NASA Contractor Report 4531

Three-Dimensional Boundary-Layer Program (BL3D) for Swept Subsonic or Supersonic Wings With Application to Laminar Flow Control

Venkit Iyer
ViGYAN, Inc.
Hampton, Virginia

Prepared for
Langley Research Center
under Contract NAS1-19672

National Aeronautics and
Space Administration
Office of Management
Scientific and Technical
Information Program
1993

Summary

This report deals with the theory, formulation, and solution of compressible three-dimensional boundary-layer equations with applications to general swept subsonic or supersonic wings in laminar flow. A number of modifications and new features are incorporated, based on an earlier general procedure described in NASA CR 4269, Jan. 1990. A more efficient algorithm has been employed, and overall improvements have been made that result in a user-friendly computer code. An interface routine is presented that uses the inviscid Euler solutions as input. Code modifications are implemented for application in laminar flow control design applications. Output of solution profiles and quantities required in boundary-layer stability analysis is included. Conversion routines to compare results with Navier-Stokes profiles are also presented.

This report is a stand-alone document that provides all the necessary details for numerical calculation of three-dimensional swept-wing boundary layers. Examples of applications and validation with thin-layer Navier-Stokes solutions are presented. A user's manual is included as an appendix.

Keywords

Boundary layer

Compressible flow

Laminar flow control

Transition prediction

Swept-wing flow

Table of Contents

Nomenclature

A_1, A_2, A_3, A_4	coefficients in the transformed continuity equation (see eqs. (47)–(50))
a_1, a_2, a_3	coefficients in the ξ-direction differencing formula (see eqs. (129)–(130))
$a^k_{l,m}$	diagonal elements of the linear system given by eq. (101) or (108)
B_i, $i = 1,6$	coefficients in the transformed ξ momentum equation (see eqs. (55)–(60))
$\tilde{B}_i$, $i = 3,6$	coefficients (see eq. (91))
$\hat{B}_3, \hat{B}_4$	coefficients (see eq. (94))
b_1, b_2, b_3,	coefficients in the η-direction differencing formula
b_4, b_5	(see eqs. (131)–(133))
$b^k_{l,m}$	superdiagonal elements of the linear system given by eq. (101) or (108)
C_i, $i = 1,6$	coefficients in the transformed η momentum equation (see eqs. (62)–(67))
$\check{C}_i$, $i = 3,6$	coefficients (see eq. (92))
$\hat{C}_4, \hat{C}_5$	coefficients (see eq. (95))
C_p	pressure coefficient
C_{13}, C_{24}, C_{25}, C_{26}, C_{34}, C_{35}, C_{36}	metric coefficients (see eqs. (6)–(12))
$C_{f,x}$	skin-friction coefficient in x direction normalized with free-stream values
D_i, $i = 1,5$	coefficients in the transformed energy equation (see eqs. (69)–(70))
$\tilde{D}_3, \tilde{D}_4$	coefficients (see eq. (96))
ds_1, ds_2	incremental arc lengths, nondimensional, in the x and y directions (see eqs. (4)–(5))
E_i, $i = 1,4$	coefficients (see eq. (87))
F	u / u_e
f	an arbitrary function
f_e	$\frac{\partial u_e}{\partial \xi}$
G	v / v_r
g_{12}	metric coefficient (see eq. (3))
H	total enthalpy, nondimensional (see eq. (24))
H^*_∞	free-stream total enthalpy, dimensional (see eq. (23))
h_1, h_2	metric coefficient (see eqs. (1)–(2))
h_s	metric term (see eq. (8))
I	H_ζ
i, j, k	indices in the ξ, η, and ζ directions
ke	index k that corresponds to the boundary-layer edge
k_s	factor for stretching the grid in the ζ direction (see eq. (128))
L	F_ζ

L^*_∞	reference length, dimensional
l	$(\rho\mu/\rho_e\mu_e)$
l_p	l/Pr
M	G_ζ
M_∞	free-stream Mach number
nx, ny	maximum number of boundary-layer grid points in x and y directions
nxlim, nylim	limits set on nx, ny to restrict computation to a smaller region
P	static pressure, nondimensional
Pr	laminar Prandtl number
P^*_∞	free-stream pressure, dimensional
Q	vector (see eq. (85))
q	absolute velocity, nondimensional (see eq. (25))
q_s	normalized suction rate defined as $q_s = (\rho^*_1 \hat{w}^*_1)/(\rho^*_\infty U^*_\infty)$
$\dot{q}^*_w$	wall heat flux, dimensional
R^*	gas constant
Re_{CF}	crossflow Reynolds number (see eq. (138))
Re_∞	free-stream Reynolds number, based on reference length L^*_∞ (see eq. (29))
Re_θ	momentum-thickness Reynolds number (see eq. (139))
$\{r^k_l\}$	residual, right-hand side of equation (108)
$\{S\}$	solution vector at location (i, j)
s_1, s_2	nondimensional arc lengths in the x and y directions (see eqs. (4)–(5))
T	temperature, nondimensional
T^*_∞	free-stream temperature, dimensional
U^*_∞	free-stream velocity, dimensional
u, v	velocities in streamwise and spanwise directions, nondimensional
u', v', w'	velocities, nondimensional, in Cartesian coordinate directions
u_s, v_s	boundary-layer velocities along and orthogonal to the edge streamline
v_r	reference velocity for v
w	transformed normal velocity (see eqs. (44)–(45))
$\tilde{w}$	scaled normal velocity (see eq. (28))
$\hat{w}$	surface-normal velocity, nondimensional
x, y, z	boundary-layer coordinates in streamwise, spanwise, and normal directions, nondimensional
x', y', z'	Cartesian coordinates, nondimensional
$\tilde{z}$	stretched boundary-layer normal coordinate (see eq. (27))
α^k, β^k, γ^k, δ^k	elements of block tridiagonal system (see eqs. (122)–(124))
β	angle between x- and y-coordinate lines
γ	ratio of specific heats
$\Delta\zeta_k$	step size in ζ (see eq. (110))
ζ	transformed normal coordinate (see eq. (36))

δ	prefix used to indicate change in a solution vector or solution vector element at iteration level n and at location (i, j) (see eq. (105), for example)
$\delta^*_{0.1}$	boundary-layer thickness, dimensional, at which v_s reduces to 10 percent of its maximum value
η, ξ	transformed boundary-layer surface coordinates
θ	(ρ_e/ρ)
Λ	sweep angle
λ_0, λ_1, λ_2, λ_3	coefficients (see eq. (97))
μ	absolute viscosity, nondimensional
ν	kinematic viscosity, nondimensional
ρ	density, nondimensional
ϕ	$\sqrt{\rho_e \mu_e s_1 u_e}$
χ_1, χ_2, χ_3	coefficients (see eq. (87))
ψ, ψ_1, ψ_2, ψ_3	surface partial derivative functions (see eqs. (14)–(17))
ψ_w	coefficient in normal velocity transformation (see eq. (115))
ψ_q	coefficient in wall heat flux transformation (see eq. (118))
ω	relaxation parameter
ω_{at}	relaxation parameter for attachment-line iteration
ω_i	factor used in finite differencing in ξ direction

Subscripts:

e	boundary-layer edge
$k = 1$	at the wall
$k = ke$	at boundary-layer edge
max	maximum
r	reference value
w	wall quantity
x, y, z	partial derivatives in x, y, and z directions
ξ, η, ζ	partial derivatives in ξ, η, and ζ directions
∞	free-stream quantity
1, 2	x and y directions

Superscripts:

*	dimensional quantity
'	Cartesian coordinate (as in x', y', z')
'	partial derivative in ζ (except for x', y', z')
n	iteration number
T	transpose

Abbreviations:

BL	Boundary layer
BL3D	Boundary layer three dimensional
INV	Inviscid
L	Left-pointing
LISW	Locally infinite swept wing
LHS	Left-hand side
NS	Navier-Stokes
RHS	Right-hand side
Z	Zig-zag

1. INTRODUCTION

A renewed interest has developed in the design of wings with extensive lengths of laminar flow in the subsonic and supersonic regimes. Design for laminar flow by passive or active means is a multiparameter optimization problem that involves such variables as surface pressure gradients, leading-edge radius, sweep, suction rates, and free-stream conditions. To aid in the design process, a reliable computational procedure is needed to predict boundary-layer stability. An important part of this computational prediction is the accurate generation of smooth mean-flow profiles. This report addresses the issue of generating these profiles.

Two options are available for mean-flow prediction. The first one is the use of an accurate thin-layer Navier-Stokes solver in which particular attention is paid to such issues as grid resolution and numerical dissipation. However, for repeated preliminary design calculations, the Navier-Stokes solution is expensive. The second option is the use of an accurate boundary-layer method coupled with an inviscid Euler solution, which is particularly attractive for experimentation with different pressure and suction distributions.

This report deals with the theory, formulation, and solution of compressible three-dimensional boundary-layer equations, with specific reference to general swept subsonic or supersonic wings in laminar flow. A number of modifications and new features are incorporated from an earlier general procedure described in NASA CR 4269, Jan. 1990 (i.e., ref. 1; see also ref. 2). However, the present report is a stand-alone document that provides all of the necessary details for numerical calculation of three-dimensional swept-wing boundary layers.

The modifications to the original procedure provide a more efficient algorithm. The

solution scheme has been modified to solve the continuity, energy, and momentum equations simultaneously, with iterative update of nonlinear terms. Streamwise and spanwise differencing schemes have been modified to ensure that the boundary-layer solution is consistent with the boundary-layer-edge boundary conditions. Overall improvements have been made that result in a more user-friendly computer code. An interface routine has been developed to use the Euler solutions as input. Code modifications have been implemented for application in laminar flow control design. The modified code also provides the output of profiles and quantities that are required in boundary-layer stability analysis. Conversion routines that enable one to compare the boundary-layer solution profiles with Navier-Stokes solution profiles are also provided.

Two applications of the code are presented: a subsonic case and a supersonic case. For the subsonic case, validations with the thin-layer Navier-Stokes solutions are presented. Detailed comparisons are made of the solution profiles and other boundary-layer properties. For the supersonic case, comparisons are given of the present code with a conical swept wing boundary-layer code developed by Kaups and Cebeci (ref. 3).

A user's manual is included as an appendix to this report. The complete program package is archived in the NASA Langley computer system mass storage and can be made available per individual request.

2. FORMULATION

2.1 Three-Dimensional Boundary-Layer Coordinates

We start with the definition of the surface-oriented curvilinear nonorthogonal coordinates used in the three-dimensional boundary-layer equations.

Let us assume that the surface of interest is defined in terms of Cartesian coordinates (x'^*, y'^*, z'^*) in dimensional units (see Figure 1(a)). The free-stream quantities are (M_∞, P^*_∞, T^*_∞) with a corresponding free-stream velocity U^*_∞.

The body coordinates are normalized with a reference length L^*_∞; the Cartesian components of velocity (u'^*, v'^*, w'^*) are normalized by the reference velocity U^*_∞. The resulting normalized coordinates are (x', y', z'), and the normalized velocity components are (u', v', w'). (See Figure 1(b).) The normalization of other flow quantities is discussed in the next section.

The boundary-layer coordinates are defined in the two surface directions x and y, where x is the predominant streamwise direction and y is the general spanwise direction (not necessarily along the constant percent chord direction for a wing). The coordinate z is mutually perpendicular to both x and y. The coordinates x and y are surface conforming, but do not need to be measured as surface arc lengths. For example, for the case of the attachment-line flow on a swept wing, the boundary-layer coordinate y may be defined along the attachment line on the surface, but can be expressed as distance in the spanwise direction perpendicular to the chord. The coordinates x and y can also be normalized to the (0, 1) range in the computational domain. The three basic metric quantities (h_1, h_2, g_{12}) defined later in this section characterize the stretching and shearing of the physical grid into the computational grid.

The grid line $x = 0$ coincides with the starting location of the boundary layer as

shown in Figure 1(c) (in this case, the attachment line of a swept wing). The choice of $x = 0$ is important because the system of equations becomes singular at the boundary-layer origination point, and a special set of equations must be solved here to initialize the solution.

The transformation of quantities from the (x', y', z') to the (x, y, z) system is determined by the set of six partial derivatives $(x'_x, y'_x, z'_x, x'_y, y'_y, z'_y)$. Note that in boundary-layer theory, the planes where z = constant are assumed to be parallel to the surface, which means that the surface partial derivatives are sufficient to characterize the transformation from one system to another. These partial derivatives enter into the three-dimensional boundary-layer equations via the three metric quantities (h_1, h_2, g_{12}) defined as

$$h_1 = \sqrt{(x'_x)^2 + (y'_x)^2 + (z'_x)^2} \tag{1}$$

$$h_2 = \sqrt{(x'_y)^2 + (y'_y)^2 + (z'_y)^2} \tag{2}$$

$$g_{12} = h_1 h_2 \cos\beta = x'_x x'_y + y'_x y'_y + z'_x z'_y \tag{3}$$

The metric coefficients h_1 and h_2 represent the stretching in the two surface coordinate directions with reference to the physical grid. The nondimensional surface arc lengths in the two directions s_1 and s_2 are defined by the two incremental relations

$$ds_1 = h_1\, dx \tag{4}$$

$$ds_2 = h_2\, dy \tag{5}$$

Further, the quantity $g_{12}/h_1 h_2$ is the cosine of the angle β between the two coordinates x and y. The additional coefficients, based on h_1, h_2 and g_{12}, are defined as

$$C_{13} = \sqrt{h_1^2 h_2^2 - g_{12}^2} \tag{6}$$

$$C_{24} = \frac{g_{12}}{C_{13}^2}\left\{\frac{g_{12}}{h_1^2} h_{1x} + h_{1y} - \frac{1}{h_1} g_{12x}\right\} \tag{7}$$

$$C_{25} = \frac{1}{C_{13}^2}\left\{h_s h_{1y} - 2 g_{12} h_{2x}\right\}\ ;\ h_s = h_1 h_2\left\{1 + \frac{g_{12}^2}{h_1^2 h_2^2}\right\} \tag{8}$$

$$C_{26} = \frac{h_1}{C_{13}^2}\left\{g_{12y} - h_2 h_{2x} - \frac{g_{12}}{h_2} h_{2y}\right\} \tag{9}$$

$$C_{34} = \frac{h_2}{C_{13}^2}\left\{g_{12x} - h_1 h_{1y} - \frac{g_{12}}{h_1} h_{1x}\right\} \tag{10}$$

$$C_{35} = \frac{1}{C_{13}^2}\left\{h_s h_{2x} - 2 g_{12} h_{1y}\right\} \tag{11}$$

$$C_{36} = \frac{g_{12}}{C_{13}^2}\left\{\frac{g_{12}}{h_2^2} h_{2y} + h_{2x} - \frac{1}{h_2} g_{12y}\right\} \tag{12}$$

The transformation of velocities from $(u',\ v',\ w')$ to $(u,\ v,\ \hat{w})$ is accomplished by the inversion of the system given below. Note that $\hat{w}$ is the symbol used for the nondimensional surface-normal velocity; the symbol w is reserved for later use as

transformed normal velocity.

$$\begin{bmatrix} x'_x & x'_y & \frac{\psi_1}{\psi} \\ y'_x & y'_x & \frac{\psi_2}{\psi} \\ z'_x & z'_x & \frac{\psi_3}{\psi} \end{bmatrix} \begin{bmatrix} u \\ v \\ \hat{w} \end{bmatrix} = \begin{bmatrix} u' \\ v' \\ w' \end{bmatrix} \tag{13}$$

where

$$\psi_1 = y'_x z'_y - z'_x y'_y \tag{14}$$

$$\psi_2 = x'_y z'_x - z'_y x'_x \tag{15}$$

$$\psi_3 = x'_x y'_y - x'_y y'_x \tag{16}$$

$$\psi = \sqrt{\psi_1^2 + \psi_2^2 + \psi_3^2} \tag{17}$$

The metric terms defined above allow the flow to be described in terms of surface-oriented quantities. As a result, the flow can be treated as equivalent to that on a developed flat surface described by two families of nonorthogonal coordinates. However, the metric terms do not represent the effects of surface curvature on the physics of the flow. Note that the effect of surface shape on the boundary layer is felt only through the inviscid pressure distribution.

2.2 Three-Dimensional Boundary-Layer Equations

The three-dimensional laminar, compressible boundary-layer equations in surface-oriented curvilinear nonorthogonal coordinates are given below (subscripts indicate partial derivatives).

The continuity equation is

$$\left(\frac{C_{13}}{h_1}\rho u\right)_x + \left(\frac{C_{13}}{h_2}\rho v\right)_y + (C_{13}\,\rho\,\tilde{w})_{\tilde{z}} = 0 \tag{18}$$

The momentum equation in the x direction is

$$\begin{aligned}\rho\left(\frac{u}{h_1}u_x + \frac{v}{h_2}u_y + \tilde{w}\,u_{\tilde{z}} + C_{24}\,u^2 + C_{25}\,uv + C_{26}\,v^2\right) - (\mu u_{\tilde{z}})_{\tilde{z}} \\ = \left(-\frac{h_1 h_2^2}{C_{13}^2}P_x + \frac{h_1 g_{12}}{C_{13}^2}P_y\right)\frac{1}{\gamma M_\infty^2}\end{aligned} \tag{19}$$

The momentum equation in the y direction is

$$\begin{aligned}\rho\left(\frac{u}{h_1}v_x + \frac{v}{h_2}v_y + \tilde{w}\,v_{\tilde{z}} + C_{34}\,u^2 + C_{35}\,uv + C_{36}\,v^2\right) - (\mu v_{\tilde{z}})_{\tilde{z}} \\ = \left(\frac{h_2 g_{12}}{C_{13}^2}P_x - \frac{h_1^2 h_2}{C_{13}^2}P_y\right)\frac{1}{\gamma M_\infty^2}\end{aligned} \tag{20}$$

The energy equation is written in terms of the nondimensional total enthalpy H. When perfect gas and constant specific heats are assumed, the dimensional total enthalpy H^* is defined as

$$H^* = \frac{R^*\gamma}{\gamma - 1}T^* + \frac{1}{2}q^{*2} \tag{21}$$

where

$$q^{*2} = u'^{*2} + v'^{*2} + w'^{*2} \approx u^{*2} + v^{*2} + 2\,u^*\,v^*\cos\beta \tag{22}$$

The nondimensional total enthalpy $H = H^*/H_\infty^*$ is based on the reference value

$$H_\infty^* = \frac{R^*\gamma}{\gamma - 1}T_\infty^* + \frac{1}{2}U_\infty^{*2} \tag{23}$$

which results in the definition

$$H = \frac{T + 0.5\,(\gamma - 1)\,M_\infty^2\,q^2}{1 + 0.5\,(\gamma - 1)\,M_\infty^2} \tag{24}$$

with $T = T^*/T^*_\infty$ and

$$q^2 = u^2 + v^2 + 2\,u\,v\cos\beta \tag{25}$$

The resulting energy equation is

$$\rho\,(u\,H_x + v\,H_y + \tilde{w}\,H_{\tilde{z}}) = \left[\frac{\mu}{Pr}\,H_{\tilde{z}} + \frac{\mu}{2}\left(1 - \frac{1}{Pr}\right)(q^2)_{\tilde{z}}\right]_{\tilde{z}} \tag{26}$$

In the equations above, $\tilde{z}$ and $\tilde{w}$ are stretched quantities with a free-stream Reynolds number scaling applied as

$$\tilde{z} = z\sqrt{Re_\infty} \tag{27}$$

$$\tilde{w} = \hat{w}\sqrt{Re_\infty} \tag{28}$$

where

$$Re_\infty = U^*_\infty L^*_\infty \,/\, \nu^*_\infty \tag{29}$$

Other variables are normalized as ρ^* by ρ^*_∞; T^* by T^*_∞; P^* by P^*_∞; and μ^* by μ^*_∞. The equation of state is then written as

$$P = \rho\,T \tag{30}$$

The pressure coefficient can be written as

$$C_p = \frac{2\,(P-1)}{\gamma M^2_\infty} \tag{31}$$

The variation of viscosity with temperature is modeled by the Sutherland law as

$$\mu^* = \frac{\mu^*_r\,T^{*1.5}}{T^* + T^*_r}$$

$$T^*_r = 198.6\,^\circ\mathrm{R} = 110.33\ \mathrm{K} \tag{32}$$

$$\mu^*_r = 2.27 \times 10^{-8}\,\frac{\mathrm{lb-sec}}{\mathrm{ft}^2\,^\circ\mathrm{R}^{1/2}} = 1.458 \times 10^{-6}\,\frac{\mathrm{N-sec}}{\mathrm{m}^2\,\mathrm{K}^{1/2}}$$

In nondimensional form, the Sutherland law is expressed as

$$\mu = \frac{T^{1.5}(1+T_r)}{T+T_r};\ \mu_r = \frac{\mu_r^*}{\mu_\infty^*};\ T_r = \frac{T_r^*}{T_\infty^*} \tag{33}$$

With the assumption that pressure is constant in the normal direction and that the normal derivatives tend to zero at the boundary-layer edge (which is denoted by the subscript e), the right-hand sides (RHS) of equations (15) and (16) can be replaced by the edge quantities to yield

$$\begin{aligned} &\rho\left(\frac{u}{h_1}u_x + \frac{v}{h_2}u_y + \tilde{w}\,u_{\tilde{z}} + C_{24}\,u^2 + C_{25}\,uv + C_{26}\,v^2\right) - (\mu u_{\tilde{z}})_{\tilde{z}} \\ &\quad = \rho_e\left(\frac{u_e}{h_1}u_{e,x} + \frac{v_e}{h_2}u_{e,y} + C_{24}\,u_e^2 + C_{25}\,u_e v_e + C_{26}\,v_e^2\right) \end{aligned} \tag{34}$$

$$\begin{aligned} &\rho\left(\frac{u}{h_1}v_x + \frac{v}{h_2}v_y + \tilde{w}\,v_{\tilde{z}} + C_{34}\,u^2 + C_{35}\,uv + C_{36}\,v^2\right) - (\mu v_{\tilde{z}})_{\tilde{z}} \\ &\quad = \rho_e\left(\frac{u_e}{h_1}v_{e,x} + \frac{v_e}{h_2}v_{e,y} + C_{34}\,u_e^2 + C_{35}\,u_e v_e + C_{36}\,v_e^2\right) \end{aligned} \tag{35}$$

The equations are hyperbolic in the stream-surface directions and parabolic in the surface-normal direction. The boundary conditions $(u_e,\ v_e,\ H_e)$ are specified at the boundary-layer edge. The value of $\tilde{w}_w$ and one of the values, T_w, H_w, or H'_w, are specified at the surface. The solution profiles at $x = 0$ and $y = 0$ are required to initiate the solution marching procedure.

2.3 Transformation

A transformation is required for the $\tilde{z}$ and $\tilde{w}$ variables to handle the singularity of the equations at $x = 0$. The transformation also reduces the boundary-layer growth in the computational coordinates. Further, a transformation for $\tilde{w}$ is necessary to express the resulting equations in a closed form.

The transformation is defined as

$$\zeta = \sqrt{\frac{u_e}{\rho_e \mu_e s_1}} \int_0^{\tilde{z}} \rho \, d\tilde{z} \tag{36}$$

$$\xi = x; \ \eta = y; \ s_1 = \int_0^x h_1 \, dx \tag{37}$$

Although $\xi = x$, the partial derivative $\frac{\partial}{\partial x}$ is actually $\frac{\partial}{\partial x}|_{y,\tilde{z}}$, and the partial derivative $\frac{\partial}{\partial \xi}$ is $\frac{\partial}{\partial \xi}|_{\eta,\zeta}$. A similar distinction exists between $\frac{\partial}{\partial y}$ and $\frac{\partial}{\partial \eta}$. The transformations of the gradients of an arbitrary function f between the $(x, y, \tilde{z})$ and (ξ, η, ζ) systems are given by

$$\begin{bmatrix} f_\xi \\ f_\eta \\ f_\zeta \end{bmatrix} = \begin{bmatrix} 1 & 0 & \tilde{z}_\xi \\ 0 & 1 & \tilde{z}_\eta \\ 0 & 0 & \tilde{z}_\zeta \end{bmatrix} \begin{bmatrix} f_x \\ f_y \\ f_{\tilde{z}} \end{bmatrix} \tag{38}$$

$$\begin{bmatrix} f_x \\ f_y \\ f_{\tilde{z}} \end{bmatrix} = \begin{bmatrix} 1 & 0 & \zeta_x \\ 0 & 1 & \zeta_y \\ 0 & 0 & \zeta_{\tilde{z}} \end{bmatrix} \begin{bmatrix} f_\xi \\ f_\eta \\ f_\zeta \end{bmatrix} \tag{39}$$

Because the (3 × 3) matrices are inverses of each other, the following relations are valid:

$$\frac{\partial \zeta}{\partial \tilde{z}} = \frac{1}{\left(\frac{\partial \tilde{z}}{\partial \zeta}\right)} = \rho \sqrt{\frac{u_e}{\rho_e \mu_e s_1}} \tag{40}$$

$$\frac{\partial \zeta}{\partial x} = -\tilde{z}_\xi \rho \sqrt{\frac{u_e}{\rho_e \mu_e s_1}} \tag{41}$$

$$\frac{\partial \zeta}{\partial y} = -\tilde{z}_\eta \rho \sqrt{\frac{u_e}{\rho_e \mu_e s_1}} \tag{42}$$

We also define the new variables F and G and a transformed normal velocity variable w such that

$$F = u/u_e; \ G = v/v_r \tag{43}$$

$$w = \tilde{w}\,\frac{s_1}{u_e}\,\frac{\partial \zeta}{\partial \tilde{z}} + \frac{s_1}{h_1}\,F\,\frac{\partial \zeta}{\partial x} + \frac{s_1}{h_2}\,G\,\frac{v_r}{u_e}\,\frac{\partial \zeta}{\partial y} \tag{44}$$

where v_r is an arbitrary reference velocity for v. The transformed velocity w simplifies the continuity equation by the explicit removal of the density term. The transformation for w can also be rewritten as

$$w = \rho\,\sqrt{\frac{s_1}{\rho_e\,\mu_e\,u_e}}\left(\tilde{w} - \frac{u}{h_1}\,\tilde{z}_\xi - \frac{v}{h_2}\,\tilde{z}_\eta\right) \tag{45}$$

2.4 Transformed Equations

The application of the transformations for $\tilde{z}$ and $\tilde{w}$ to equations (18), (34), (35), and (26) is straightforward and is described in detail in reference 1. (Note that in the present report the notations for coefficients have been simplified.) The results are summarized here. The continuity equation reduces to

$$w_\zeta = A_1\,F_\xi + A_2\,F + A_3\,G_\eta + A_4\,G \tag{46}$$

$$A_1 = -\frac{s_1}{h_1} \tag{47}$$

$$A_2 = -\frac{s_1}{C_{13}\,\phi}\left\{C_{13}\,\frac{\phi}{h_1}\right\}_{,x} \tag{48}$$

$$A_3 = -\frac{s_1\,v_r}{h_2\,u_e} \tag{49}$$

$$A_4 = -\frac{s_1}{C_{13}\,\phi}\left\{C_{13}\,\frac{\phi\,v_r}{h_2\,u_e}\right\}_{,y} \tag{50}$$

$$\phi = \sqrt{\rho_e \mu_e s_1 u_e} \tag{51}$$

Also note that at the boundary-layer edge the transformed normal velocity becomes

$$w_{e,\zeta} = A_2 + A_3 G_{e,\eta} + A_4 G_e \tag{52}$$

At the boundary-layer edge, the partial derivatives of F, G, ϕ and the metric coefficients in the x or y direction are the same as the corresponding partial derivatives in the ξ or η direction.

To set up the fourth-order Pade differencing, we introduce three new variables L, M, and I, defined as the partial derivatives with respect to ζ of the basic variables F, G, and H, respectively. The ξ momentum equation reduces to

$$(l\,L - w\,F)_\zeta = B_1 \left(F^2\right)_\xi + B_2 (F\,G)_\eta + B_3\,F^2 + B_4\,F\,G + B_5\,G^2 + B_6\,\theta \tag{53}$$

The new variables introduced are defined as

$$L = F_\zeta;\ M = G_\zeta;\ I = H_\zeta;\ \theta = \left(\frac{\rho_e}{\rho}\right);\ l = \left(\frac{\rho\mu}{\rho_e \mu_e}\right) \tag{54}$$

The coefficients B_i are given as

$$B_1 = -A_1 \tag{55}$$

$$B_2 = -A_3 \tag{56}$$

$$B_3 = \frac{s_1}{h_1\,u_e} u_{e,\xi} - A_2 + C_{24}\,s_1 \tag{57}$$

$$B_4 = \frac{s_1\,v_r}{h_2\,u_e^2} u_{e,\eta} - A_4 + C_{25}\frac{s_1\,v_r}{u_e} \tag{58}$$

$$B_5 = C_{26} \frac{s_1 v_r^2}{u_e^2} \tag{59}$$

The coefficient B_6 is evaluated at the boundary-layer edge from equation (53) as

$$B_6 = -\left\{ w_{e,\zeta} + B_2 G_{e,\eta} + B_3 + B_4 G_e + B_5 G_e^2 \right\} \tag{60}$$

where $w_{e,\zeta}$ is given by equation (52).

The η momentum reduces to

$$(l M - w G)_\zeta = C_1 (F G)_\xi + C_2 \left(G^2\right)_\eta + C_3 F^2 + C_4 F G + C_5 G^2 + C_6 \theta \tag{61}$$

The coefficients C_i are given as

$$C_1 = -A_1 \tag{62}$$

$$C_2 = -A_3 \tag{63}$$

$$C_3 = \frac{C_{34} s_1 u_e}{v_r} \tag{64}$$

$$C_4 = -A_2 + s_1 C_{35} + \frac{s_1}{h_1 v_r} v_{r,\xi} \tag{65}$$

$$C_5 = -A_4 + C_{36} \frac{s_1 v_r}{u_e} + \frac{s_1}{h_2 u_e} v_{r,\eta} \tag{66}$$

The coefficient C_6 is evaluated at the boundary-layer edge from equation (61) as

$$C_6 = -\left\{ w_{e,\zeta} G_e + C_1 G_{e,\xi} + C_2 \left(G_e^2\right)_\eta + C_3 + C_4 G_e + C_5 G_e^2 \right\} \tag{67}$$

The energy equation in terms of the transformed variables becomes

$$\left(\frac{l}{Pr} I - w H\right)_{\zeta} = D_1 (F H)_{\xi} + D_2 (G H)_{\eta} + D_3 F H + D_4 G H + D_5$$

$$D_5 = \frac{U_{\infty}^{*2}}{2 H_{\infty}^{*}} \left\{ l \left(\frac{1 - Pr}{Pr} \right) (q^2)_{\zeta} \right\}_{\zeta} \tag{68}$$

The coefficients D_i are given as

$$D_1 = -A_1;\ D_2 = -A_3;\ D_3 = -A_2;\ D_4 = -A_4 \tag{69}$$

The term D_5 can be rewritten with equation (25) as

$$D_5 = \frac{U_{\infty}^{*2}}{H_{\infty}^{*}} \left(\frac{1 - Pr}{Pr} \right) \left\{ l \left[u_e^2 F L + v_r^2 G M + u_e v_r \left(\frac{g_{12}}{h_1 h_2} \right) (F M + G L) \right] \right\}_{\zeta} \tag{70}$$

2.5 Quasi-Two-Dimensional Equations for Initial Conditions

The solution of the transformed three-dimensional boundary-layer equations requires the specification of profiles of F, G, and H at the $\xi = 0$ and $\eta = 0$ planes as initial conditions. In the ideal case, a plane of symmetry flow or a conical flow will exist at these planes. As a result, the equations simplify to quasi-two-dimensional form (i.e., either ξ or η derivatives reduce to zero). This simplification permits the solution and generation of initial solution planes independent of the full three-dimensional flow region.

In the case of flow past a wing attached to a fuselage, certain assumptions are necessary for simplification of the initial profiles. For a swept wing with a nonsymmetrical chordwise wing section at an angle of attack, the attachment-line boundary layer (at $\xi = 0$) is a true symmetry plane only if we assume that the coefficient $C_{26} = 0$. This

assumption is reasonable if the curvature of the attachment line is not significant. A more drastic assumption is necessary for the $\eta = 0$ plane. We restrict the calculation to a certain region on the wing, where the boundary-layer assumptions are valid. At the $\eta = 0$ boundary, we assume that the η gradients of the flow variables are equal to zero. However, we permit variation of the metric terms as well as the boundary-layer edge quantities in both the ξ and η directions. With this assumption, the equations again reduce to quasi-two-dimensional form. This assumption is a more general version of the conical flow assumption and is termed as the locally infinite, swept-wing (LISW) assumption. The profiles at the $\xi = 0$, $\eta = 0$ location are generated by assuming that the attachment line is infinite swept locally as well.

The equations that are valid for an LISW flow are obtained by setting the coefficients A_3 (hence, B_2, C_2, and D_2) to zero. In the finite-differencing scheme, the η-direction differencing coefficients are also set to zero. To obtain smooth solutions near this boundary, the full three-dimensional solution is relaxed to the LISW solution by incorporating a factor $\omega = \omega(\eta)$ to be applied to these coefficients for a few planes adjacent to the $\eta = 0$ plane. A value of $\omega = 0$ gives the LISW solution, whereas a value of $\omega = 1$ gives the full three-dimensional solution. A similar assumption of LISW flow is used at the $\eta = \eta_{\max}$ boundary as well.

The quasi-two-dimensional equations that are valid for an attachment line are more involved because the ξ momentum equation becomes singular at $\xi = 0$ by substituting $u = 0$. The gradient $\partial u/\partial \xi$ is finite, however. The effect of the strong inviscid flow acceleration $f_e = \partial u_e/\partial \xi$ on the attachment-line boundary layer is characterized by taking the ξ derivative of the ξ momentum equation. The new definitions for the transformed

normal coordinate and normal velocity are

$$\zeta = \sqrt{\frac{f_e}{\rho_e \mu_e h_1}} \int_0^{\tilde{z}} \rho \, d\tilde{z} \tag{71}$$

$$w = \rho \sqrt{\frac{h_1}{\rho_e \mu_e f_e}} \left(\tilde{w} - \frac{v}{h_2} \tilde{z}_\eta \right) \tag{72}$$

With these special transformations, the transformed equations are in the same form as before (equations (46), (53), (61), and (68)) except that the following coefficients are changed:

$$A_1 = 0 \tag{73}$$

$$A_2 = -1 \tag{74}$$

$$A_3 = -\frac{h_1 v_r}{h_2 f_e} \tag{75}$$

$$A_4 = -\frac{h_1}{C_{13} \phi} \left\{ C_{13} \frac{\phi v_r}{h_2 f_e} \right\}_{,y} \tag{76}$$

$$\phi = \sqrt{\rho_e \mu_e h_1 f_e} \tag{77}$$

$$B_3 = 2 \tag{78}$$

$$B_4 = \frac{h_1 v_r}{h_2 f_e^2} f_{e,\eta} - A_4 + C_{25} \frac{h_1 v_r}{f_e} \tag{79}$$

$$B_5 = C_{26,x} \frac{h_1 v_r^2}{f_e^2} \tag{80}$$

$$C_3 = 0 \tag{81}$$

$$C_4 = -A_2 \tag{82}$$

$$C_5 = -A_4 + C_{36}\frac{h_1 v_r}{f_e} + \frac{h_1}{h_2 f_e} v_{r,\eta} \tag{83}$$

$$D_5 = \frac{U_\infty^{*2}}{H_\infty^*}\left(\frac{1-Pr}{Pr}\right) v_r^2 (l\,GM)_\zeta \tag{84}$$

In the finite-differencing scheme for the attachment-line solution, the ξ-direction differencing coefficients are also set to zero.

As before for the case of the LISW equations, the equations that characterize the flow at $\xi = 0$, $\eta = 0$ are obtained from the attachment-line equations with the added condition $A_3 = 0$.

2.6 Equations in Vector Form

To apply the fourth-order Pade differencing formula to the set of equations, the equation set is expressed in vectorial form for convenience. The vector Q is defined as

$$Q = \left(w,\ lL - wF,\ lM - wG,\ l_p I - wH,\ F,\ G,\ H\right)^T \tag{85}$$

where

$$l_p = \frac{l}{Pr} \tag{86}$$

The normal derivative $Q' = \partial Q/\partial\zeta$ (note that the prime denotes the partial derivative with respect to ζ) can be written from the boundary-layer equations. Before the expression for Q' is presented, the following equations are given.

The density ratio θ can be written from equation (24) in terms of the elements of Q as

$$\theta = E_1 F^2 + E_2 FG + E_3 G^2 + E_4 H$$

$$E_1 = -\frac{\chi_2}{\chi_3} u_e^2;\ E_2 = -2\frac{\chi_2}{\chi_3} u_e v_r \cos\beta$$

$$E_3 = -\frac{\chi_2}{\chi_3} v_r^2;\ E_4 = \frac{\chi_1}{\chi_3} \tag{87}$$

$$\chi_1 = 1 + \frac{\gamma - 1}{2} M_\infty^2;\ \chi_2 = \chi_1 - 1;\ \chi_3 = H_e \chi_1 - \chi_2 q_e^2$$

The viscosity ratio l can be written from equation (33) as

$$l = \sqrt{\theta}\left(\frac{1 + T_r/T_e}{\theta + T_r/T_e}\right) \tag{88}$$

The normal derivatives l' and θ' can be derived in the form

$$\theta' = 2E_1 F L + E_2 (FM + GL) + 2E_3 GM + E_4 I \tag{89}$$

$$l' = \frac{l\,\theta'}{\sqrt{\theta}}\left\{\frac{1}{2\sqrt{\theta}} - \frac{l}{(1 + T_r/T_e)}\right\} \tag{90}$$

The Q_1' element is obtained from equation (46). The Q_2' element is obtained by substituting for θ from equation (87) into equation (53).

$$Q_2' = B_1 \left(F^2\right)_\xi + B_2 (FG)_\eta + \tilde{B}_3 F^2 + \tilde{B}_4 FG + \tilde{B}_5 G^2 + \tilde{B}_6 H$$

$$\tilde{B}_3 = B_3 + E_1 B_6;\ \tilde{B}_4 = B_4 + E_2 B_6;\ \tilde{B}_5 = B_5 + E_3 B_6;\ \tilde{B}_6 = B_6 E_4 \tag{91}$$

The element Q_3' is similarly obtained as

$$Q_3' = C_1 (FG)_\eta + C_2 \left(G^2\right)_\eta + \tilde{C}_3 F^2 + \tilde{C}_4 FG + \tilde{C}_5 G^2 + \tilde{C}_6 H$$

$$\tilde{C}_3 = C_3 + E_1 C_6;\ \tilde{C}_4 = C_4 + E_2 C_6;\ \tilde{C}_5 = C_5 + E_3 C_6;\ \tilde{C}_6 = C_6 E_4 \tag{92}$$

The second derivatives $L' = F''$, $M' = G''$, and $I' = H''$ required subsequently in the vector representation are obtained by differentiation. For example, differentiation of Q_2' yields

$$Q_2' = lL' + Ll' - wL - Fw' = \text{RHS of equation (91)} \tag{93}$$

If w' is substituted from equation (46) and rearranged, then

$$\begin{aligned} L' = \frac{1}{l}\Big[&B_1\left(F^2\right)_\xi + B_2\left(FG\right)_\eta + \hat{B}_3 F^2 + \hat{B}_4 FG + \tilde{B}_5 G^2 + \tilde{B}_6 H \\ &-Ll' + wL + A_1 F F_\xi + A_3 F G_\eta\Big]; \end{aligned} \tag{94}$$

$$\hat{B}_3 = \tilde{B}_3 + A_2;\ \hat{B}_4 = \tilde{B}_4 + A_4$$

The expressions for M' and I' are similarly obtained as

$$\begin{aligned} M' = \frac{1}{l}\Big[&C_1\left(FG\right)_\eta + C_2\left(G^2\right)_\eta + \tilde{C}_3 F^2 + \hat{C}_4 FG + \hat{C}_5 G^2 + \tilde{C}_6 H \\ &-Ml' + wM + A_1 G F_\xi + A_3 G G_\eta\Big]; \end{aligned} \tag{95}$$

$$\hat{C}_4 = \tilde{C}_4 + A_2;\ \hat{C}_5 = \tilde{C}_5 + A_4$$

$$\begin{aligned} I' = \frac{1}{l_p}\Big[&D_1\left(FH\right)_\xi + D_2\left(GH\right)_\eta + \tilde{D}_3 FH + \tilde{D}_4 GH + D_5 \\ &-Il_p' + wI + A_1 H F_\xi + A_3 H G_\eta\Big]; \end{aligned} \tag{96}$$

$$\tilde{D}_3 = D_3 + A_2;\ \tilde{D}_4 = D_4 + A_4$$

The expression for D_5 can be obtained from equation (70) as

$$D_5 = l\left[\lambda_1\left(FL' + L^2\right) + \lambda_2\left(GM' + M^2\right) + \lambda_3\left(FM' + ML + GL' + LM\right)\right]$$

$$+ l'\left[\lambda_1 FL + \lambda_2 GM + \lambda_3\left(FM + GL\right)\right]; \tag{97}$$

$$\lambda_0 = \frac{U_\infty^{*2}}{H_\infty^*}\frac{1 - Pr}{Pr};\ \lambda_1 = \lambda_0 u_e^2;\ \lambda_2 = \lambda_0 v_r^2;\ \lambda_3 = \lambda_0 u_e v_r \cos\beta$$

Note that $\lambda_1 = \lambda_3 = 0$ for the attachment-line equations. The final vector representation is given as

$$Q = \begin{pmatrix} w \\ lL - wF \\ lM - wG \\ l_p I - wH \\ F \\ G \\ H \end{pmatrix} \tag{98}$$

$$Q' = \begin{pmatrix} A_1 F_\xi + A_2 F + A_3 G_\eta + A_4 G \\ B_1\left(F^2\right)_\xi + B_2(FG)_\eta + \tilde{B}_3 F^2 + \tilde{B}_4 FG + \tilde{B}_5 G^2 + \tilde{B}_6 H \\ C_1(FG)_\xi + C_2\left(G^2\right)_\eta + \tilde{C}_3 F^2 + \tilde{C}_4 FG + \tilde{C}_5 G^2 + \tilde{C}_6 H \\ D_1(FH)_\xi + D_2(GH)_\eta + D_3 FH + D_4 GH + D_5 \\ L \\ M \\ I \end{pmatrix} \tag{99}$$

$$Q'' = \begin{pmatrix} A_1 L_\xi + A_2 L + A_3 M_\eta + A_4 M \\ 2B_1(FL)_\xi + B_2(FM + GL)_\eta + 2\tilde{B}_3 FL + \tilde{B}_4(FM + GL) + 2\tilde{B}_5 GM + \tilde{B}_6 I \\ C_1(FM + GL)_\xi + 2C_2(GM)_\eta + 2\tilde{C}_3 FL + \tilde{C}_4(FM + GL) + 2\tilde{C}_5 GM + \tilde{C}_6 I \\ D_1(FI + HL)_\xi + D_2(GI + HM)_\eta + D_3(FI + HL) + D_4(GI + HM) + D_5' \\ L' \text{ (equation (94))} \\ M' \text{ (equation (95))} \\ I' \text{ (equation (96))} \end{pmatrix} \tag{100}$$

3. DISCRETIZATION

3.1 Differencing Formulas

We apply the fourth-order Pade differencing formula in the normal direction. This two-point compact scheme is defined in terms of the variable and its two higher derivatives. In the present case, if we assume that the indices in the two surface directions (i, j) remain constant and that k is the normal direction index, then the discretization at the midpoint of k and $(k-1)$ is written as

$$Q_k - Q_{k-1} - \frac{\Delta\zeta}{2}\left(Q'_k + Q'_{k-1}\right) + \frac{\Delta\zeta^2}{12}\left(Q''_k - Q''_{k-1}\right) + O(\Delta\zeta^5) = 0 \tag{101}$$

$$\Delta\zeta = \zeta_k - \zeta_{k-1} \tag{102}$$

The differencing in the surface directions ξ and η are second order (or first order in some regions). For example, in the ξ direction, if we assume that the indices (j, k) are fixed, then

$$\begin{aligned} Q_\xi &= a_1 Q_i + \{aQ\} \\ \{aQ\} &= a_2 Q_{i-1} + a_3 Q_{i-2} \end{aligned} \tag{103}$$

Similarly, in the η direction, if we assume that the indices k are fixed, then

$$\begin{aligned} Q_\eta &= b_1 Q_{i,j} + \{bQ\} \\ \{bQ\} &= b_2\, Q_{i,j-1} + b_3 Q_{i,j-2} + b_4\, Q_{i-1,j} + b_5 Q_{i-1,j+1} \end{aligned} \tag{104}$$

The value of the coefficients a_i and b_i are dependent on the location of the point (i, j) in the streamwise and the crossflow direction. At present, we restrict the discussion to the discretization in the ζ direction and will use the short notation given above for the ξ- and η-direction differencing. (See " Discretization in the (i, j) Directions" for more details.)

We define a solution vector $\{S\} = \{w,\ F,\ G,\ H,\ L,\ M,\ I\}^T$. Because the equations are nonlinear in $\{S\}$, Newton linearization is used to convert the system to a linear matrix

inversion problem. If superscript n denotes the current iteration stage, let us define $\{\delta S\}$ as

$$\{\delta S\} \;=\; S^n - S^{n-1} \tag{105}$$

A linear system is now set up to solve for $\{\delta S\}$ in terms of the solution at iteration level $n-1$. For example, a term that involves $(F^n)^2$ is written as

$$(F^n)^2 \;=\; \left(F^{n-1} + \delta F\right)^2 \approx \left(F^{n-1}\right)^2 + 2F^{n-1}\,\delta F \tag{106}$$

In what follows, the superscript $n-1$ is dropped and is taken to imply the known values of $\{S\}$ at iteration $n-1$. A few examples of the linearized formulas with this notation are given below:

$$\begin{aligned}
(F^n)^2 &= F^2 + 2F\,\delta F \\
F^n_\xi &= F_\xi + a_1\delta F \\
F^n_\eta &= F_\eta + b_1\delta F \\
(FG)^n_\xi &= a_1 G\delta F \\
F^n F^n_\xi &= FF_\xi + \delta F\left(a_1 F + F_\xi\right)
\end{aligned} \tag{107}$$

3.2 Linearized system at (*i,j*)

The system is explicit in ξ and η because of our choice of the finite-differencing scheme and is implicit in the surface-normal direction. The linearized system is represented at location (i,j), which corresponds to the solution at iteration level n as

$$\left[\cdots\; a^k_{l,m}\; b^k_{l,m}\cdots\right]\left\{\delta S^k_l\right\} \;=\; \left\{r^k_l\right\} \tag{108}$$

where $a^k_{l,m}$ and $b^k_{l,m}$ are elements of the (7 x 7) blocks in the diagonal and superdiagonal locations of the linearized block bidiagonal system. The superscript k denotes that the

discretization corresponds to the midpoint of k and $(k-1)$ points. The index l varies from 1 to 7, depending on which element of equation (101) is being discretized; m varies from 1 to 7, depending on which element of $\{\delta S\}$ it multiplies. The (7 x 7) blocks $\left[a^k_{l,m}\right]$ and $\left[b^k_{l,m}\right]$ are the only nonzero blocks in the system above because we have a two-point compact scheme in the k direction. The (7 x 1) vector $\{r^k_l\}$ corresponds to the residual of equation (101), based on the solution $\{S\}$ at iteration $(n-1)$.

For example, examine the discretization of the second element of the system represented by equation (101), which can be written as

$$
\begin{aligned}
&(lL - wF)_k - (lL - wF)_{k-1} \\
&- \frac{\Delta\zeta_k}{2}\Big\{\Big[B_1F_\xi^2 + B_2(FG)_\eta + \tilde{B}_3F^2 + \tilde{B}_4FG + \tilde{B}_5G^2 + \tilde{B}_6H\Big]_k \\
&\qquad + \Big[B_1F_\xi^2 + B_2(FG)_\eta + \tilde{B}_3F^2 + \tilde{B}_4FG + \tilde{B}_5G^2 + \tilde{B}_6H\Big]_{k-1}\Big\} \\
&+ \frac{\Delta\zeta_k^2}{12}\Big\{\Big[2B_1(FL)_\xi + B_2(FM+GL)_\eta + 2\tilde{B}_3FL + \tilde{B}_4(FM+GL) + 2\tilde{B}_5GM + \tilde{B}_6I\Big]_k \\
&- \Big[2B_1(FL)_\xi + B_2(FM+GL)_\eta + 2\tilde{B}_3FL + \tilde{B}_4(FM+GL) + 2\tilde{B}_5GM + \tilde{B}_6I\Big]_{k-1}\Big\} = 0
\end{aligned}
\tag{109}
$$

where

$$\Delta\zeta_k = \zeta_k - \zeta_{k-1} \tag{110}$$

We can now construct the elements of the blocks $\left[a^k_{l,m}\right]$, $\left[b^k_{l,m}\right]$, and $\{r^k_l\}$ for the case $l = 2$ from above by using the linearization procedure explained earlier. Some examples are given below. The coefficient a^k_{21} is the coefficient of δw_{k-1} from the second element of equation (101), which is discretized at $(k-\frac{1}{2})$, and b^k_{21} is the corresponding coefficient

$$a_{21} = F_{k-1}$$

$$b_{21} = -F_k$$

$$a_{22}^k = w_{k-1} - \frac{\Delta\zeta_k}{2}\left(2B_1a_1F + B_2b_1G + 2\tilde{B}_3F + \tilde{B}_4G\right)_{k-1}$$

$$b_{22}^k = -w_k - \frac{\Delta\zeta_k}{2}\left(2B_1a_1F + B_2b_1G + 2\tilde{B}_3F + \tilde{B}_4G\right)_{k}$$

$$a_{25}^k = -l_{k-1} - \frac{\Delta\zeta_k^2}{12}\left(2B_1a_1F + B_2b_1G + 2\tilde{B}_3F + \tilde{B}_4G\right)_{k-1}$$

$$r_2^k = \text{negative of LHS of equation (109)}$$

Similar expressions can be derived from the 7 elements of the system that are represented by equations (98)–(100). These expressions for the 49 elements of $\left[a_{l,m}^k\right]$, the 49 elements of $\left[b_{l,m}^k\right]$, and the 7 elements of $\left\{r_l^k\right\}$ are given in appendix A.

3.3 Boundary Conditions

The boundary conditions at the boundary-layer edge ($k = ke,\ \zeta = \zeta_e$) are given as

$$F_{k=ke} = 1;\ \ G_{k=ke} = G_e = \frac{v_e}{v_r};\ \ H_{k=ke} = H_e \tag{112}$$

The boundary conditions at the wall ($k = 1,\ \zeta = 0$) are given as

$$F_{k=1} = G_{k=1} = 0$$

$$H_{k=1} = H_1 \ \text{ or } \ I_{k=1} = I_1 \tag{113}$$

$$w_{k=1} = w_w$$

The transformed normal velocity at the wall ($w_{k=1}$ or w_1 or w_w) is specified from equation (45) as

$$w_1 = \left(\frac{\rho_1^*\hat{w}_1^*}{\rho_\infty^* U_\infty^*}\right)\psi_w\sqrt{Re_\infty} \tag{114}$$

where ψ_w is defined for general three-dimensional flow or attachment-line flow as

$$\psi_w = \sqrt{\frac{s_1}{\rho_e \mu_e u_e}} \quad \text{or} \quad \psi_w = \sqrt{\frac{h_1}{\rho_e \mu_e f_e}} \tag{115}$$

Suction rate is usually specified in terms of the suction-rate momentum value scaled by the free-stream momentum as $q_s = \rho_1^* \hat{w}_1^* / \rho_\infty^* U_\infty^*$.

For an adiabatic wall, I_1 is specified as equal to zero. For a nonadiabatic case, if the wall heat flux is known in dimensional units as $\dot{q}_w^*$, then the wall heat flux equation can be written as

$$\dot{q}_w^* = -\frac{\gamma R^*}{(\gamma - 1) Pr} \mu_w^* \left(\frac{\partial T^*}{\partial z^*} \right)_w \tag{116}$$

If we apply the transformation formulas and note that at the wall $\theta_w' = E_4 I_1$ (from equation (89)), then we obtain

$$\dot{q}_w^* = -\frac{\gamma R^*}{(\gamma - 1).Pr} \left(\frac{T_\infty^* \mu_\infty^*}{L_\infty^*} \right) \sqrt{Re_\infty}\, \psi_q T_e \rho_e \mu_e E_4 l_1 I_1 \tag{117}$$

where ψ_q is defined for general three-dimensional flow or attachment-line flow as

$$\psi_q = \sqrt{\frac{u_e}{\rho_e \mu_e s_1}} \quad \text{or} \quad \psi_q = \sqrt{\frac{f_e}{\rho_e \mu_e h_1}} \tag{118}$$

Application of the heat flux boundary condition involves the specification of I_1 with equation (117). A negative value of $\dot{q}_w^*$ corresponds to a cold-wall situation (i.e., heat flow in the negative z direction). If the wall temperature T_w is the known quantity, then H_1 is specified (from equation (24)) as

$$H_1 = H_w = \frac{T_w}{\left(1 + \frac{\gamma - 1}{2} M_\infty^2\right)} \tag{119}$$

The incorporation of the boundary conditions into the linear discretized system results in a shift of the rows downward by four. This produces a system that is block tridiagonal. The block tridiagonal system is defined by

$$[\ldots \quad \alpha^k \quad \beta^k \quad \gamma^k \quad \ldots] \left[\delta S^k\right] = \left[\delta^k\right] \qquad (k = 1, 2, .., ke) \tag{120}$$

where

$$\left[\delta S^k\right] = \begin{bmatrix} \delta w_k \\ \delta F_k \\ \delta G_k \\ \delta H_k \\ \delta L_k \\ \delta M_k \\ \delta I_k \end{bmatrix}$$

$$\left[\delta^k\right] = \begin{bmatrix} r_1^k \\ r_2^k \\ r_3^k \\ r_4^k \\ r_5^{k+1} \\ r_6^{k+1} \\ r_7^{k+1} \end{bmatrix} \tag{121}$$

Note that the index k on α^k, β^k, and γ^k corresponds to the location of a particular block in the $(ke \times ke)$ system of (7×7) blocks. The index k of each of the elements in a block refers to the discretization location. The subdiagonal, diagonal, and superdiagonal blocks at row location k are obtained as

$$\left[\alpha^k\right] = \begin{bmatrix} a_{11}^k & a_{12}^k & a_{13}^k & a_{14}^k & a_{15}^k & a_{16}^k & a_{17}^k \\ a_{21}^k & a_{22}^k & a_{23}^k & a_{24}^k & a_{25}^k & a_{26}^k & a_{27}^k \\ a_{31}^k & a_{32}^k & a_{33}^k & a_{34}^k & a_{35}^k & a_{36}^k & a_{37}^k \\ a_{41}^k & a_{42}^k & a_{43}^k & a_{44}^k & a_{45}^k & a_{46}^k & a_{47}^k \\ 0 & 0 & 0 & 0 & 0 & 0 & 0 \\ 0 & 0 & 0 & 0 & 0 & 0 & 0 \\ 0 & 0 & 0 & 0 & 0 & 0 & 0 \end{bmatrix} \tag{122}$$

$$\left[\beta^k\right] = \begin{bmatrix} b_{11}^k & b_{12}^k & b_{13}^k & b_{14}^k & b_{15}^k & b_{16}^k & b_{17}^k \\ b_{21}^k & b_{22}^k & a_{23}^k b & b_{24}^k & b_{25}^k & b_{26}^k & b_{27}^k \\ b_{31}^k & b_{32}^k & b_{33}^k & b_{34}^k & b_{35}^k & b_{36}^k & b_{37}^k \\ b_{41}^k & b_{42}^k & b_{43}^k & b_{44}^k & b_{45}^k & b_{46}^k & b_{47}^k \\ a_{51}^{k+1} & a_{52}^{k+1} & a_{53}^{k+1} & a_{54}^{k+1} & a_{55}^{k+1} & a_{56}^{k+1} & a_{57}^{k+1} \\ a_{61}^{k+1} & a_{62}^{k+1} & a_{63}^{k+1} & a_{64}^{k+1} & a_{65}^{k+1} & a_{66}^{k+1} & a_{67}^{k+1} \\ a_{71}^{k+1} & a_{72}^{k+1} & a_{73}^{k+1} & a_{74}^{k+1} & a_{75}^{k+1} & a_{76}^{k+1} & a_{77}^{k+1} \end{bmatrix} \tag{123}$$

$$\left[\gamma^k\right] = \begin{bmatrix} 0 & 0 & 0 & 0 & 0 & 0 & 0 \\ 0 & 0 & 0 & 0 & 0 & 0 & 0 \\ 0 & 0 & 0 & 0 & 0 & 0 & 0 \\ 0 & 0 & 0 & 0 & 0 & 0 & 0 \\ b_{51}^{k+1} & b_{52}^{k+1} & b_{53}^{k+1} & b_{54}^{k+1} & b_{55}^{k+1} & b_{56}^{k+1} & b_{57}^{k+1} \\ b_{61}^{k+1} & b_{62}^{k+1} & b_{63}^{k+1} & b_{64}^{k+1} & b_{65}^{k+1} & b_{66}^{k+1} & b_{67}^{k+1} \\ b_{71}^{k+1} & b_{72}^{k+1} & b_{73}^{k+1} & b_{74}^{k+1} & b_{75}^{k+1} & b_{76}^{k+1} & b_{77}^{k+1} \end{bmatrix} \tag{124}$$

The boundary conditions at the boundary-layer edge result in a diagonal and RHS block as

$$\left[\beta^{ke}\right] = \begin{bmatrix} b_{11}^k & b_{12}^k & b_{13}^k & b_{14}^k & b_{15}^k & b_{16}^k & b_{17}^k \\ b_{21}^k & b_{22}^k & a_{23}^k b & b_{24}^k & b_{25}^k & b_{26}^k & b_{27}^k \\ b_{31}^k & b_{32}^k & b_{33}^k & b_{34}^k & b_{35}^k & b_{36}^k & b_{37}^k \\ b_{41}^k & b_{42}^k & b_{43}^k & b_{44}^k & b_{45}^k & b_{46}^k & b_{47}^k \\ 0 & 1 & 0 & 0 & 0 & 0 & 0 \\ 0 & 0 & 1 & 0 & 0 & 0 & 0 \\ 0 & 0 & 0 & 1 & 0 & 0 & 0 \end{bmatrix}; \quad \left[\delta^{ke}\right] = \begin{bmatrix} r_1^k \\ r_2^k \\ r_3^k \\ r_4^k \\ 0 \\ 0 \\ 0 \end{bmatrix}; \; k = ke \qquad (125)$$

The diagonal block β_1 and RHS block δ_1 that result from a specified wall heat flux condition (adiabatic or otherwise) are as given below (which corresponds to $\delta I_1 = 0$):

$$\left[\beta^1\right] = \begin{bmatrix} 1 & 0 & 0 & 0 & 0 & 0 & 0 \\ 0 & 1 & 0 & 0 & 0 & 0 & 0 \\ 0 & 0 & 1 & 0 & 0 & 0 & 0 \\ 0 & 0 & 0 & 0 & 0 & 0 & 1 \\ a_{51}^{k+1} & a_{52}^{k+1} & a_{53}^{k+1} & a_{54}^{k+1} & a_{55}^{k+1} & a_{56}^{k+1} & a_{57}^{k+1} \\ a_{61}^{k+1} & a_{62}^{k+1} & a_{63}^{k+1} & a_{64}^{k+1} & a_{65}^{k+1} & a_{66}^{k+1} & a_{67}^{k+1} \\ a_{71}^{k+1} & a_{72}^{k+1} & a_{73}^{k+1} & a_{74}^{k+1} & a_{75}^{k+1} & a_{76}^{k+1} & a_{77}^{k+1} \end{bmatrix}; \quad \left[\delta^1\right] = \begin{bmatrix} 0 \\ 0 \\ 0 \\ 0 \\ r_5^{k+1} \\ r_6^{k+1} \\ r_7^{k+1} \end{bmatrix}; \; k = 1 \qquad (126)$$

For a specified wall temperature condition, the system becomes

$$\left[\beta^1\right] = \begin{bmatrix} 1 & 0 & 0 & 0 & 0 & 0 & 0 \\ 0 & 1 & 0 & 0 & 0 & 0 & 0 \\ 0 & 0 & 1 & 0 & 0 & 0 & 0 \\ 0 & 0 & 0 & 1 & 0 & 0 & 0 \\ a_{51}^{k+1} & a_{52}^{k+1} & a_{53}^{k+1} & a_{54}^{k+1} & a_{55}^{k+1} & a_{56}^{k+1} & a_{57}^{k+1} \\ a_{61}^{k+1} & a_{62}^{k+1} & a_{63}^{k+1} & a_{64}^{k+1} & a_{65}^{k+1} & a_{66}^{k+1} & a_{67}^{k+1} \\ a_{71}^{k+1} & a_{72}^{k+1} & a_{73}^{k+1} & a_{74}^{k+1} & a_{75}^{k+1} & a_{76}^{k+1} & a_{77}^{k+1} \end{bmatrix}; \quad \left[\delta^1\right] = \begin{bmatrix} 0 \\ 0 \\ 0 \\ 0 \\ r_5^{k+1} \\ r_6^{k+1} \\ r_7^{k+1} \end{bmatrix}; \; k = 1 \qquad (127)$$

Appendix A summarizes the information required to construct the block tridiagonal system. Implementation of the boundary conditions also requires an update that is based on the current solution, which is done with the update of the nonlinear terms.

Because the Pade formula is a compact scheme based on the solution variables and their derivatives at two points that span the local cell center, a stretched grid can be employed without degradation of the fourth-order accuracy of the method. A stretching

constant k_s is defined to exponentially stretch the grid in the ζ direction as

$$\zeta_k = \zeta_{ke}\left(\frac{k_s^{k-1}-1}{k_s^{ke-1}-1}\right) \tag{128}$$

3.4 Discretization in the (*i,j*) Directions

In the fully three-dimensional region (away from the attachment line and side boundaries, $j = 1$ or $j = nylim$), the differencing in the surface directions ξ and η is done to second-order accuracy. In accordance with the parabolic nature of the equations, the ξ derivative is obtained by the three-point upwind-differenced formula

$$(f_\xi)_{i,j} = a_1 f_{i,j} + a_2 f_{i-1,j} + a_3 f_{i-2,j}$$

$$a_1 = (\Delta\xi_i^2 - \Delta\xi_{i-1}^2)/\Delta;\ a_2 = -\Delta\xi_i^2/\Delta;\ a_3 = \Delta\xi_{i-1}^2/\Delta \tag{129}$$

$$\Delta = \Delta\xi_i\Delta\xi_{i-1}(\Delta\xi_i + \Delta\xi_{i-1});\ \Delta\xi_i = \xi_{i,j} - \xi_{i-1,j};\ \Delta\xi_{i-1} = \xi_{i-1,j} - \xi_{i-2,j}$$

When $i = 2$, the first-order formula with just two points is used, which results in the coefficients

$$a_1 = 1/\Delta\xi_2 = 1/(\xi_2 - \xi_1);\ a_2 = -a_1;\ a_3 = 0 \tag{130}$$

A function ω_i is used to blend the first-order and second-order formulas in a small number of marching steps. The short notation $\{aF\}$ used in equation (103) can thus be expanded in terms of the coefficients given above. At $\xi = 0$, the attachment-line equations do not contain any $\partial/\partial\xi$ terms; this condition is incorporated into the solution scheme by setting up a flag set to zero for the attachment-line solution and to unity for $i > 1$.

The η differencing is accomplished with a combination of two schemes. For situations where the profile G is positive at all normal grid-point locations, the standard left-pointing three-point second-order scheme (which we refer to as the L scheme) is used. When

the profile has negative values, the "zig zag" scheme (also called the Z scheme), first proposed by Krause (ref. 4), is employed. For moderate crossflow situations, this scheme automatically satisfies the zone-of-dependence principle that is outlined by Wang (ref. 5). The finite-differencing formula that combines the above two schemes can be written as

$$(f_\eta)_{i,j} = b_1 f_{i,j} + b_2 f_{i,j-1} + b_3 f_{i,j-2} + b_4 f_{i-1,j} + b_5 f_{i-1,j+1} \tag{131}$$

The coefficients take these values for the L scheme:

$$b_1 = (\Delta\eta_j^2 - \Delta\eta_{j-1}^2)/\Delta; \quad b_2 = -\Delta\eta_j^2/\Delta; \quad b_3 = \Delta\eta_{j-1}^2/\Delta; \quad b_4 = b_5 = 0$$

$$\Delta = \Delta\eta_j \Delta\eta_{j-1}(\Delta\eta_j + \Delta\eta_{j-1}); \quad \Delta\eta_j = \eta_{i,j} - \eta_{i,j-1}; \quad \Delta\eta_{j-1} = \eta_{i,j-1} - \eta_{i,j-2} \tag{132}$$

The coefficients take these values for the Z scheme:

$$b_1 = \frac{1}{2}(\eta_{i,j} - \eta_{i,j-1} + \eta_{i-1,j+1} - \eta_{i-1,j})$$

$$b_2 = -\frac{1}{2}(\eta_{i,j} - \eta_{i,j-1}); \quad b_3 = 0; \quad b_4 = -\frac{1}{2}(\eta_{i-1,j+1} - \eta_{i-1,j}); \quad b_5 = -b_4 \tag{133}$$

At $\eta = 0$ (left boundary) or at $\eta = \eta_{\max}$ (right boundary), no $\partial/\partial\eta$ terms are present in the LISW equations; this condition is incorporated into the solution scheme by setting up a flag set to zero for the boundaries $j = 1$ and $j = nylim$. The flag is set to unity in the fully three-dimensional region. As stated earlier in section "Quasi-Two-Dimensional Equations for Initial Conditions," a factor $\omega = \omega(\eta)$ is used to blend the LISW solution to the fully three-dimensional solution at the boundary-adjacent points. The short notation $\{bF\}$ that is used in equation (104) is thus obtained directly from equations (131)–(133).

4. INVISCID INTERFACE

The three-dimensional boundary-layer solution procedure is based on the specification of the edge quantities u_e, v_e, and T_e on a surface grid defined in the coordinate directions ξ and η. In addition, the computation of the edge density ρ_e requires the specification of the inviscid pressure P or the pressure coefficient C_p (for flows that involve a shock between the free stream and the attachment line). In the general case, for a nonorthogonal boundary-layer grid, the metric quantities h_1, h_2, and g_{12} are also assumed to be given. Further, the edge value of viscosity μ_e is computed from T_e with the Sutherland formula (equation (33)). The above quantities are referenced to the free-stream quantities (U^*_∞, P^*_∞, and T^*_∞) and the reference length L^*_∞.

If we assume that a negligible interaction occurs between the viscous and inviscid regions, the edge conditions can be obtained by solving the three-dimensional Euler equations on a sufficiently fine mesh. In some cases such as low-speed flow, a potential panel code may be substituted in place of the Euler solver, after which an interface procedure is necessary to process the inviscid results to express them in the form required by the boundary-layer code. Specifically, this procedure involves (a) the accurate location of the inviscid attachment line, (b) the generation of the boundary-layer grid which originates from the attachment line on the upper or lower surface, (c) the calculation of the edge velocities in surface grid-oriented directions, and (d) the output of quantities in the required form for the boundary-layer code.

Two approaches are used to calculate the edge velocities (u_e, v_e) and edge temperature T_e. The first approach is to interpolate the inviscid pressure distribution onto the boundary-layer grid and then calculate the edge velocities and temperature by solving the limiting equations of the boundary-layer equations at the boundary-layer edge.

These limiting equations (henceforth called the BL–EDGE equations) are hyperbolic and can be solved with a marching method that is analogous to the boundary-layer solution procedure. The source term in these equations is the pressure gradient in the two directions ξ and η. The second method involves the interpolation of all the required edge quantities from the inviscid grid to the boundary-layer grid.

The first procedure is, in principle, more consistent with the boundary-layer solution method; however, the solution of the BL–EDGE equations may be slightly different from the solution of the Euler equations. This mismatch in the edge quantities from the two solutions is attributed to (a) the terms dropped in the BL–EDGE equations, based on the boundary-layer assumption, and (b) variations in the finite-differencing schemes. In one case, we have the edge velocities computed from the Euler equations, whereas, in the other case, the edge velocities are computed from the limiting boundary-layer equations, based on the Euler pressure gradient. The BL–EDGE equations also assume that the edge total enthalpy is a constant, which is not necessarily true for the Euler solution. Note also that accurate enforcement of the condition $\partial P/\partial x = 0$ at the attachment line is difficult from a coarse inviscid grid, which may necessitate that the interpolation near the attachment line be linear rather than spline to ensure a negative pressure gradient at the attachment line. The interface program includes an option to calculate the edge conditions by either method.

4.1 Attachment-Line Relocation

After the surface pressure distribution is obtained from the inviscid calculation, the initial location of the attachment line is obtained by scanning for a maximum pressure in the vicinity of the leading edge of the wing. However, note that the true attachment-point location may be located within a bandwidth of one grid point on either side. The true

location of the attachment point is where the surface velocity in the direction normal to the attachment line is equal to zero.

In this procedure, the Cartesian velocity components of the Euler solution are converted to surface-oriented velocities that correspond to a boundary-layer surface grid generated from the initial attachment-line location. This velocity conversion is based on equations (13)–(17). In general, the component u_e at the initial attachment point will be nonzero. This point is then relocated in the positive or negative direction, depending on the value and sign of u_e and the local estimated value of $\partial u_e/\partial s_1$. For example, for the upper surface at an angle of attack, a relocation in the positive direction means that the point is moved to include more of the lower surface; this is done when u_e has a positive value. After the points are relocated with this logic, a new boundary-layer surface grid is generated from these attachment-line locations. New values of velocity components are obtained by interpolation. This procedure is repeated until the value of u_e at each attachment point is less than a specified tolerance value. A parameter ω_{at} is used to relax the relocation displacement and to ensure that the iterated locations remain within the grid-point bandwidth mentioned above. Upon convergence, the pressure is interpolated with a spline routine from the inviscid grid to the final boundary-layer grid.

4.2 Edge Values by Interpolation

Edge velocities and temperature are obtained by spline interpolation. For a fine inviscid grid, this method usually produces smooth edge conditions comparable to the solution from the BL–EDGE equations.

4.3 Edge Values from BL–EDGE Equations

The three-dimensional boundary-layer equations (eqs. (19) and (20)), when applied

at the edge of the boundary layer, result in the BL–EDGE equations and are given as

$$\frac{u_e}{h_1}u_{e,x} + \frac{v_e}{h_2}u_{e,y} + C_{24}\,u_e^2 + C_{25}\,u_e v_e + C_{26}v_e^2 = \left(-\frac{h_1 h_2^2}{C_{13}^2}P_x + \frac{h_1 g_{12}}{C_{13}^2}P_y\right)\frac{1}{\gamma\rho_e M_\infty^2} \quad (134)$$

$$\frac{u_e}{h_1}v_{e,x} + \frac{v_e}{h_2}v_{e,y} + C_{34}\,u_e^2 + C_{35}\,u_e v_e + C_{36}v_e^2 = \left(\frac{h_2 g_{12}}{C_{13}^2}P_x - \frac{h_1^2 h_2}{C_{13}^2}P_y\right)\frac{1}{\gamma\rho_e M_\infty^2} \quad (135)$$

Further, H_e is assumed to be constant. With P specified from the inviscid solution, the following equation provides closure for this hyperbolic set of equations:

$$T_e = H_e\left(1 + \frac{\gamma-1}{2}M_\infty^2\right) - \frac{\gamma-1}{2}M_\infty^2 q_e^2$$
$$\rho_e = P/T_e \quad (136)$$

The solution to the above system is obtained with a discretization that is identical to the full three-dimensional boundary-layer equations in the two surface directions. With the abbreviated notations for the ξ and η directions, a discretization with Newton linearization yields the system

$$\begin{bmatrix} \frac{1}{h_1}\left(2a_1u_e + \{au_e\} + \underline{b_1 v_e \frac{h_1}{h_2}}\right) & \underline{\frac{1}{h_2}(b_1u_e + \{bu_e\})} \\ \frac{1}{h_1}(a_1v_e + \{av_e\}) & \frac{1}{h_2}\left(a_1u_e\frac{h_2}{h_1} + \underline{2b_1v_e + \{bv_e\}}\right) \end{bmatrix} \begin{Bmatrix} \partial u_e \\ \partial v_e \end{Bmatrix} = \begin{Bmatrix} r_1 - \frac{u_e}{h_1}\frac{\partial u_e}{\partial x} - \frac{v_e}{h_2}\frac{\partial u_e}{\partial y} \\ r_2 - \frac{u_e}{h_1}\frac{\partial v_e}{\partial x} - \frac{v_e}{h_2}\frac{\partial v_e}{\partial y} \end{Bmatrix} \quad (137)$$

where

$$r_1 = \frac{1}{\gamma M_\infty^2\rho_e}\left\{-\frac{h_1h_2^2}{C_{13}^2}P_x + \frac{h_1g_{12}}{C_{13}^2}P_y\right\} - \left(C_{24}u_e^2 + C_{25}u_ev_e + C_{26}v_e^2\right)$$
$$r_2 = \frac{1}{\gamma M_\infty^2\rho_e}\left\{\frac{h_2g_{12}}{C_{13}^2}P_x - \frac{h_1^2h_2}{C_{13}^2}P_y\right\} - \left(C_{34}u_e^2 + C_{35}u_ev_e + C_{36}v_e^2\right)$$

The terms marked by an underline apply to the three-dimensional region only. These terms are set to zero per the LISW condition at $j = 1$ and $j = ny$. Note that the P_y terms are retained for LISW, however.

The solution is obtained by inversion of the system, which is followed by an iterative update for nonlinear terms.

5. BL3D EXAMPLE CASES

Two test cases are presented here. The first test case is that of a moderately swept ($\Lambda = 33°$) tapered wing in subsonic flow. The streamwise cross sections of this wing correspond to NACA 0012; however, for generality, calculations of metrics and other parameters are done with the assumption that the wing is defined in terms of discrete coordinates. The second test case is a highly swept ($\Lambda = 70°$) wing in supersonic flow, similar in planform to that of the F16XL aircraft, with cross sections defined in discrete coordinates. For both cases, the inviscid results are obtained by solving the Euler equations. The computer code CFL3D (ref. 6) is used for this purpose, with the viscous terms set to zero for the Euler calculation. An interface routine processes the results and feeds the resulting edge conditions to BL3D. For validation (case 1 only), the results obtained from BL3D are compared with the results from the thin-layer Navier-Stokes code, which is also obtained with CFL3D. For the supersonic wing case, we present comparisons of the BL3D results with the solution from a conical swept wing boundary-layer code developed by Kaups and Cebeci (ref. 3). In addition, runs are made with a uniform suction distribution (case 1 only). These results are also compared with the corresponding Navier-Stokes solution.

5.1 Geometry and Conditions for Case 1

The planform of this wing is a trapezoid for which the root chord is 1 ft and the leading-edge sweep is constant at 32.73°. The wing has a span of 2 ft and the trailing-edge sweep is constant at 18.88°, which results in a tip chord of 0.398 ft. The tip-section leading edge is at $x'^* = 1.286$ ft and the tip-section trailing edge is at $x'^* = 1.684$ ft. The streamwise cross section of the wing corresponds to the NACA 0012 section. The free-stream conditions are $M_\infty = 0.5$, $\alpha = 2°$, $P^*_\infty = 2116$ psf, and T^*_∞ = 520°R. The wing

is assumed to be symmetrical about the root chord plane.

5.2 Euler Solution for Case 1

The surface distribution used in the Euler grid consists of constant percent chord lines and constant percent span lines. In the spanwise direction, the grid has 41 points on the wing surface, which corresponds to a span distance of 0.05 ft between grid lines. In the chordwise wraparound direction, the grid has 257 points, and in the wall-normal direction the grid has 49 points that are stretched exponentially. The grid is further extended into the wake region and off the tip of the wing. The Euler computation is done with the code CFL3D. The results from the calculation are obtained at the centers of the grid cells; thus, 40 cell centers exist in the spanwise direction. Let us denote these locations by the symbol j(INV). To avoid the region very close to the symmetry plane and the wingtip, we restrict our analysis to the region $7 \leq j(\text{INV}) \leq 35$, which corresponds to $0.325 \leq y'^{*} \leq 1.725$. The middle location of this region is at $j(\text{INV}) = 21$, which corresponds to $y'^{*} = 1.025$.

Figure 2(a) shows the surface distribution of the Euler grid-cell center points (note that only every fourth point is plotted in the chordwise direction for clarity). Figure 2(b) shows the corresponding boundary-layer grid on the upper surface. The boundary-layer grid originates from the attachment line, and the x-coordinate is measured in terms of the surface arc length, which is normalized by a length such as the local chord length or, in the present case, by the maximum arc length. The spanwise coordinate y is defined as the local span distance from the symmetry plane.

The inviscid results used in the interface routine are the three Cartesian components of the velocity on the wing surface, the inviscid wall density, and the temperature. The pressure coefficient on the surface can be calculated from the above. Alternately, the pressure coefficient can be specified, and the edge temperature can be calculated

(assuming that the edge density is given). Figure 3 shows the variation of the pressure coefficient obtained from the Euler solution at three span locations where j(INV) = 7, 21, and 35. Note that the effect of the taper is to create a favorable pressure gradient in the spanwise direction.

5.3 Euler-BL3D Interface for Case 1

The details of the procedure for relocating the inviscid attachment line are presented in Figures 4–7. Figure 4 shows a plot of the iterated attachment-line locations. This plot is in terms of (y', z') of these surface points and corresponds to a view from upstream of the wing leading edge (not to scale). The initial attachment-line location that corresponds to the peak in the pressure coefficient near the leading edge is shown in solid symbols. The inviscid grid points on the upper and lower sides of this line are shown as dashed lines. These lines bound the uncertainty on the true attachment-line location because of the coarseness of the inviscid grid. Also shown in Figure 4 are the iterated locations of the attachment line. As explained in "Attachment-Line Relocation," the iteration is based on a relocation strategy such that the local inviscid velocity vector is exactly tangential to the attachment line. Note that the line that joins the final attachment-line locations is much smoother than the original line.

Figure 5 shows the velocity u_e interpolated at the attachment-line location that corresponds to successive iterations. Note that the initial values of u_e are relatively high (±0.04) and that the objective of driving u_e to near zero (< 0.0001) is achieved in seven iterations. Figure 6 shows the corresponding variations of the velocity v_e on the attachment line. Here again, the final v_e variation is smooth. Figure 7 shows the resulting variation of C_p on the attachment line.

The boundary-layer surface grid is generated from the attachment line on the upper

or lower side. In the present case, 40 points are generated in the chordwise direction between the attachment line and the local 5 percent chord location. Beyond this point, the boundary-layer grid coincides with the inviscid grid, and no interpolation is required. The stretching of the surface distribution near the attachment line is done so that the grid blends smoothly with the inviscid grid (at the 5 percent chord location in the present case).

After the generation of the surface grid, the inviscid pressure is interpolated to the boundary-layer grid. The boundary-layer calculation is restricted to the region that is bounded by the j(INV) = 7 and j(INV) = 35 spanwise locations. The regions outside these limits are unsuitable; the locally infinite-swept wing assumption does not apply in these regions because of the proximity of the flow to the symmetry plane or the wingtip. The boundary-layer grid notation denoted by j(BL3D) is thus based on the left boundary of j(INV) = 7. In other words, the j(BL3D) = 1 location is identical to the j(INV) = 7 location.

Figure 8 shows the chordwise variation of the interpolated C_p values on the boundary-layer grid at three spanwise locations. The interpolation is accomplished with a spline routine. In the present case, because the inviscid grid has good resolution near the leading edge and the inviscid results are smooth in this region, no smoothing is required. However, in the absence of the above, a smooth spline interpolation may be required. In this event, the amount of smoothing and the resulting interpolated pressures must be carefully monitored. If the streamwise pressure gradient at the attachment line is not negative, a marching of the boundary-layer solution away from the attachment line may not be possible. Spline and other higher order interpolation methods are likely to introduce nonnegative pressure gradients at the attachment line. Hence, in some cases, a locally linear interpolation may be required near the attachment line to ensure negative pressure gradients.

All physical distances, such as the root chord length, are normalized by a reference

length L_∞^*. Further, the boundary-layer grid x- (and ξ-) coordinate is defined as the local chordwise arc length divided by the local maximum arc length up to the trailing edge. The boundary-layer grid y- (and also η-) coordinate is defined as the local spanwise distance. With this definition, the metric quantities can be computed with equations (1)–(3). For the present case, the variation of h_1, h_2, and g_{12} in the chordwise direction at the j(BL3D) = 1 location is shown in Figure 9.

As explained in "Edge Values by Interpolation," the edge velocities can be obtained by direct interpolation. In this method, the three Cartesian velocity components from the inviscid solution are interpolated. Subsequently, the edge velocities in the x and y directions are obtained by an inversion of the system given by equations (13)–(17). The edge temperature is also interpolated to complete the interface to the BL3D program.

In the second method, the BL–EDGE equations are solved with the input pressure distribution as outlined in "Edge Values from BL–EDGE Equations." Figure 10 shows a comparison of the edge velocities obtained by either method at the j(BL3D) = 1 location. Note that the two results agree well. Figure 11 shows contour plots of the edge velocity u_e on the upper surface of the wing that are obtained from the two methods. A slight difference in the variation is caused by the fact that the BL–EDGE solution assumes a locally swept-wing condition at j(BL3D) = 1 and j(BL3D) = 29. Another cause for this difference is that the finite differencing used in the Euler solution is different from that used in the BL–EDGE solution. However, for the present case, both results are acceptable. Figure 12 shows the corresponding comparison of the edge velocity v_e. The edge temperature variations also compare well.

5.4 BL3D Solution for Case 1

The three-dimensional boundary-layer solution follows the sequence below:

(a) Input boundary-layer edge data. The input consists of the boundary-layer grid dimensions (nx, ny); the coordinates (x, y); the metric quantities h_1, h_2 and g_{12}; and edge values u_e, v_e, and T_e. Further, if the streamline between the free stream and the boundary-layer attachment line contains a shock (nonisentropic region), then the input of C_p or P is required to calculate the edge density ρ_e. Other inputs are the free-stream conditions, the reference length, and other parameters that pertain to the solution procedure.

(b) Setup of initial profiles. Solution profiles that correspond to the similarity solution for a flat plate or wedge are used as initial profiles to start the locally infinite, swept attachment-line solution at $i = 1$, $j = 1$ of the boundary-layer grid.

(c) Setup of edge coefficients. This setup is based on the edge conditions and gradients. The coefficients A_i, B_i, C_i, and D_i are calculated.

(d) LISW solution. This solution is obtained at the two boundaries $j = 1$ and $j = ny\mathrm{lim}$ by marching in the x direction. The terms that involve derivatives in the y direction are set to zero for this case. Further, at $i = 1$, the attachment-line equations are solved.

(e) Solution of the three-dimensional region. Given the initial plane solution and the side boundary solution, the three-dimensional region can now be solved with the L scheme or the Z scheme for the span derivatives. A switching from the L scheme to the Z scheme occurs when the profile of G has a negative element.

Depending on the pressure distribution, the solution region can be restricted to (1, $nx\mathrm{lim}$), (1, $ny\mathrm{lim}$). After the convergence of the solution at each (i, j) point, quantities such as the boundary-layer thickness, the skin-friction coefficient, and the crossflow Reynolds number are calculated.

5.5 BL3D Results for Case 1

Comparison of the BL3D solution is made with profiles that are obtained from the solution of the NS equations with the code CFL3D. This code was run on a grid with the same surface distribution as the Euler grid, but with 81 points in the wall-normal direction. The grid stretching was designed to include about 30 to 40 points in the boundary layer of the flow. The flow was assumed to have an abrupt transition to turbulence at the 25 percent location on the wing. This assumption ensures that the flow remains attached and thereby avoids the numerical problems caused by the laminar separated regions. The profile comparisons are restricted to locations upstream of the 25 percent chord station. Because of the large amount of data, the comparison plots are presented for a few locations in the flow that are representative of the entire flow solution.

Figures 13–18 compare of the BL3D and NS profiles at the j(BL3D) = 1 plane. We present comparisons at six locations in the chordwise direction. These locations approximately correspond to chord locations of 1, 2, 3, 6, 12, and 23 percent. Shown are the profiles of spanwise velocity v, chordwise velocity u, and temperature T. At these locations, the spanwise velocity profile assumes different shapes with inflection and reversal regions. The NS profiles are shown in open square symbols. The BL3D profiles at this j location are the solution of the LISW equations. In spite of this assumption, very good agreement is obtained until the 23 percent chord location. Note that the edge velocities used as input for the BL3D computation are the interpolated values from the inviscid code. The edge velocities that are computed from the NS solution are slightly different than those from the Euler solution. This difference is the main contributor to the lack of better agreement between the two solutions. Also, some differences are attributable to the fact that the profiles are not compared at exactly the same location. The temperature profiles at the 12 percent chord location and beyond are different

presumably because the boundary-layer interaction becomes more significant in this region. Furthermore, some differences near the attachment point are caused by the fact that the attachment point from the NS solution is shifted slightly compared with the Euler location. Overall, the agreement is satisfactory and validates the BL3D results.

The program also calculates the crossflow within the boundary layer relative to the local edge streamline direction. In the present report, crossflow is defined as negative when pointed toward the wing root. In Figure 19, we compare the streamwise velocity profiles u_s at six representative locations with the corresponding NS profiles. Figure 20 shows the corresponding crossflow velocity profiles of v_s. The crossflow that is predicted by the BL3D code is slightly larger than the NS solution in the negative crossflow region. The crossflow Reynolds number Re_{CF} is defined as

$$Re_{CF} = \frac{v^*_{s,\max}\delta^*_{0.1}\rho^*_e}{\mu^*_e} \tag{138}$$

where $v^*_{s,\max}$ is the maximum absolute value of the crossflow velocity v^*_s and $\delta^*_{0.1}$ is the normal distance at which the v^*_s profile decays to less than 10 percent of $v^*_{s,\max}$ (when scanned from the edge down to the wall). This parameter has a strong correlation to the growth of crossflow instabilities in a three-dimensional boundary layer. Figure 21 shows the variation of this parameter in the chord direction at the j(BL3D) = 1 location compared with the NS solution.

Figures 22–30 present the profiles at the j(BL3D) = 15 location at the $y' = 1.025$ spanwise station. The overall comparison is good, although in some locations differences in profiles exist mainly because of the fact that the edge conditions from the NS and Euler results are different.

Figure 31 shows the contours of the boundary-layer thickness and the skin-friction coefficient in the x direction obtained from the BL3D calculation. The contours are smooth

and blend smoothly with the infinite swept-wing solutions at the j boundary locations. Note that the flow is close to laminar separation as indicated by the near-zero values of $C_{f,x}$ at ξ = 0.25.

Figure 32 shows the contours of the crossflow Reynolds number and the maximum absolute percent crossflow on the upper surface. The values of Re_{CF} for this case are under 100, and the maximum crossflow reaches a maximum of about 12 percent.

5.6 Results With Suction for Case 1

Solutions were obtained from the NS and BL3D solvers with boundary-layer suction. A constant amount of suction q_s (equal to 0.0005) was assumed. Figure 33 shows a comparison of the resulting solution profiles at the j(BL3D) = 15 plane. The profiles with no suction are also shown for comparison. Figure 34 shows the resulting Re_{CF} values; a substantial reduction is produced in the crossflow with suction.

The attachment-line Reynolds number Re_θ is defined as

$$Re_\theta = \frac{v^*_{e,i=1}\theta^*_{m,i=1}\rho^*_{e,i=1}}{\mu^*_{e,i=1}} \tag{139}$$

where θ^*_m is the momentum thickness. This parameter is important because of attachment-line stability considerations. Figure 35 shows a comparison of the Re_θ values at the attachment line both with and without suction. The comparison with the values obtained from the NS solution is satisfactory.

5.7 Geometry and Conditions for Case 2

Case 2 is the boundary-layer flow on a supersonic wing of 70° sweep at a free-stream Mach number M_∞ of 1.6 and at an angle of attack of 0°. The planform is similar to the wing of the F16XL aircraft. The other input free-stream conditions correspond

to an altitude of 40,000 ft ($P^*_\infty = 393.13$ psf, $T^*_\infty = 390°\mathrm{R}$). The free-stream Reynolds number is 3.06×10^6 per ft.

Figure 36 shows a top view of the Euler grid used in this case, with an inset showing a chordwise section. The wing is assumed to be symmetric about the (x'^*, z'^*) plane at the span station j(INV) = 1, which is at a distance of 27 in. from the fuselage axis. The flow region of interest corresponds to the y'^* range of 72.8 to 132.2 in.

5.8 Euler Solution and BL3D Interface for Case 2

The inviscid pressure distribution on the wing upper surface, obtained from the Euler solution, is shown in Figure 37. Here, the streamwise distances are shown in terms of $x'^* - x'^*_{LE}$, which corresponds to the chordwise distance from the local leading-edge location. The variation of pressure coefficient and the wing cross section at the span location j(INV) = 16 (90.2 in. from fuselage axis) is shown in Figure 38. Attached laminar flow does not exist beyond a $x'^* - x'^*_{LE}$ distance of 3 ft; hence, the calculations reported here are for an $x'^* - x'^*_{LE}$ of less than 3 ft.

The interface program is essentially in the same form as case 1, except for minor changes in reading in and manipulation of the Euler solution input. The boundary-layer grid is specified as containing 40 points clustered within the 2 percent chordwise location. The edge velocities and temperature are calculated either by direct interpolation or by solution of the BL−EDGE equations. Good comparisons of the edge values u_e, v_e, and T_e from the two methods were obtained, as shown in Figures 39−41. Figure 42 shows a comparison at the span station j(BL3D) = 5. In the following section, the boundary-layer solution at this span station will be presented in detail.

5.9 BL3D Solution for Case 2

Following the interface run, the present code BL3D was run in a region bounded by

$1 \leq j(\text{BL3D}) \leq 9$. The results reported here correspond to the solution at $j(\text{BL3D}) = 5$. For comparison, the Kaups-Cebeci code was also run at this section.

Figure 43 shows the comparison of the u_s, v_s, T profiles at two chordwise locations close to the attachment line at the span station $j(\text{BL3D}) = 5$. The agreement is good, except for a very small reduction in the magnitude of the crossflow profile obtained from BL3D. Figure 44 shows the comparison of the profiles at two locations (1 ft and 2.26 ft in surface arc length away from the attachment line). Here, the streamwise and temperature profiles agree well. The crossflow profile from BL3D shows slightly reduced crossflow. Note that because the flow becomes increasingly three dimensional away from the attachment line the two codes are expected to differ in solutions.

Figure 45 shows a comparison of the resulting crossflow Reynolds number values from the two computations. Again, the reduced crossflow predicted by BL3D can be noted.

References

1. Iyer, V. , "Computation of three-dimensional compressible boundary layers to fourth-order accuracy on wings and fuselages," NASA CR 4269, Jan. 1990.

2. Iyer, V. and Harris, J. E. , "Fourth-order accurate three-dimensional compressible boundary-layer calculations," *Journal of Aircraft*, Vol. 27, No. 3, Mar. 1990, pp. 253–261.

3. Kaups, K. and Cebeci, T. , "Compressible laminar boundary layers with suction on swept and tapered wings," *Journal of Aircraft*, Vol. 24, No. 7, July 1977, pp. 661–667.

4. Krause, E. , Hirschel, E. and Bothmann, T. , "Die numerische integration der bewegungsgleichungen dreidimensionaler, laminarer, kompressibler grenzschichten," DGLR-Fachbuch-reihe, Band 3, Braunschweig 1969, pp. 03–1 to 03–49.

5. Wang, K. , "On the determination of the zones of influence and dependence for three-dimensional boundary-layer equations," *Fluid Mechanics*, Vol. 48, Part 2, 1971, pp. 397–404.

6. Thomas, J. L. , Taylor, S. L. and Anderson, W. K. , "Navier-Stokes computation of vortical flows over low aspect ratio wings," AIAA-87–0207, Jan. 1987.

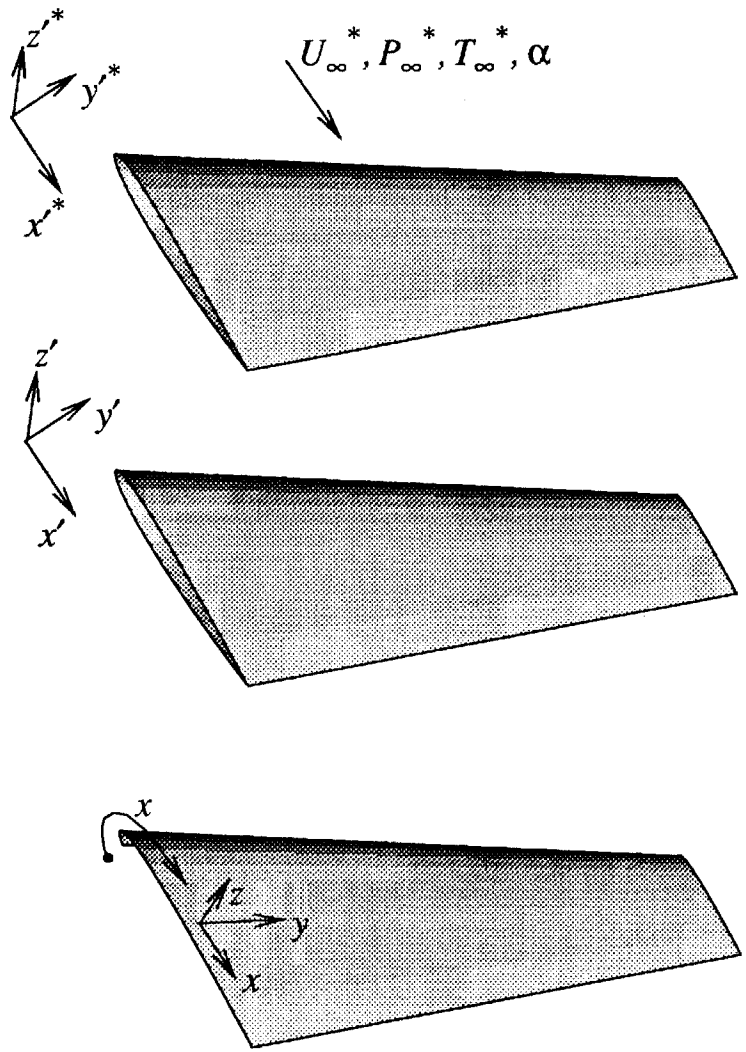

(a) Cartesian system, dimensional
Velocities: u'^*, v'^*, w'^*

(b) System normalized with L_∞^*, U_∞^*
Velocities: u', v', w'

(c) Boundary-layer coordinate system
$x = 0$ at attachment line
u, v : surface-oriented velocities

Figure 1. Three-dimensional boundary-layer coordinates for a swept wing.

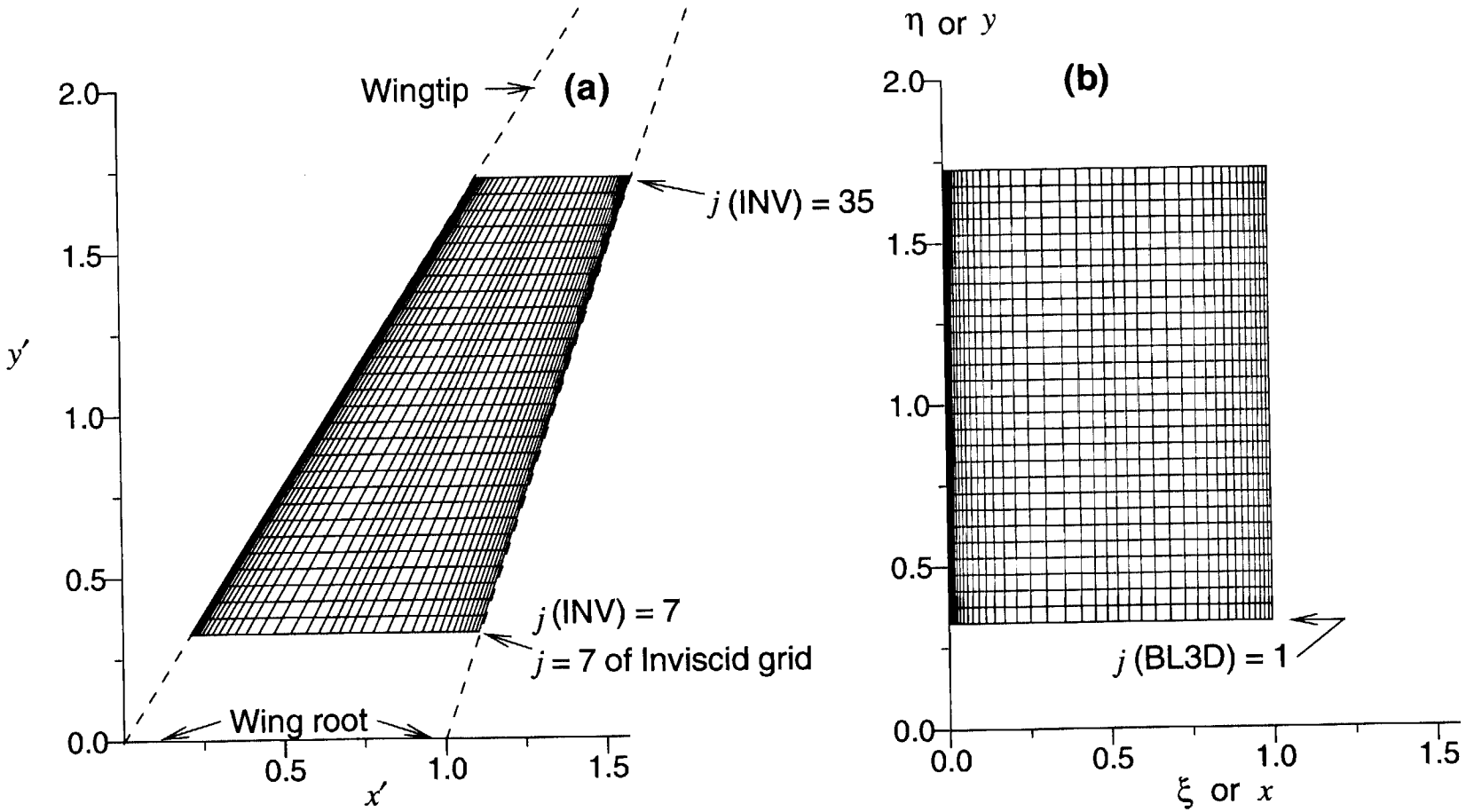

Figure 2. Cartesian grid (a) and boundary-layer grid (b) for case 1
(In the x direction, only every fourth grid line is plotted for clarity).

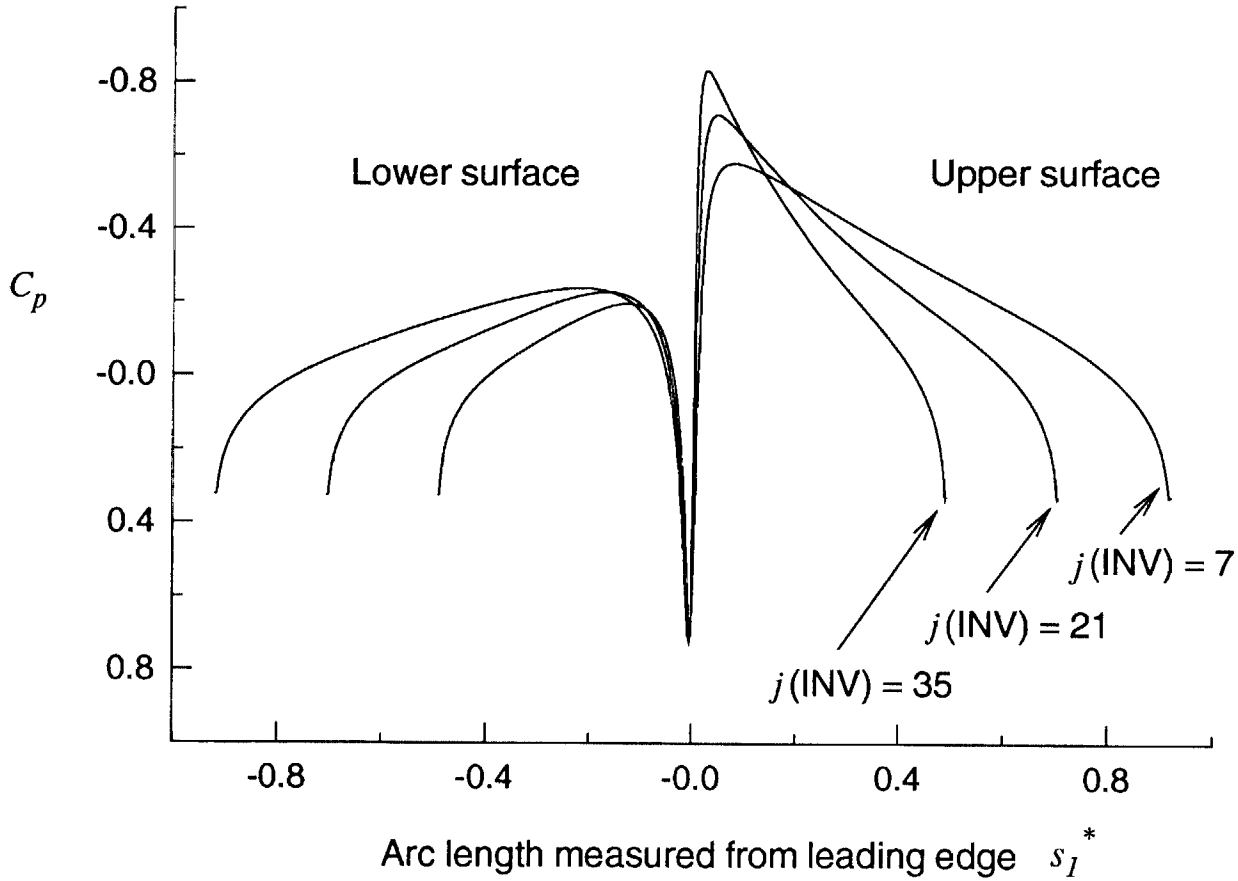

Figure 3. Pressure coefficient variation from Euler solution for case 1.

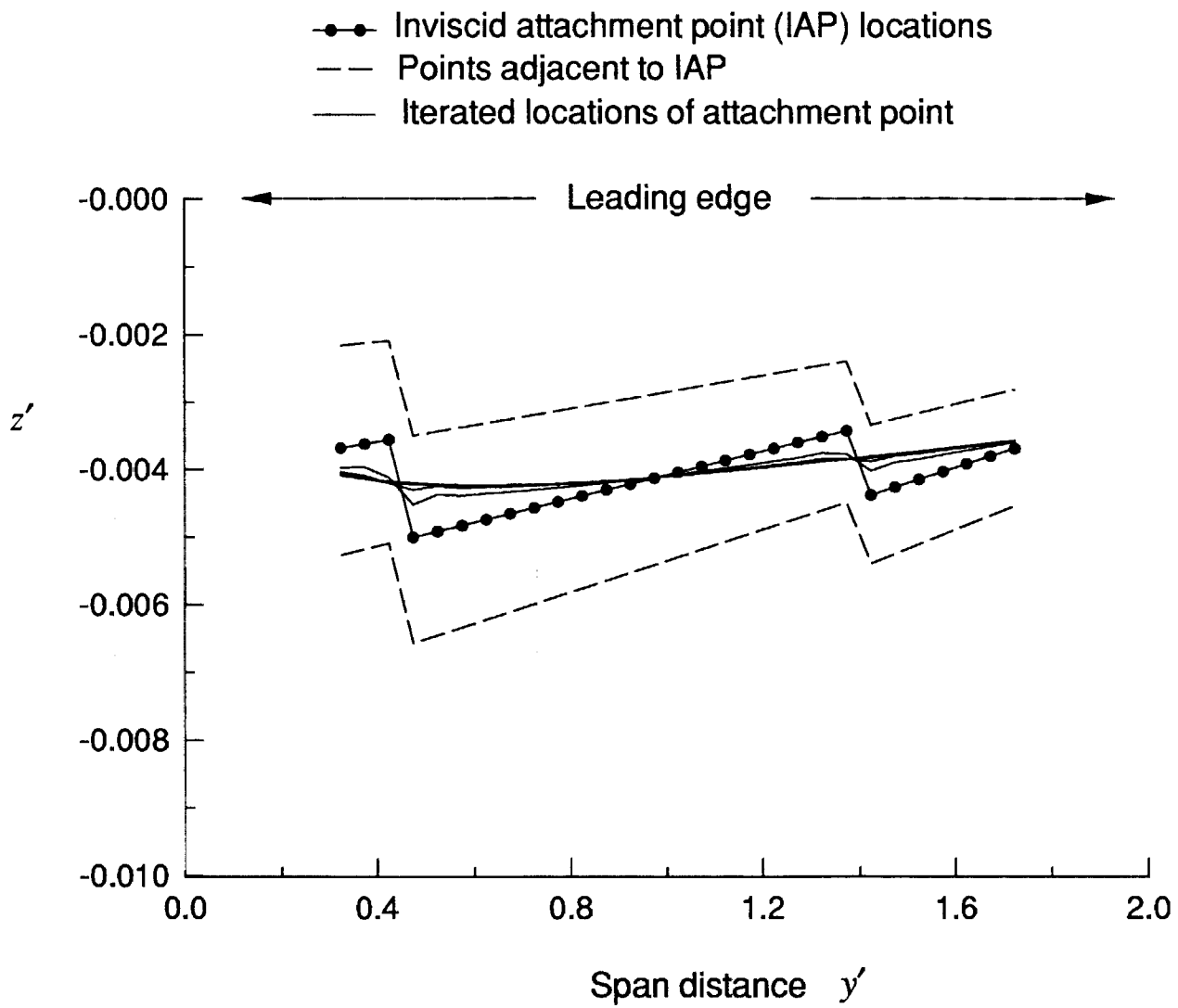

Figure 4. Iterative attachment-line relocation for case 1.

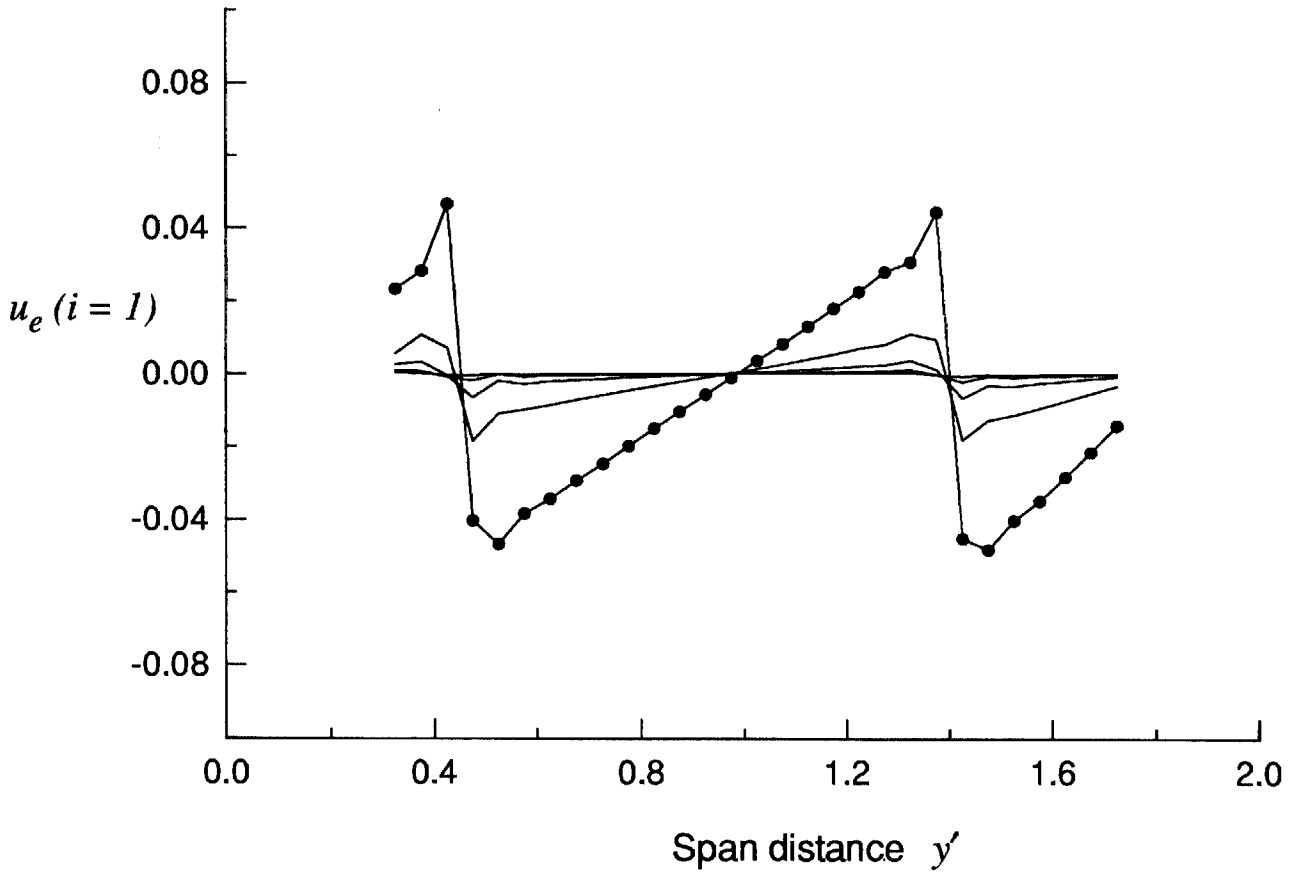

Figure 5. Convergence of velocity u_e on attachment line for case 1.

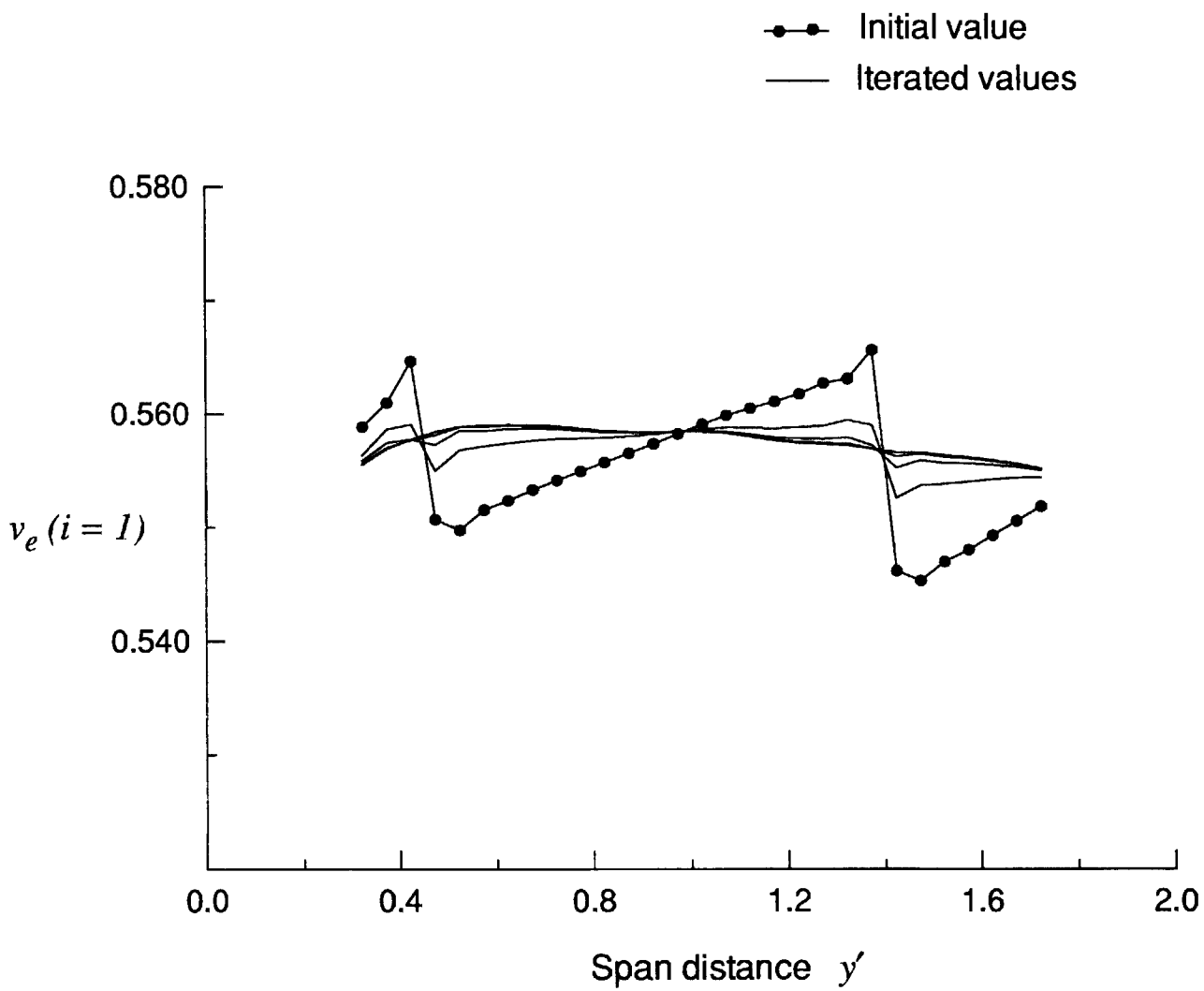

Figure 6. Convergence of velocity v_e at attachment line for case 1.

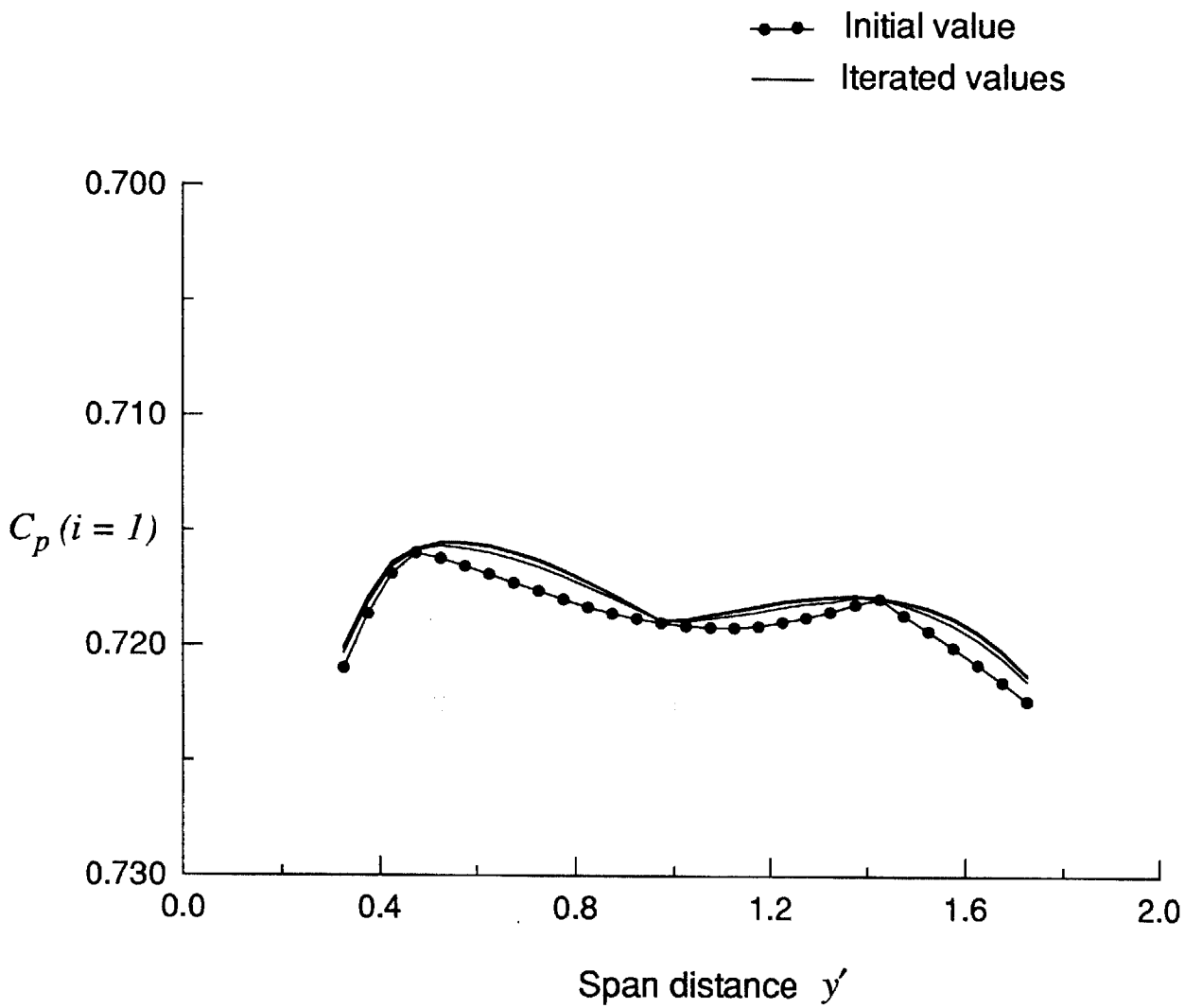

Figure 7. Convergence of pressure coefficient at attachment line for case 1.

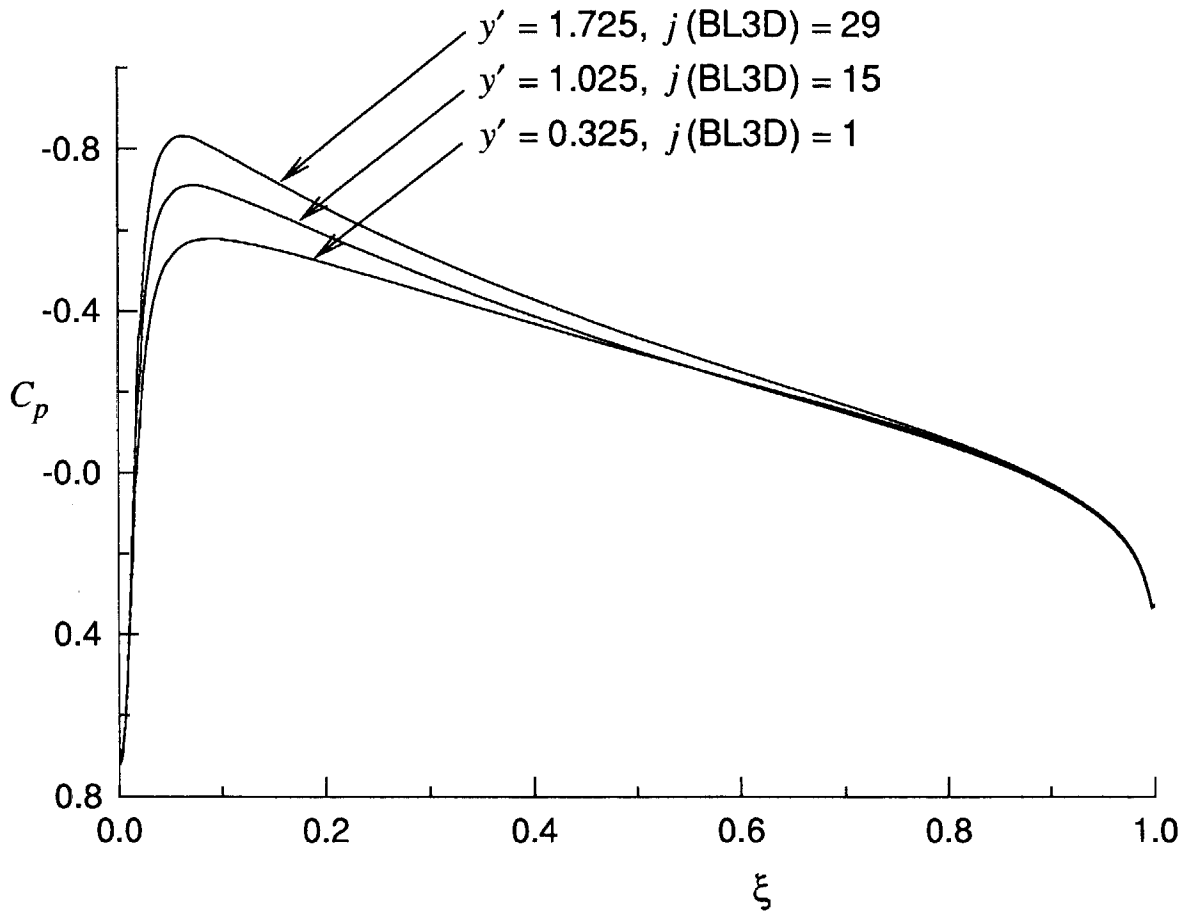

Figure 8. Variation of pressure coefficient, case 1, upper surface.

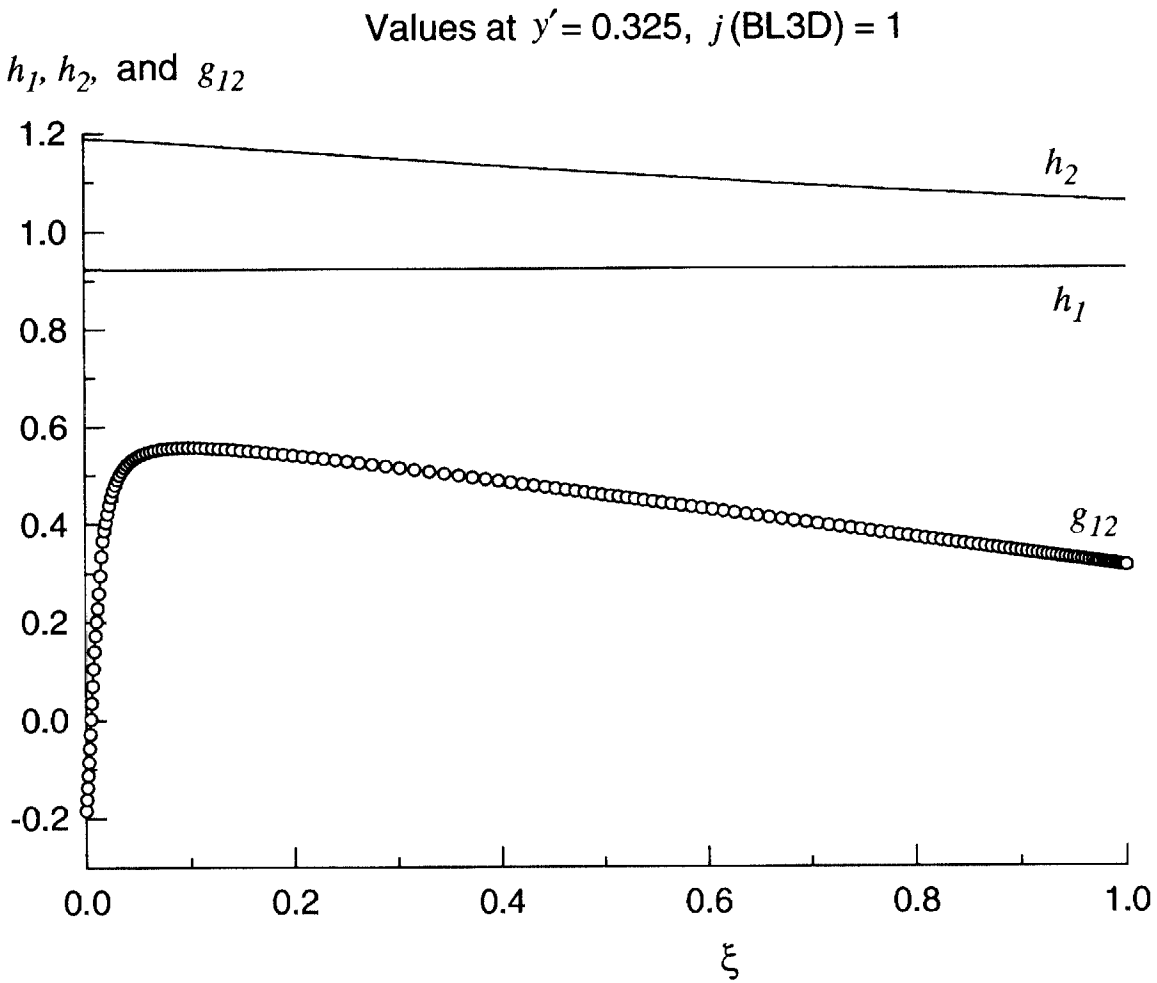

Figure 9. Variation of metric quantities, case 1, upper surface.

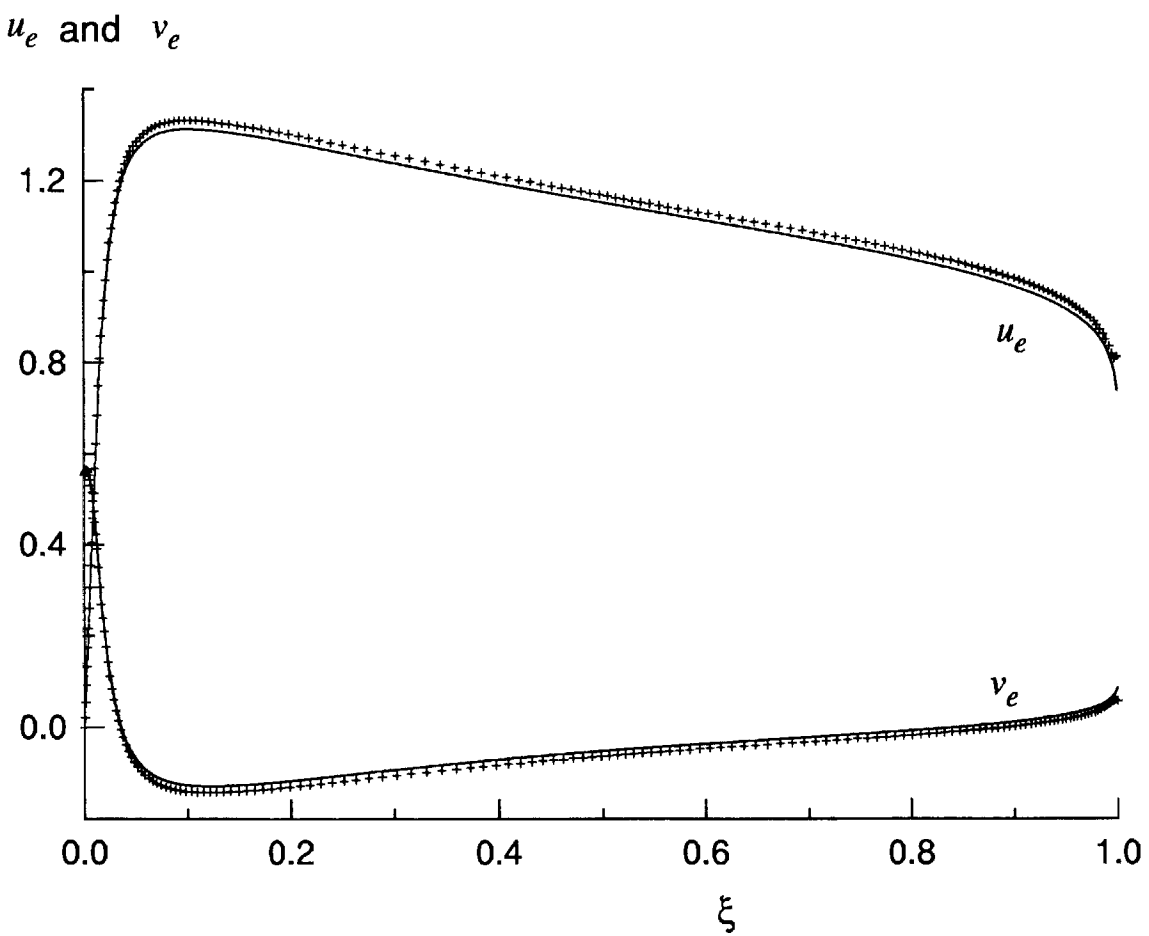

Figure 10. Comparison of BL– EDGE solution to Euler solution for case 1, upper surface.

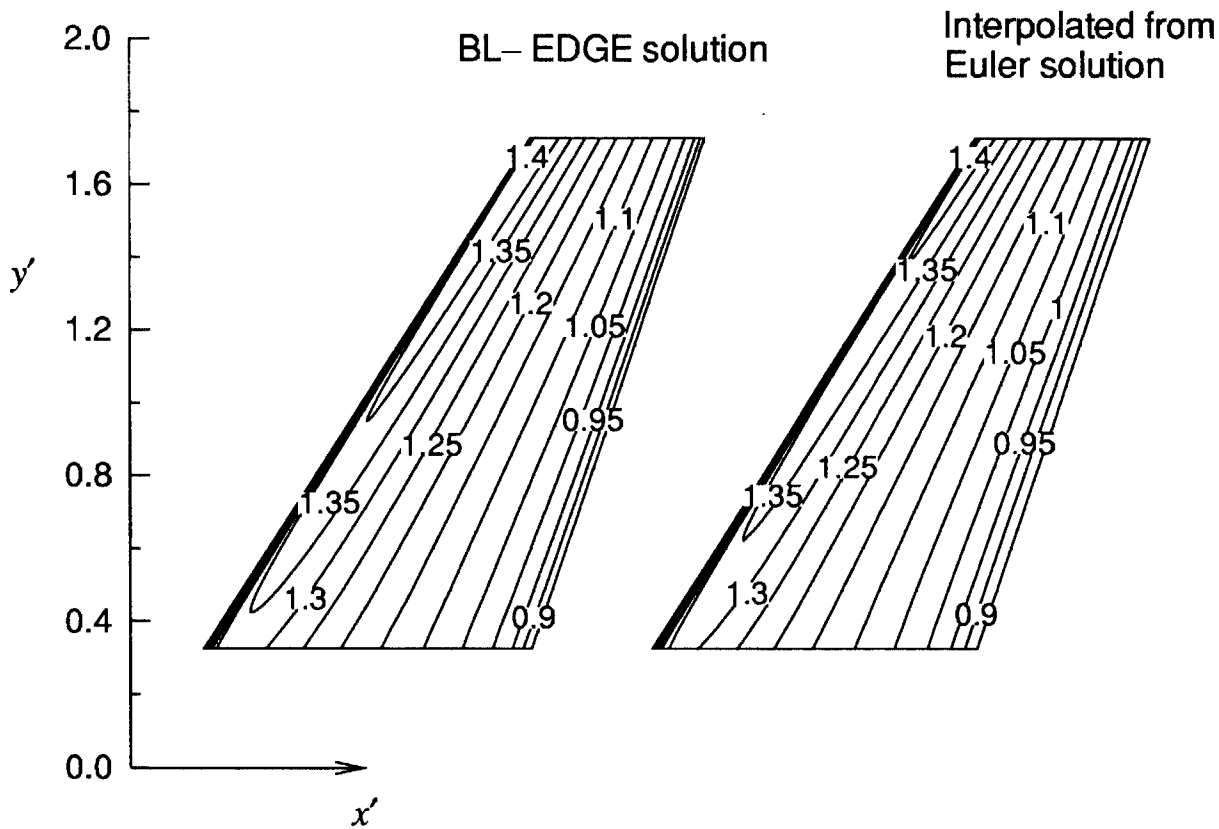

Figure 11. Comparison of edge velocity u_e for case 1, upper surface.

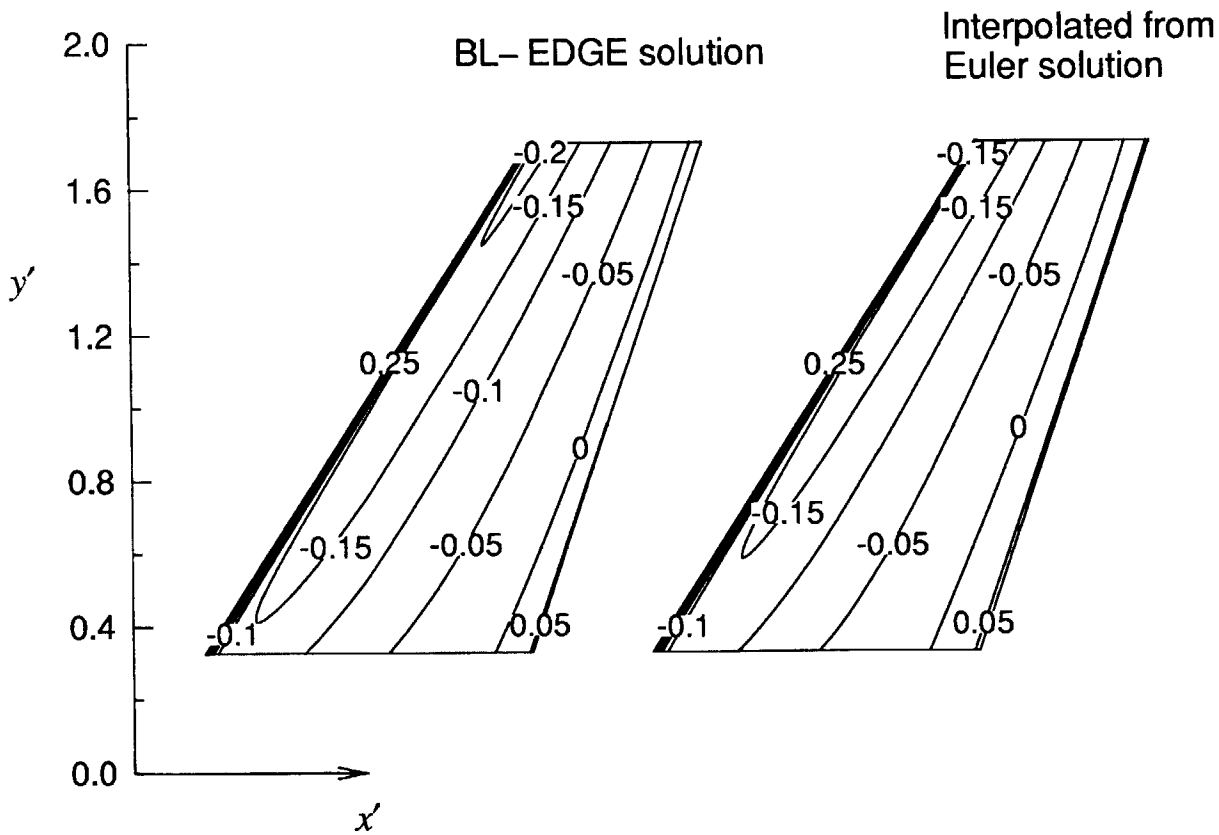

Figure 12. Comparison of edge velocity v_e for case 1, upper surface.

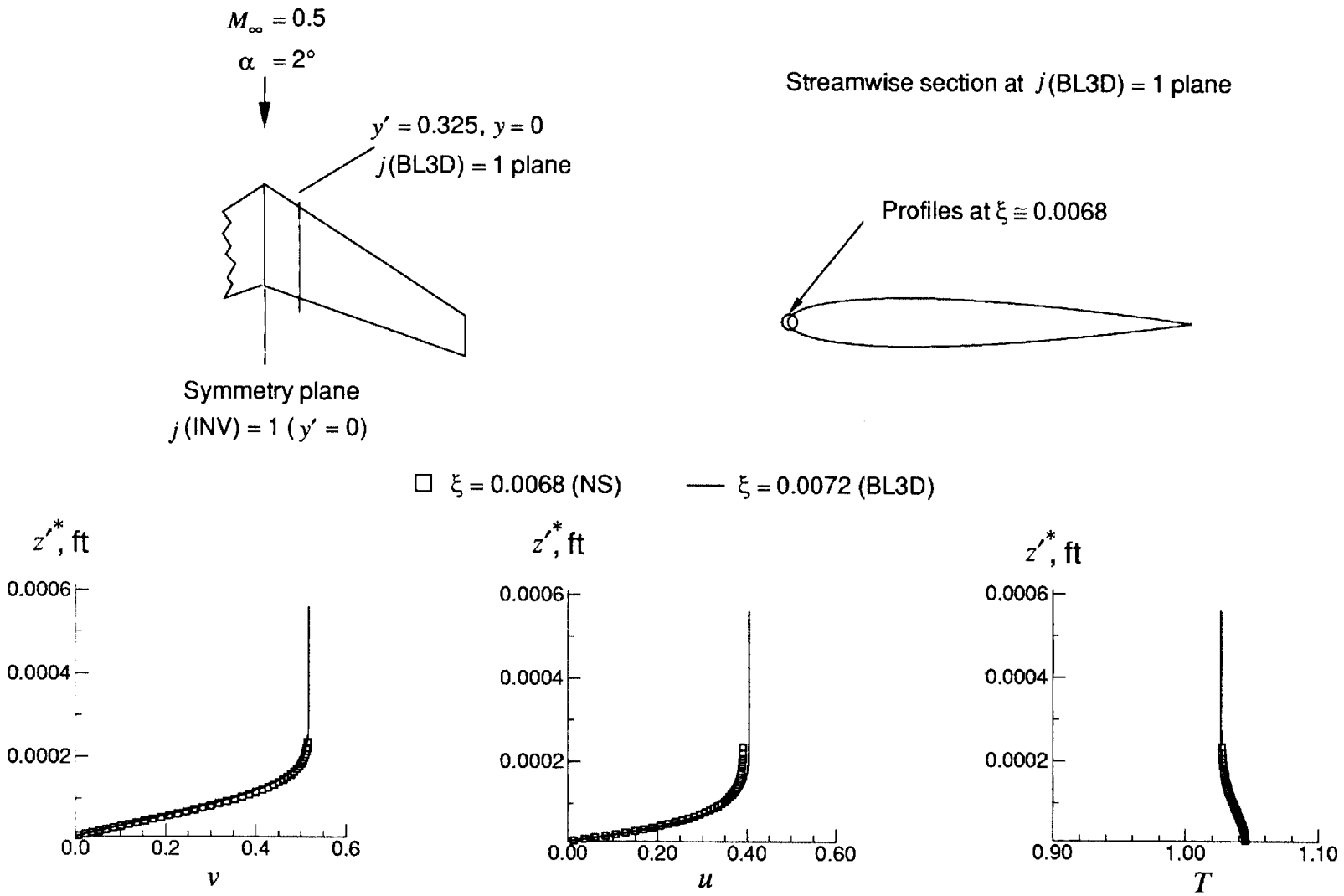

Figure 13. Comparison of NS and BL3D profiles on wing upper surface at $\xi \cong 0.0068$, $\eta = 0.0$ (Case 1).

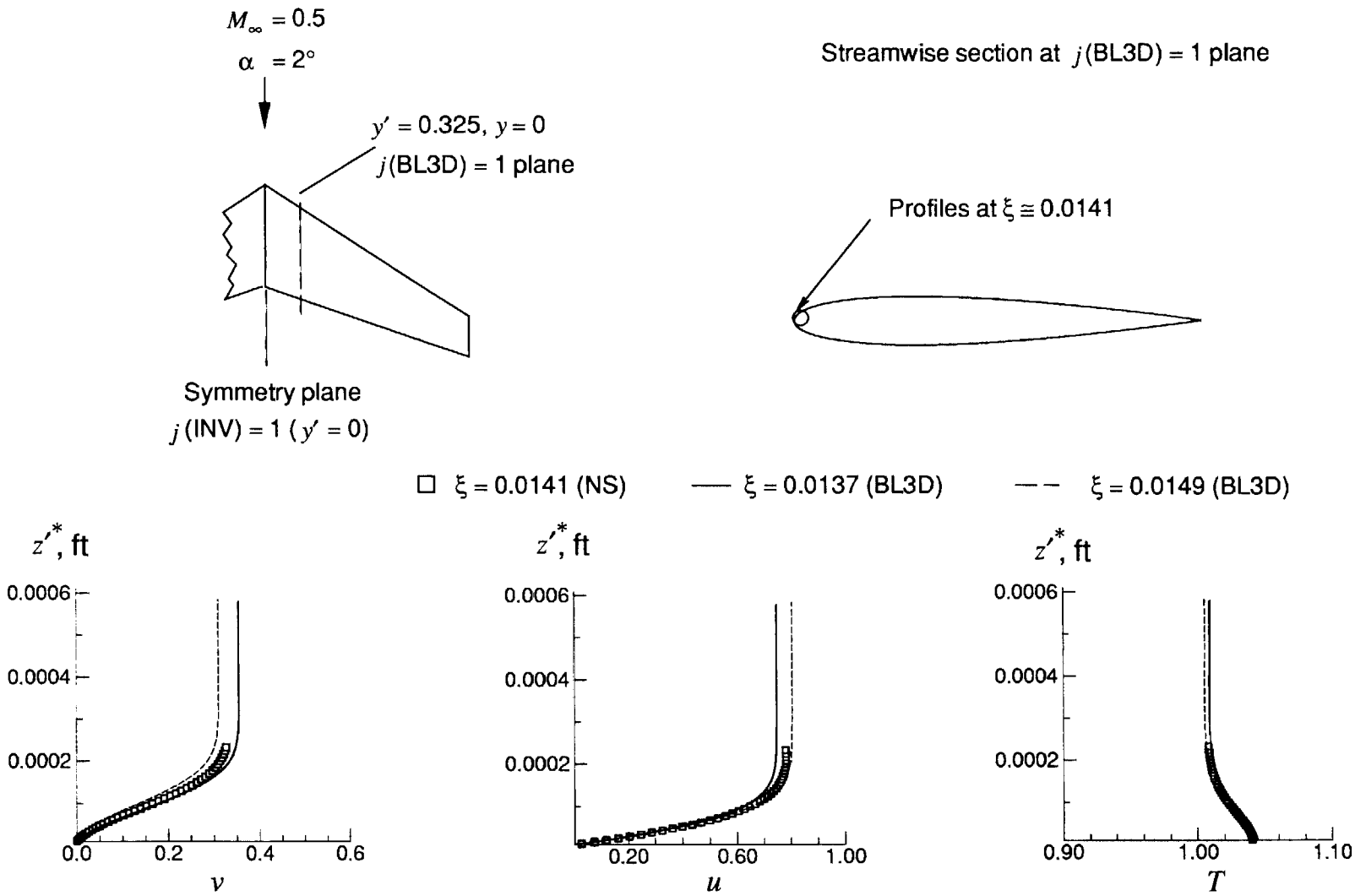

Figure 14. Comparison of NS and BL3D profiles on wing upper surface at $\xi \cong 0.0141$, $\eta = 0.0$ (Case 1).

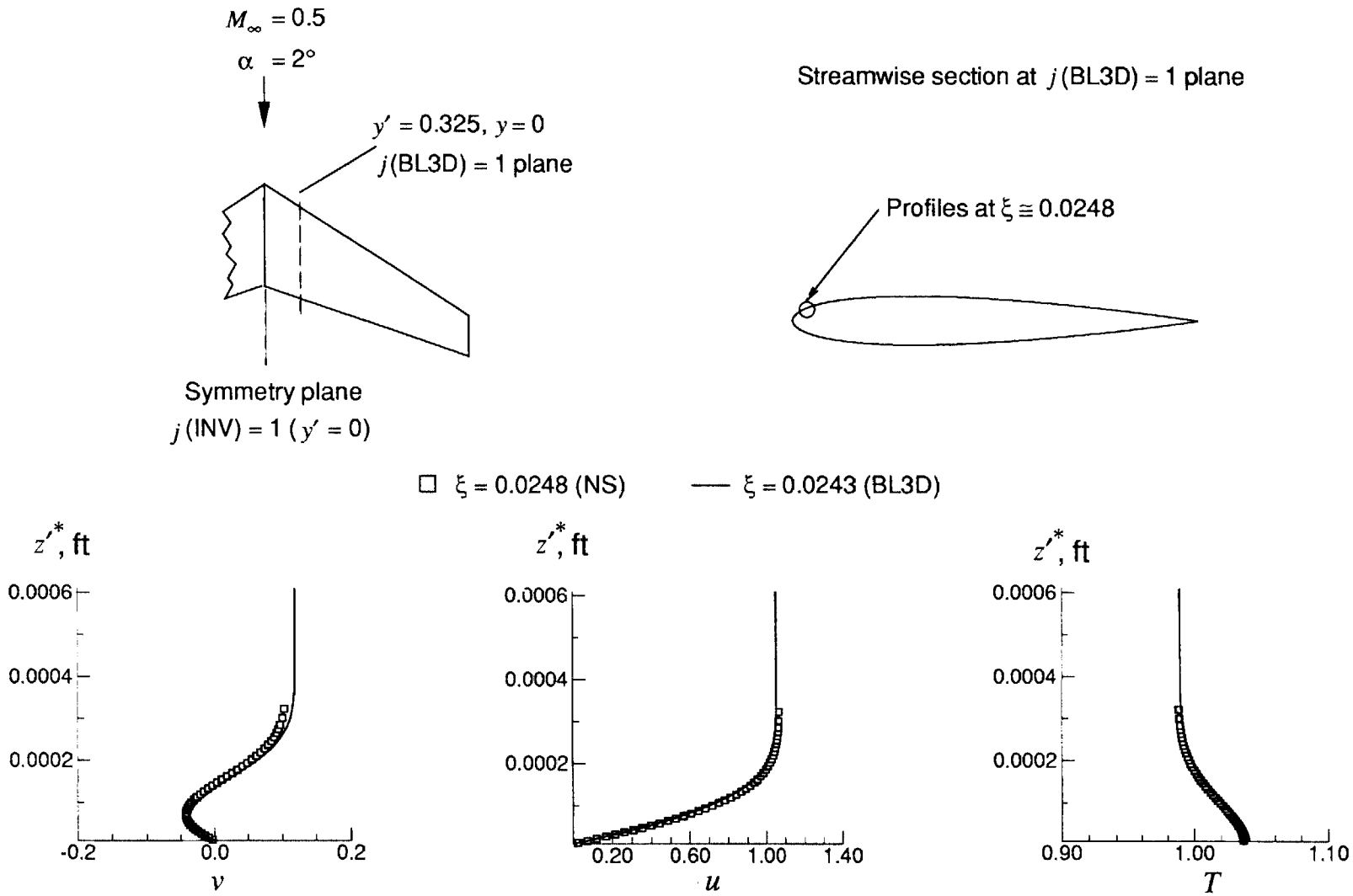

Figure 15. Comparison of NS and BL3D profiles on wing upper surface at $\xi \cong 0.0248$, $\eta = 0.0$ (Case 1).

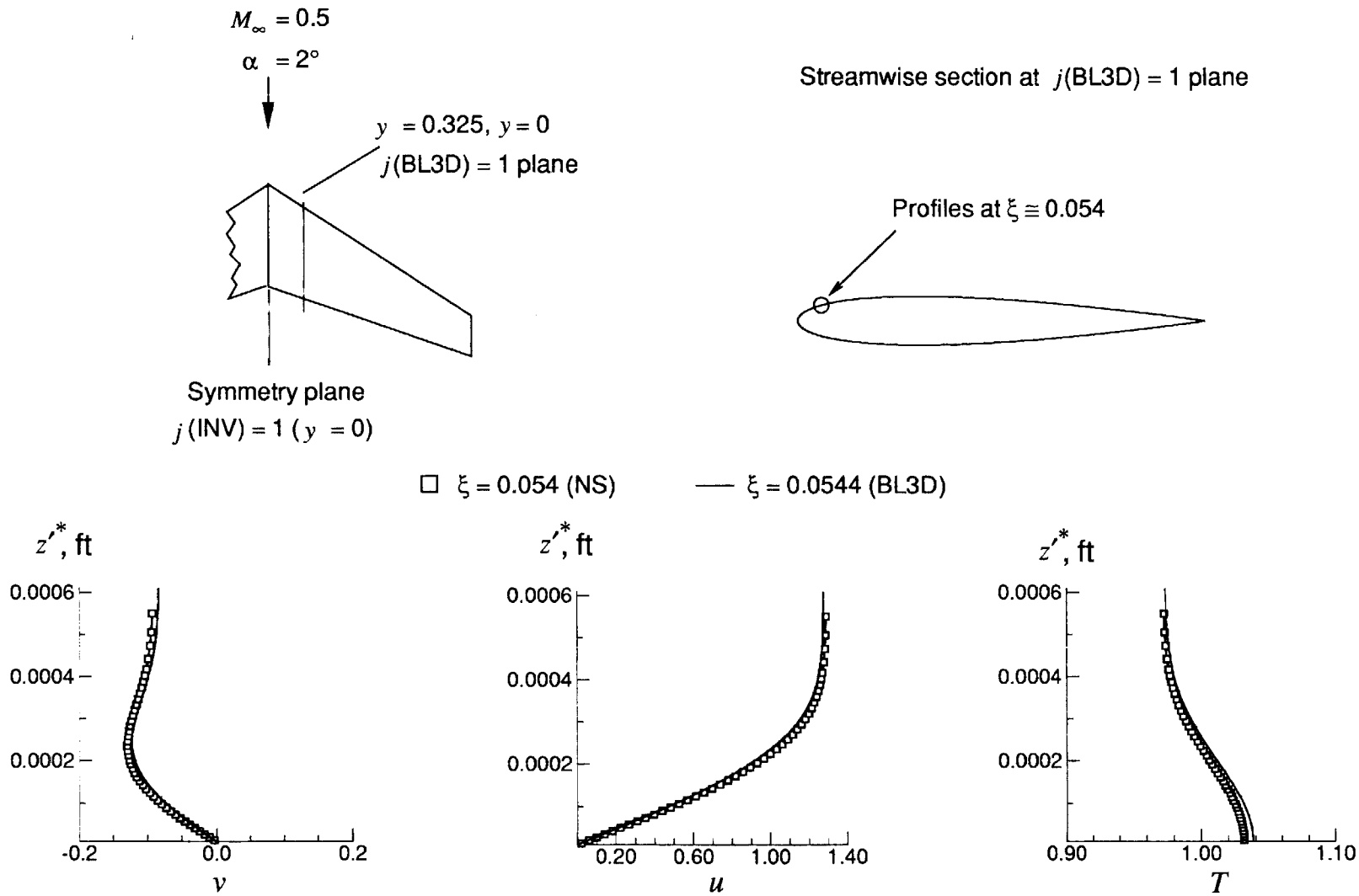

Figure 16. Comparison of NS and BL3D profiles on wing upper surface at $\xi \cong 0.054$, $\eta = 0.0$ (Case 1).

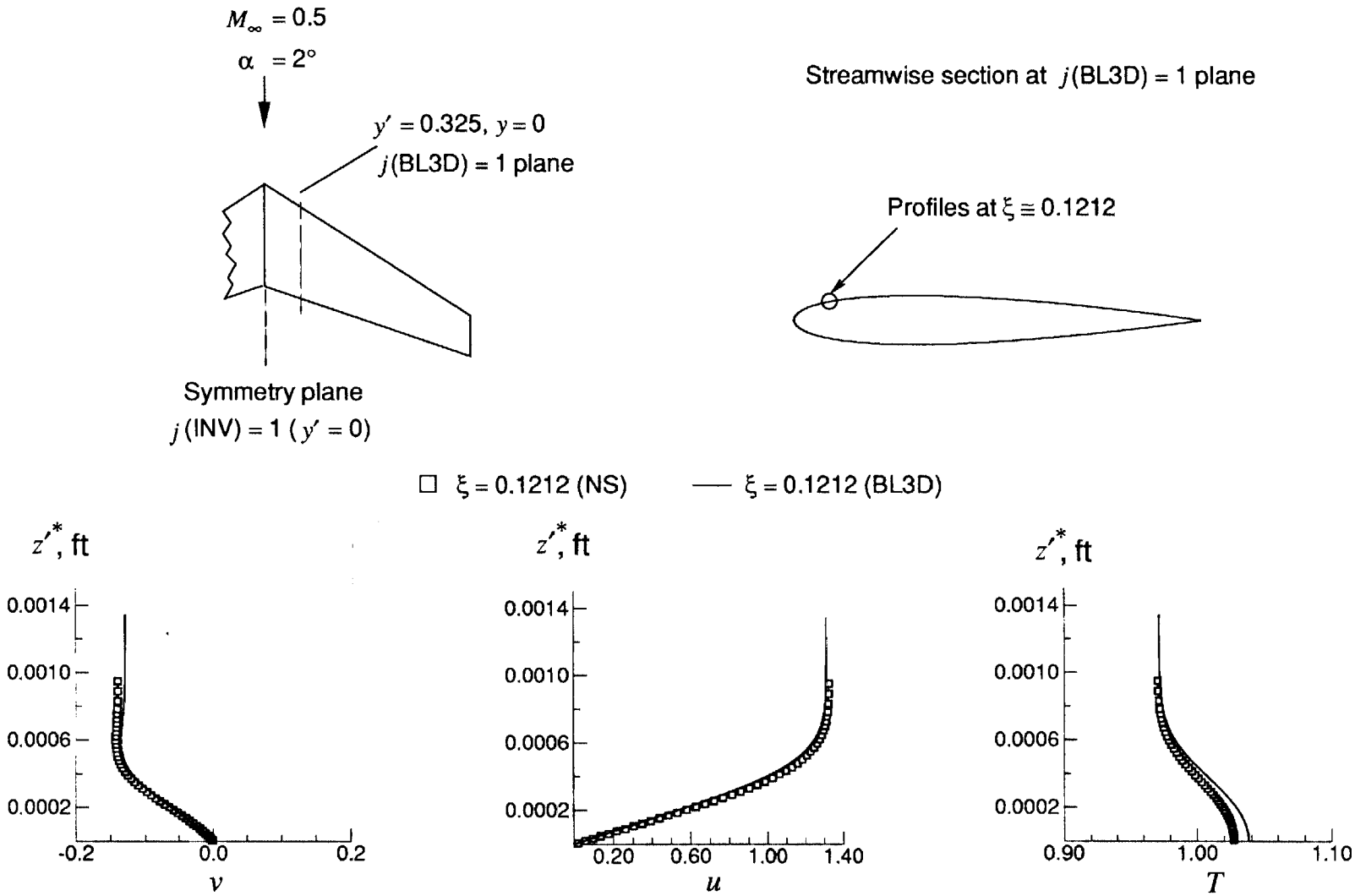

Figure 17. Comparison of NS and BL3D profiles on wing upper surface at $\xi \equiv 0.1212$, $\eta = 0.0$ (Case 1).

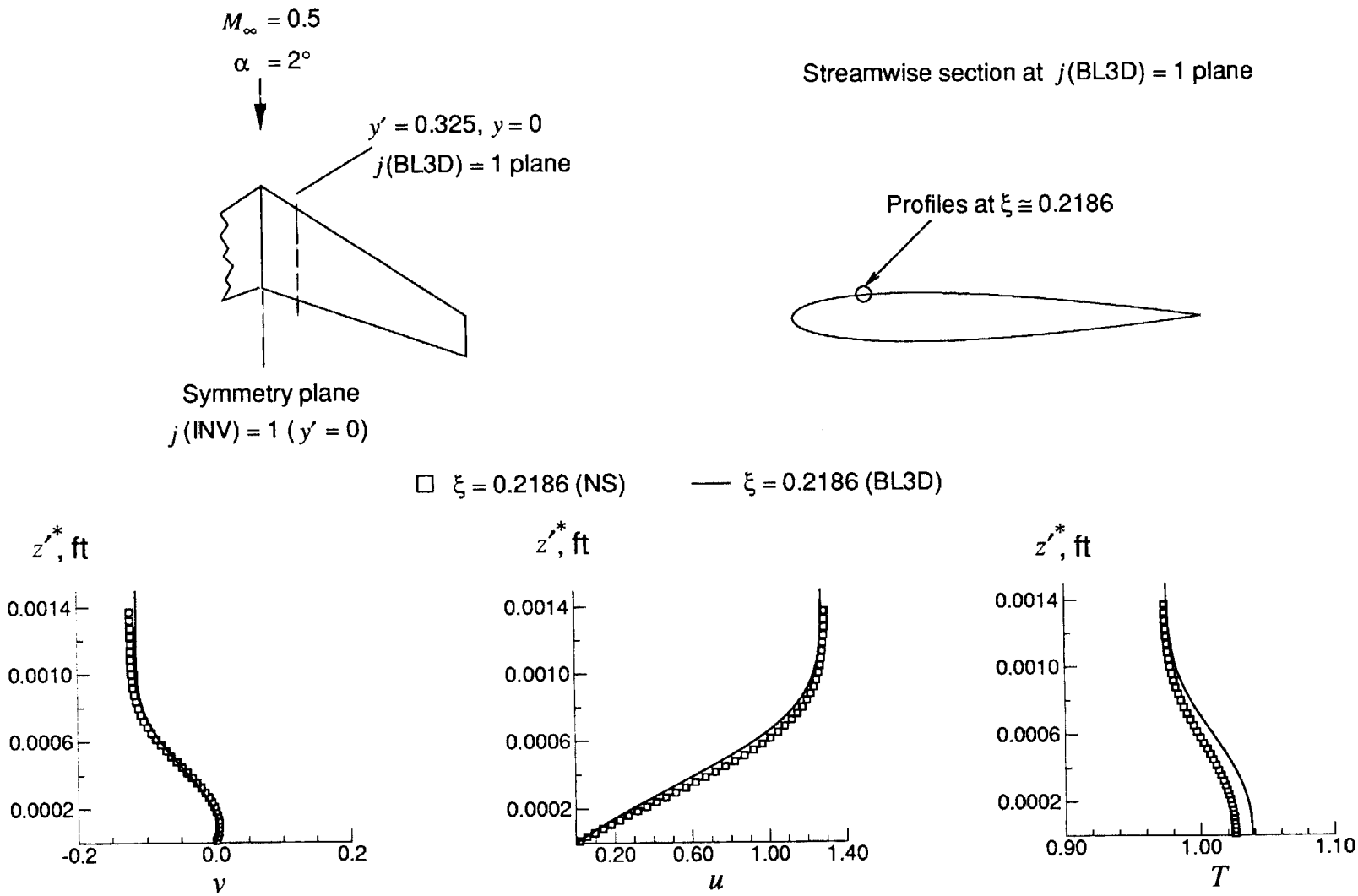

Figure 18. Comparison of NS and BL3D profiles on wing upper surface at $\xi \cong 0.2186$, $\eta = 0.0$ (Case 1).

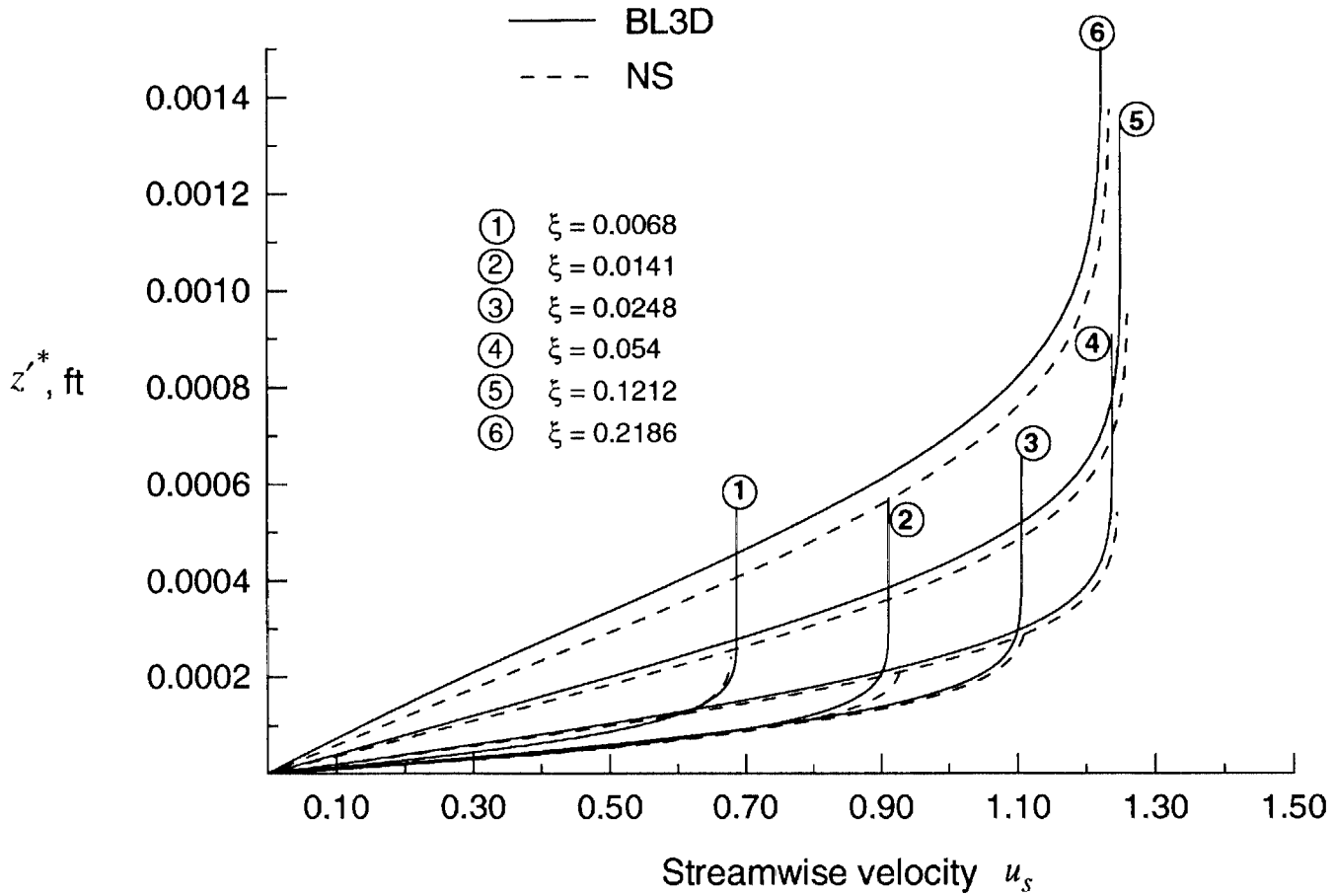

Figure 19. Comparison of streamwise flow profiles from NS and BL3D at j (BL3D) = 1.

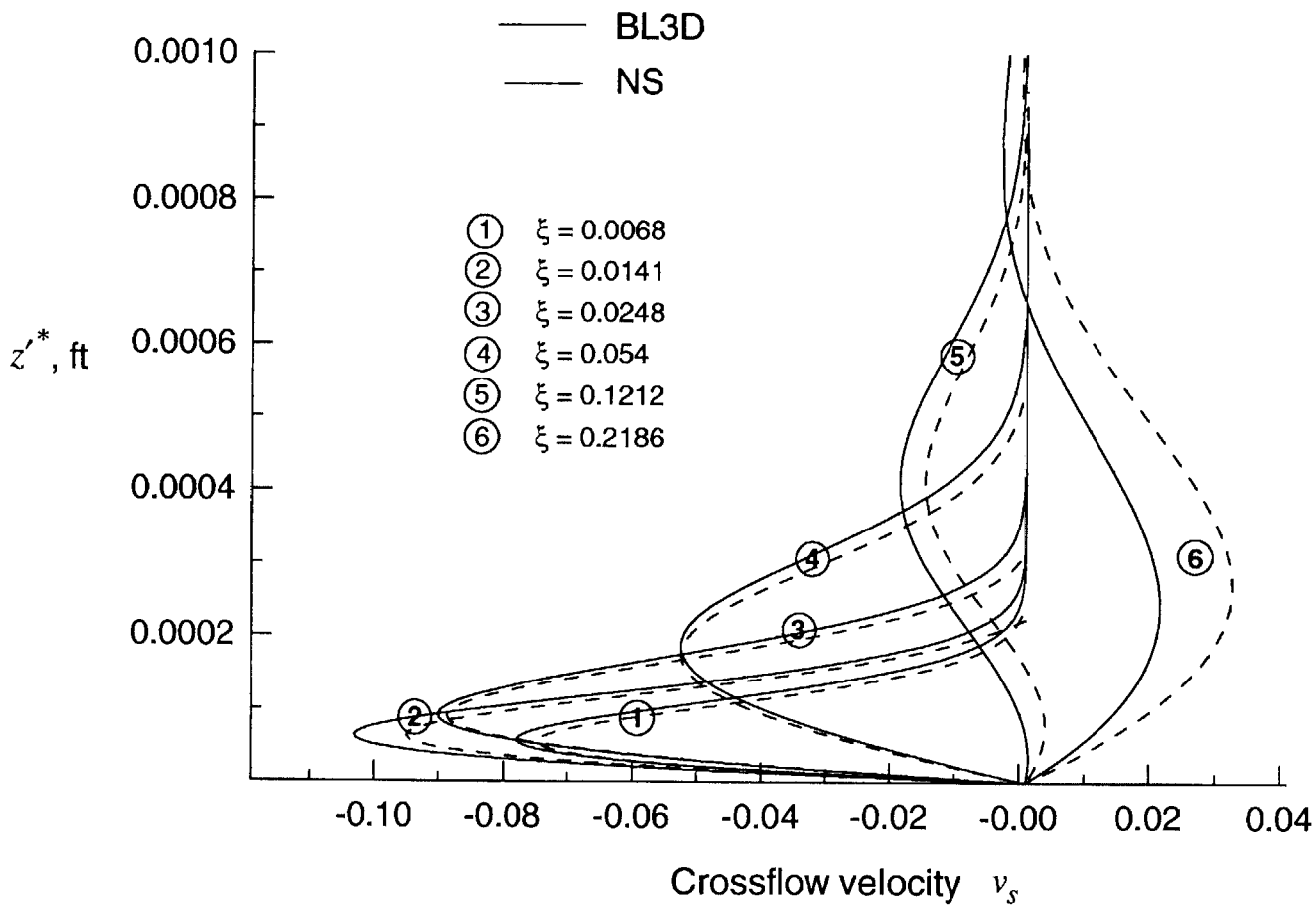

Figure 20. Comparison of crossflow profiles from NS and BL3D at j (BL3D) = 1.

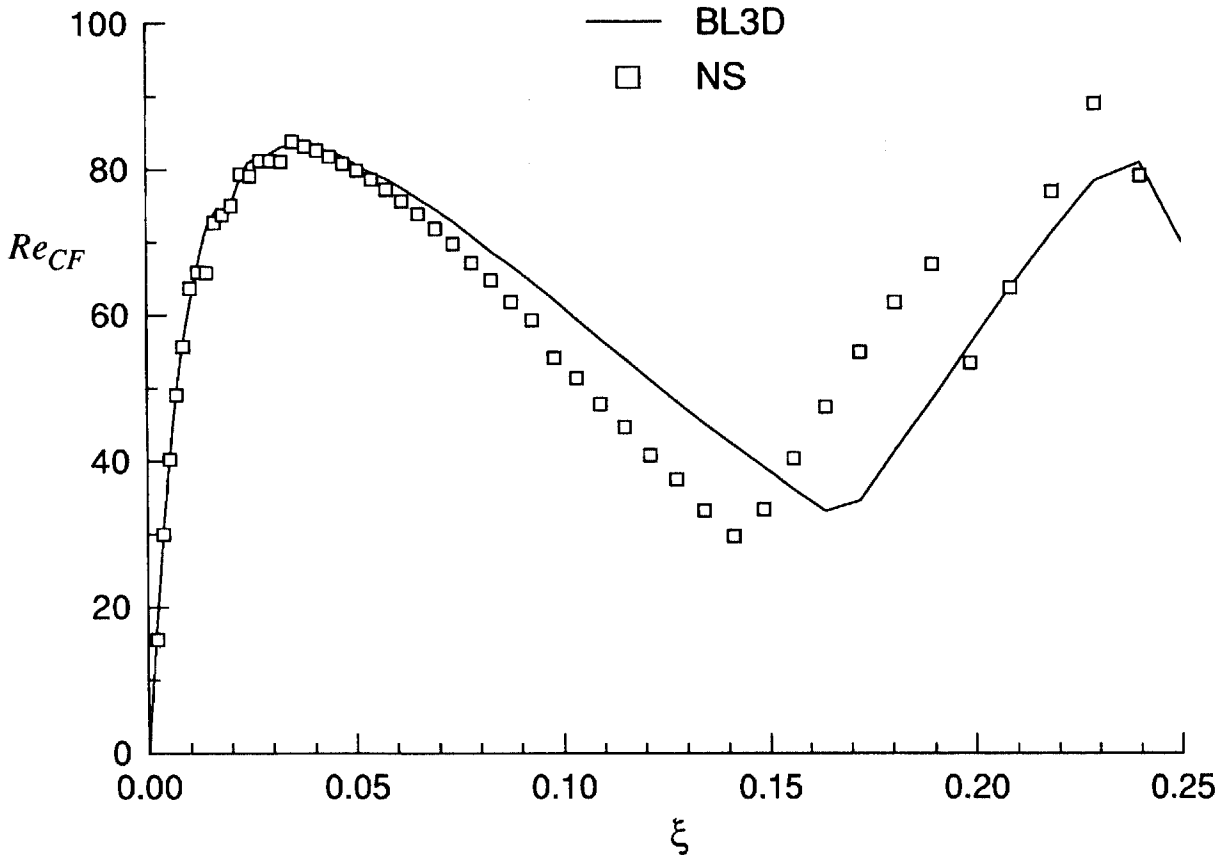

Figure 21. Comparison of crossflow Reynolds numbers from NS and BL3D at j(BL3D) = 1.

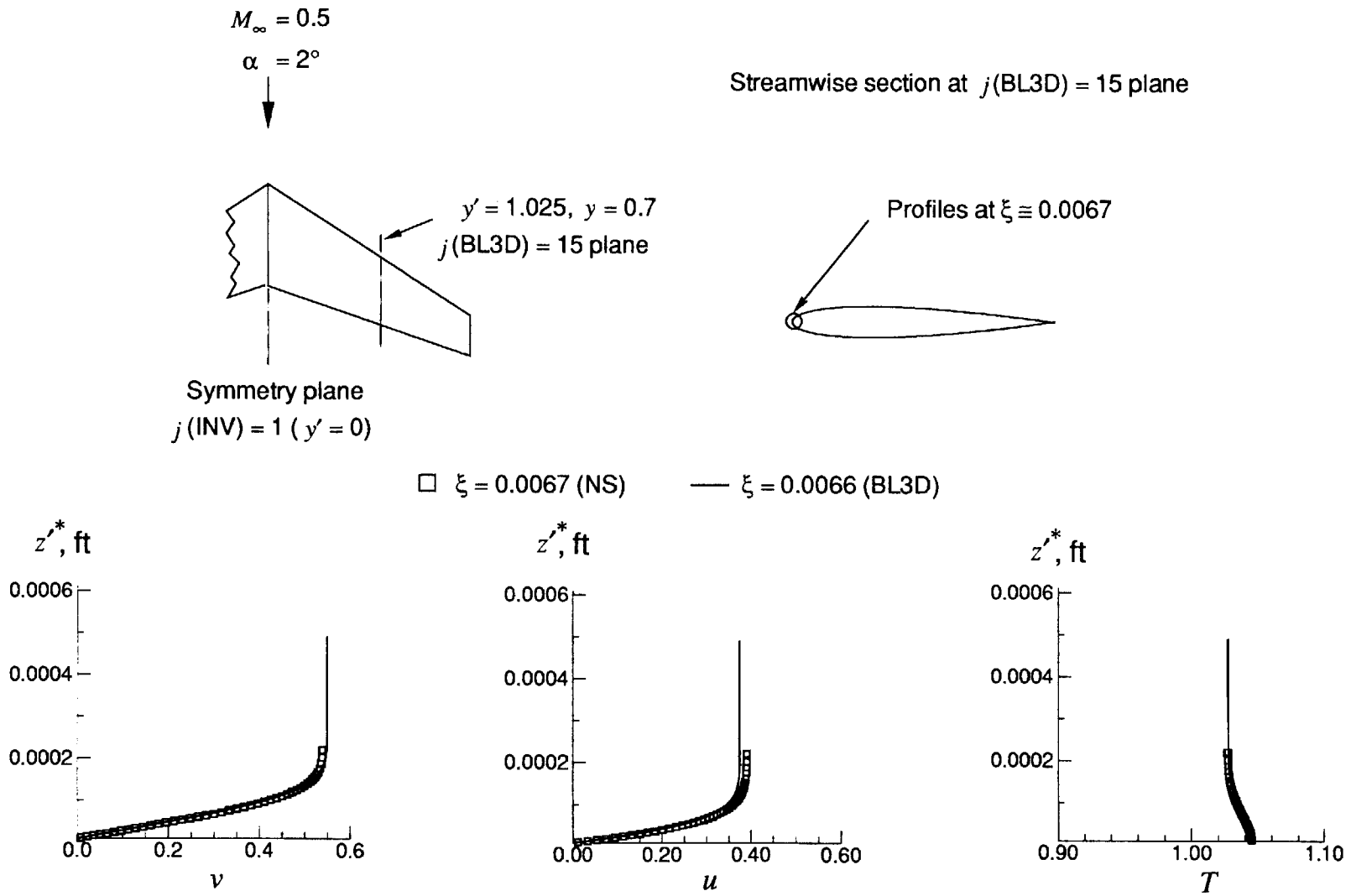

Figure 22. Comparison of NS and BL3D profiles on wing upper surface at $\xi \cong 0.0067$, $\eta = 0.7$ (Case 1).

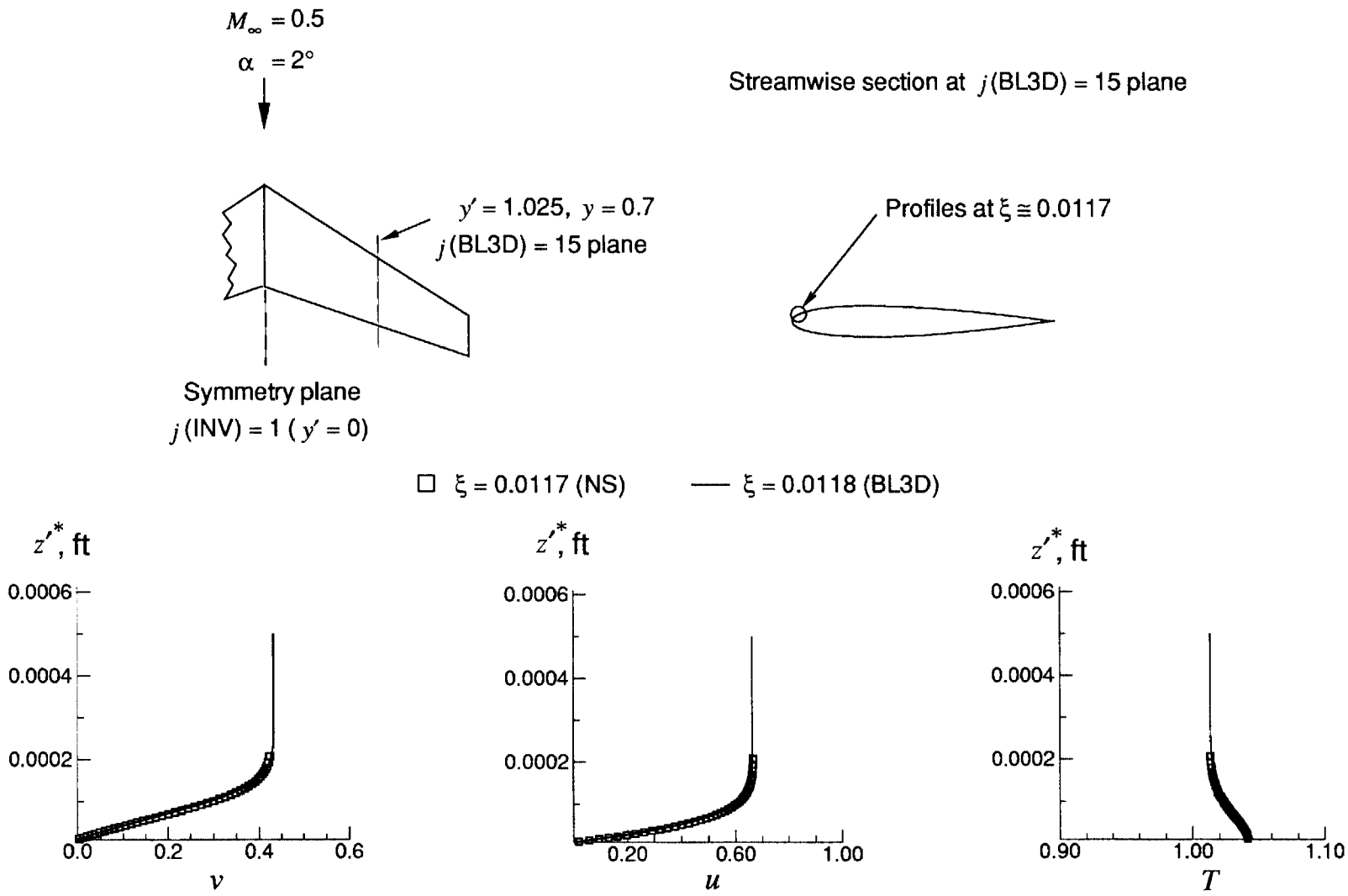

Figure 23. Comparison of NS and BL3D profiles on wing upper surface at $\xi \cong 0.0117$, $\eta = 0.7$ (Case 1).

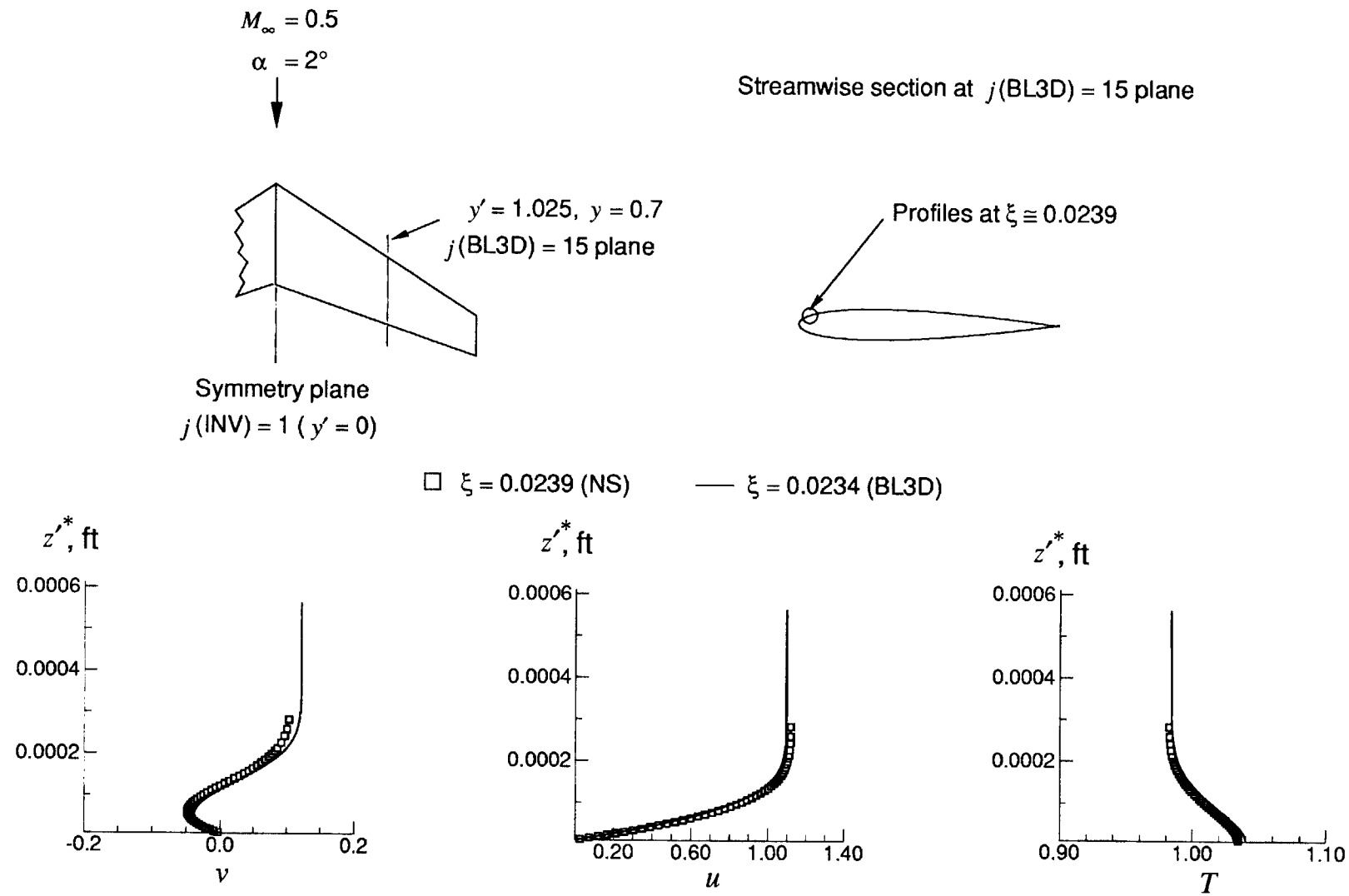

Figure 24. Comparison of NS and BL3D profiles on wing upper surface at $\xi \equiv 0.0239$, $\eta = 0.7$ (Case 1).

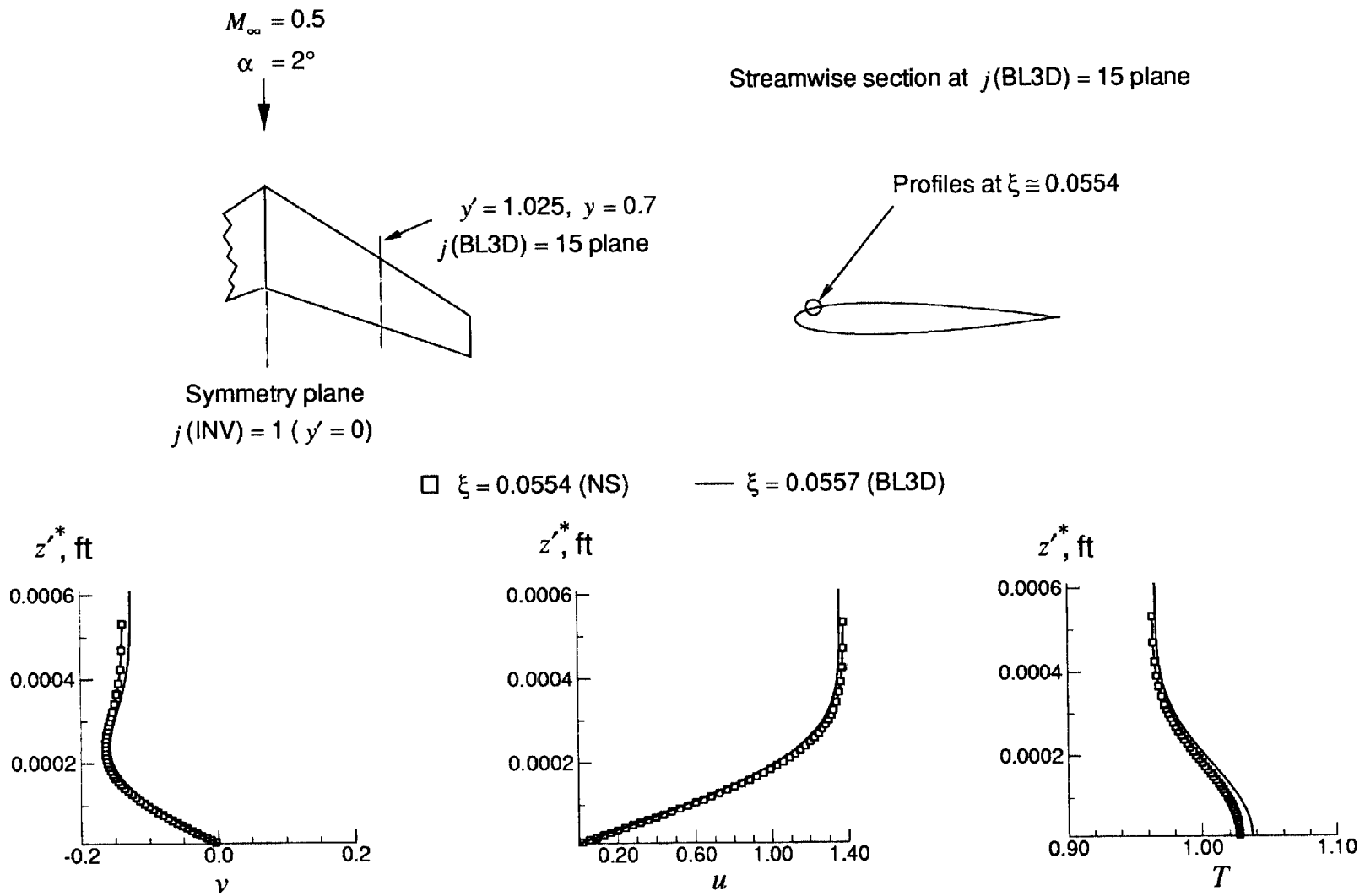

Figure 25. Comparison of NS and BL3D profiles on wing upper surface at $\xi \cong 0.0554$, $\eta = 0.7$ (Case 1).

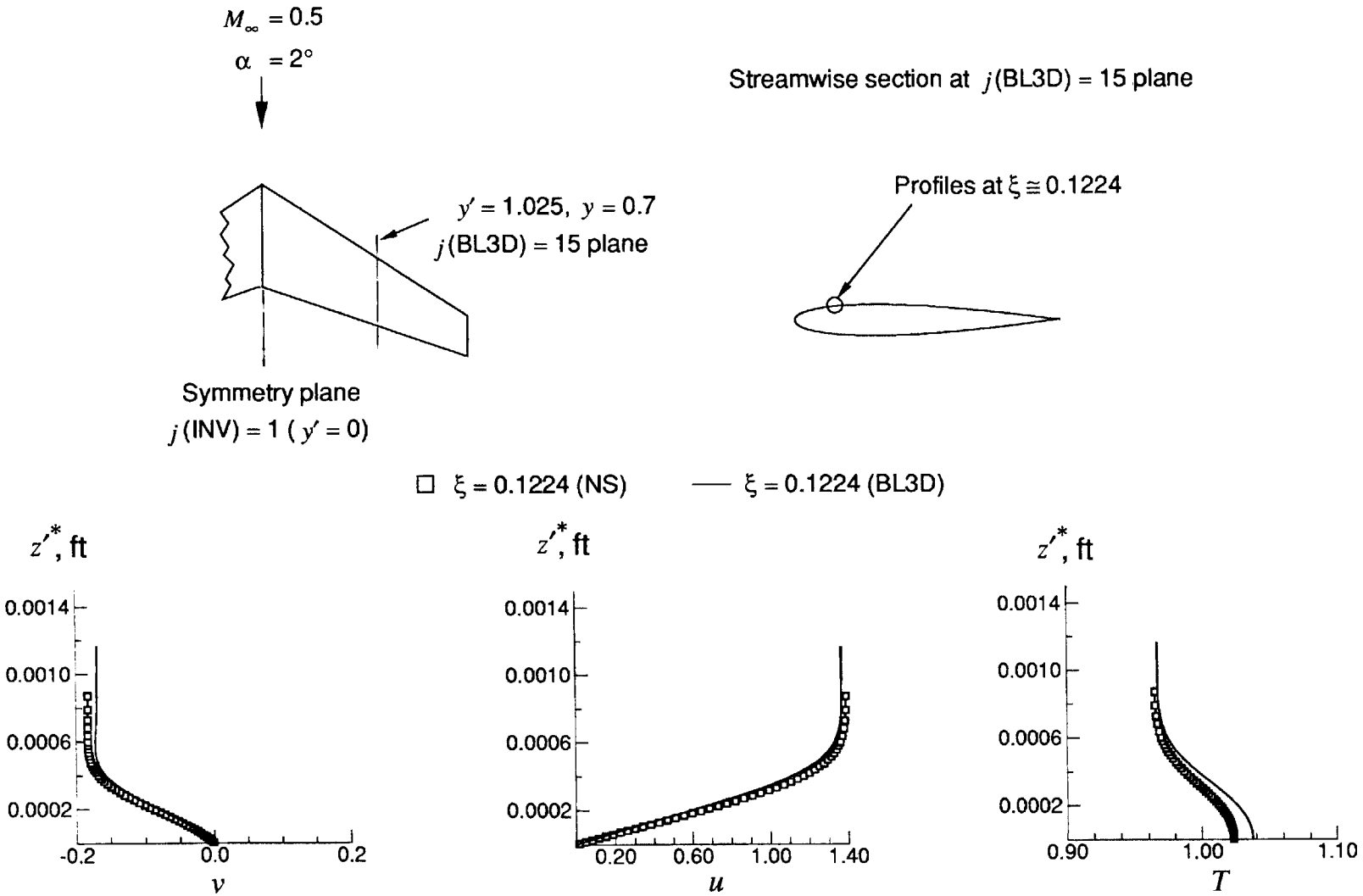

Figure 26. Comparison of NS and BL3D profiles on wing upper surface at $\xi \cong 0.1224$, $\eta = 0.7$ (Case 1).

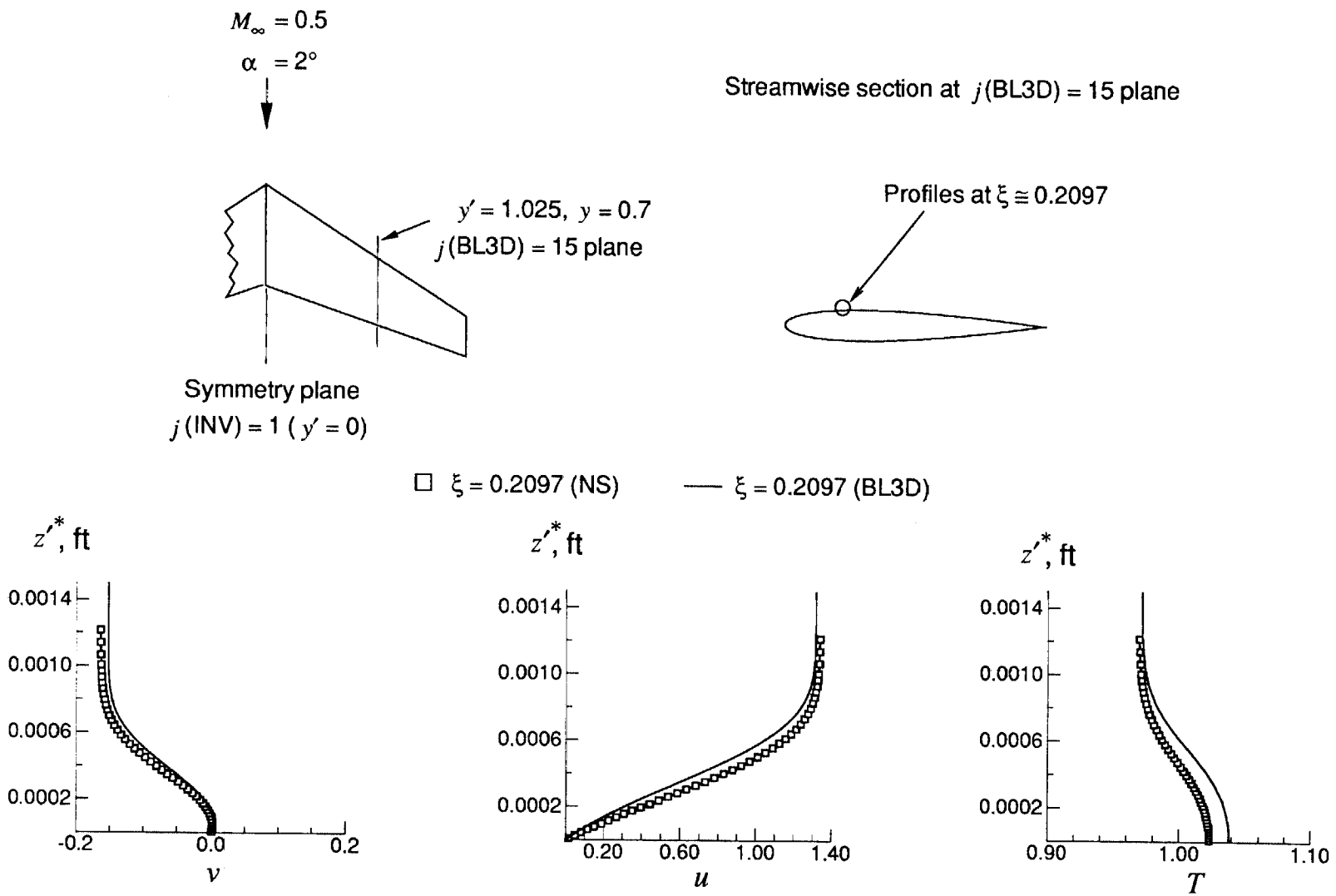

Figure 27. Comparison of NS and BL3D profiles on wing upper surface at $\xi \cong 0.2097$, $\eta = 0.7$ (Case 1).

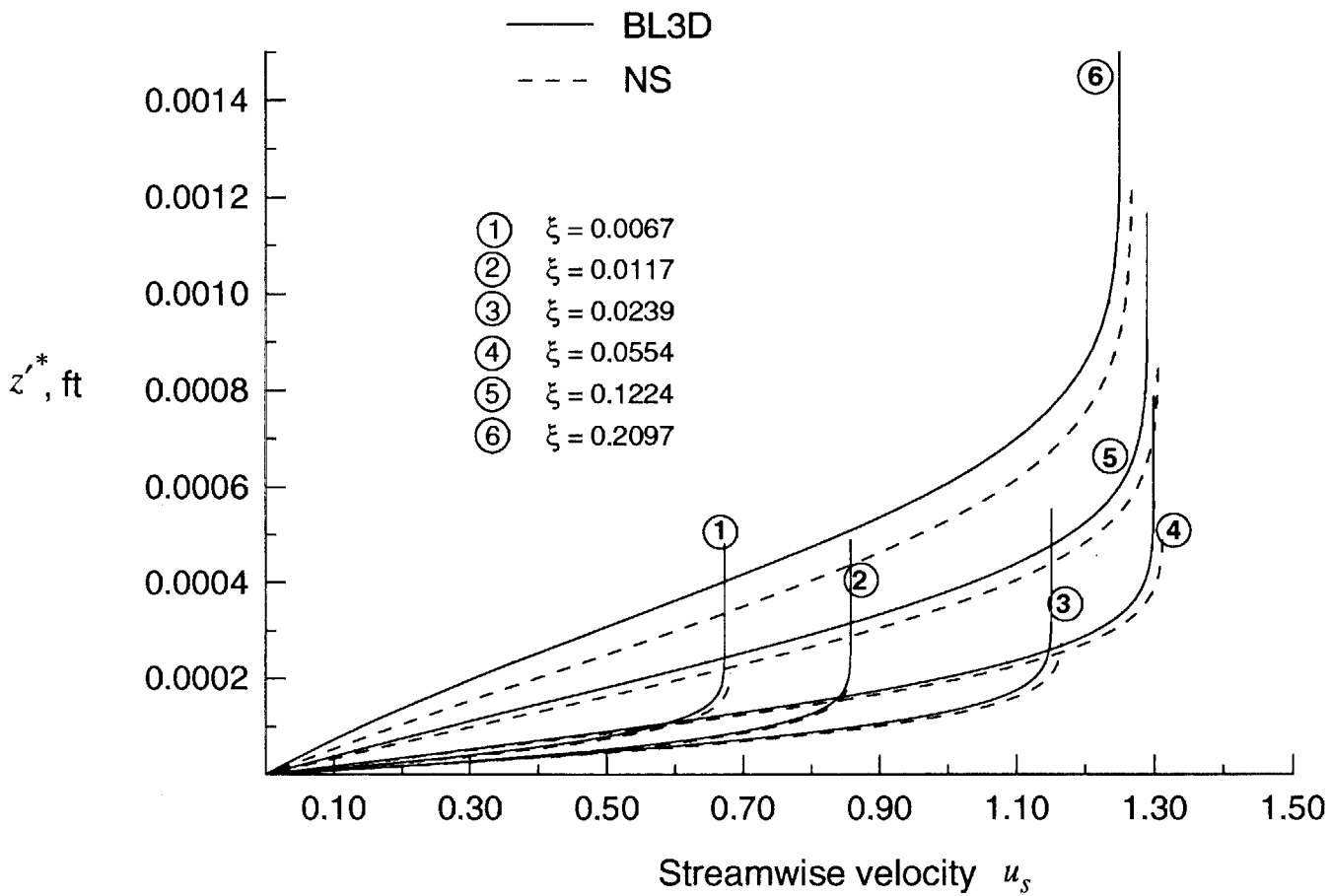

Figure 28. Comparison of streamwise flow profiles from NS and BL3D at j (BL3D) = 15.

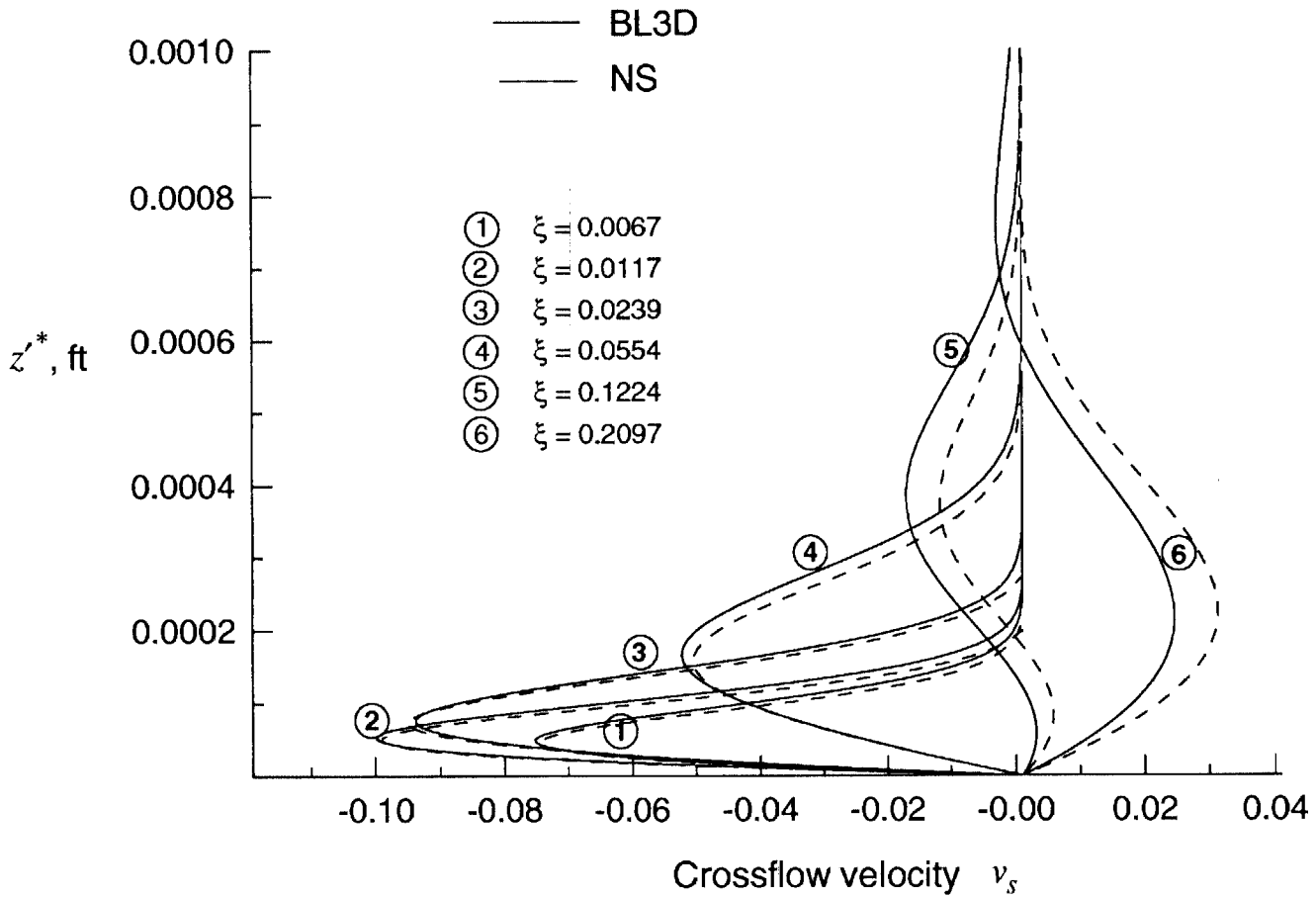

Figure 29. Comparison of crossflow profiles from NS and BL3D at j (BL3D) = 15.

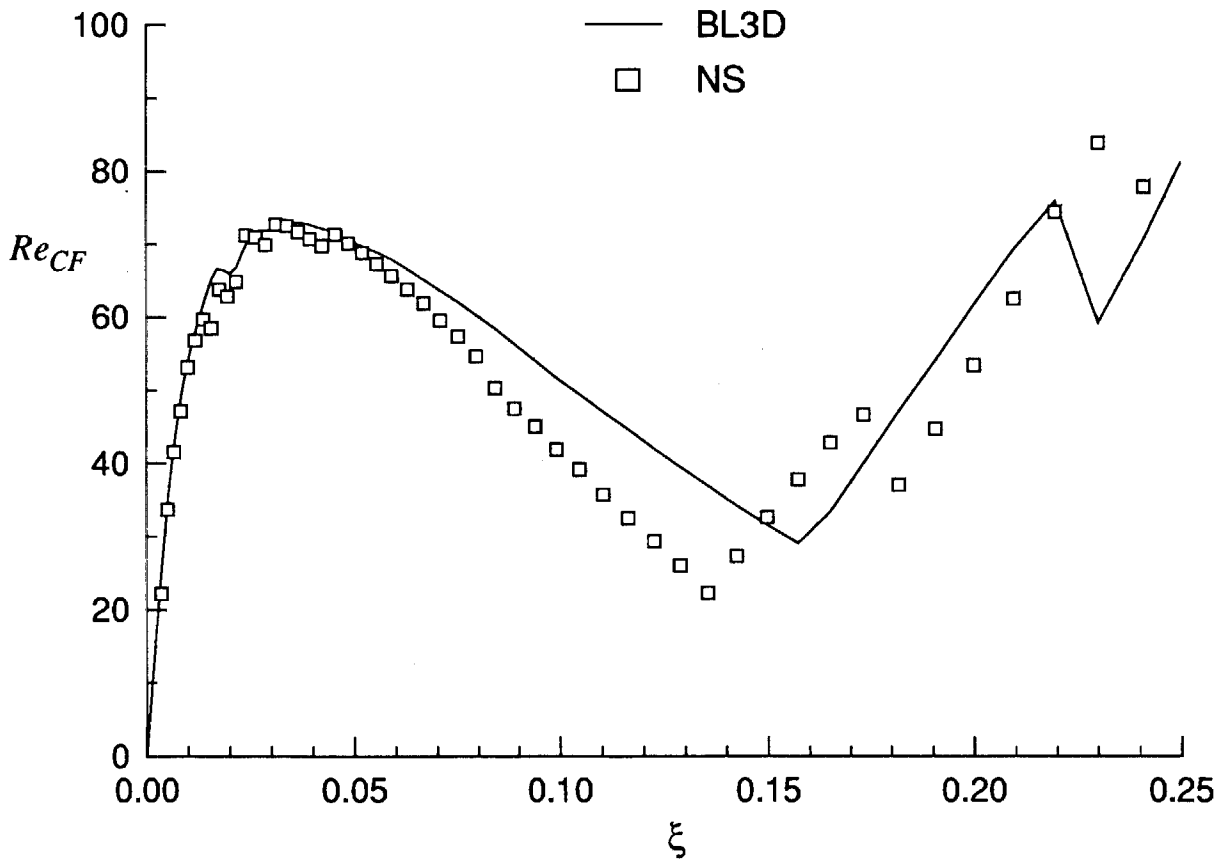

Figure 30. Comparison of crossflow Reynolds numbers from NS and BL3D at j(BL3D) = 15.

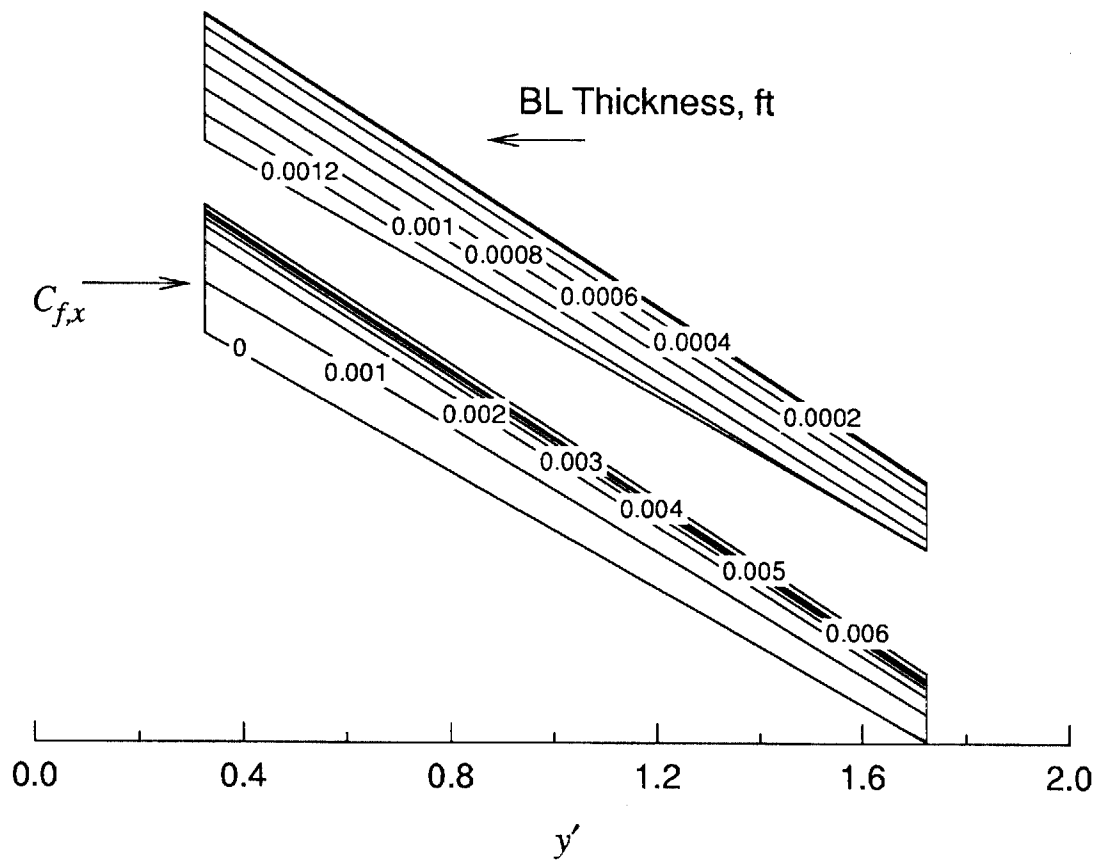

Figure 31. Contours of boundary-layer thickness and $C_{f,x}$ for case 1, upper surface.

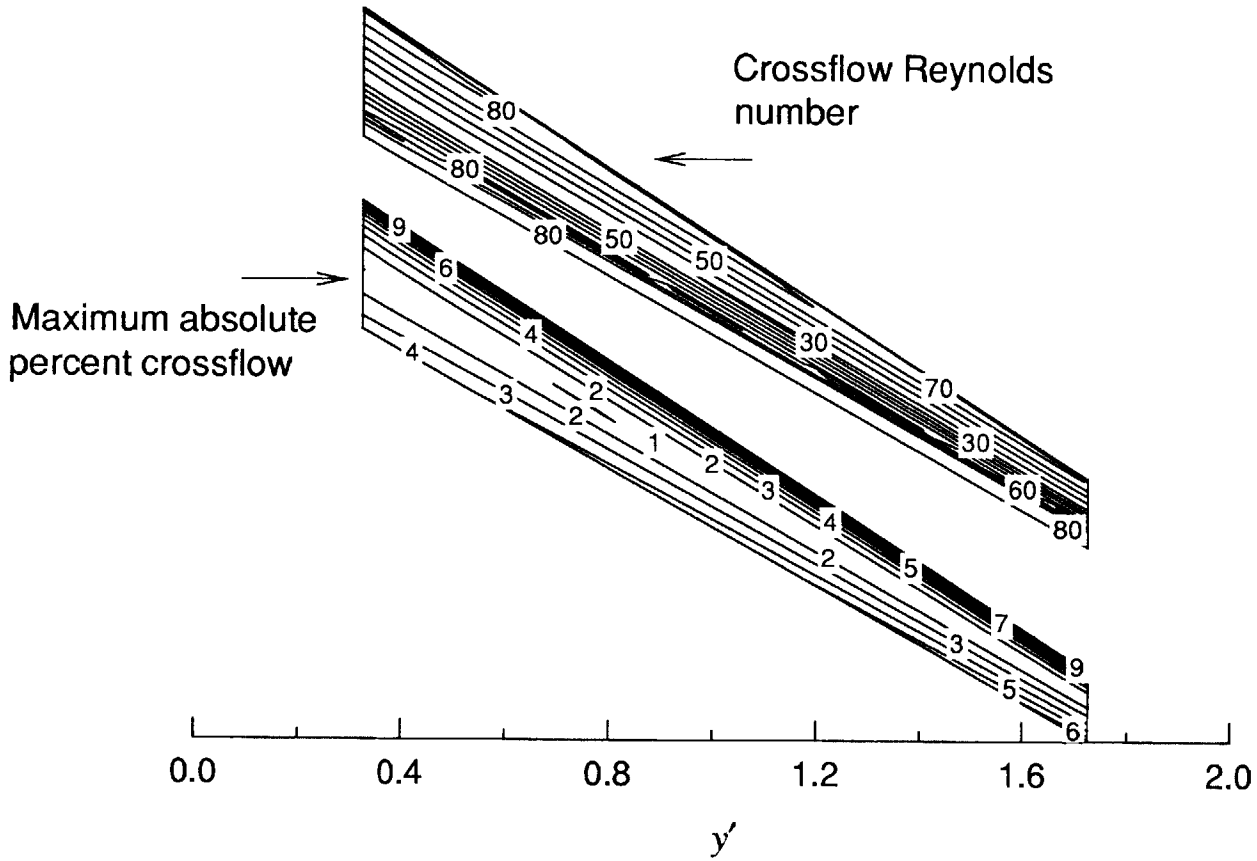

Figure 32. Contours of Re_{CF} and maximum percent crossflow for case 1, upper surface.

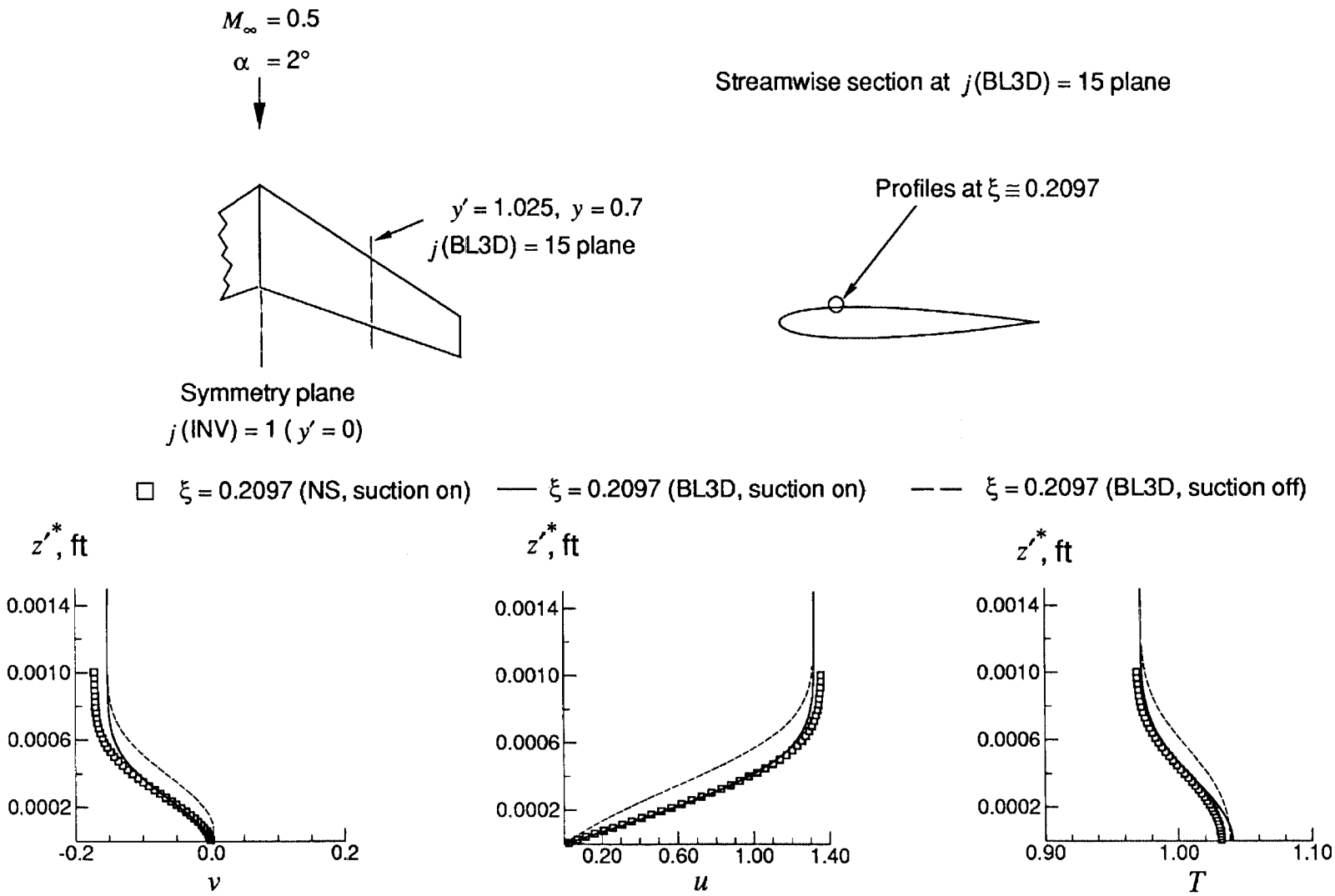

Figure 33. Comparison of NS and BL3D profiles with suction at $\xi \cong 0.2097$, $\eta = 0.7$ (Case 1).

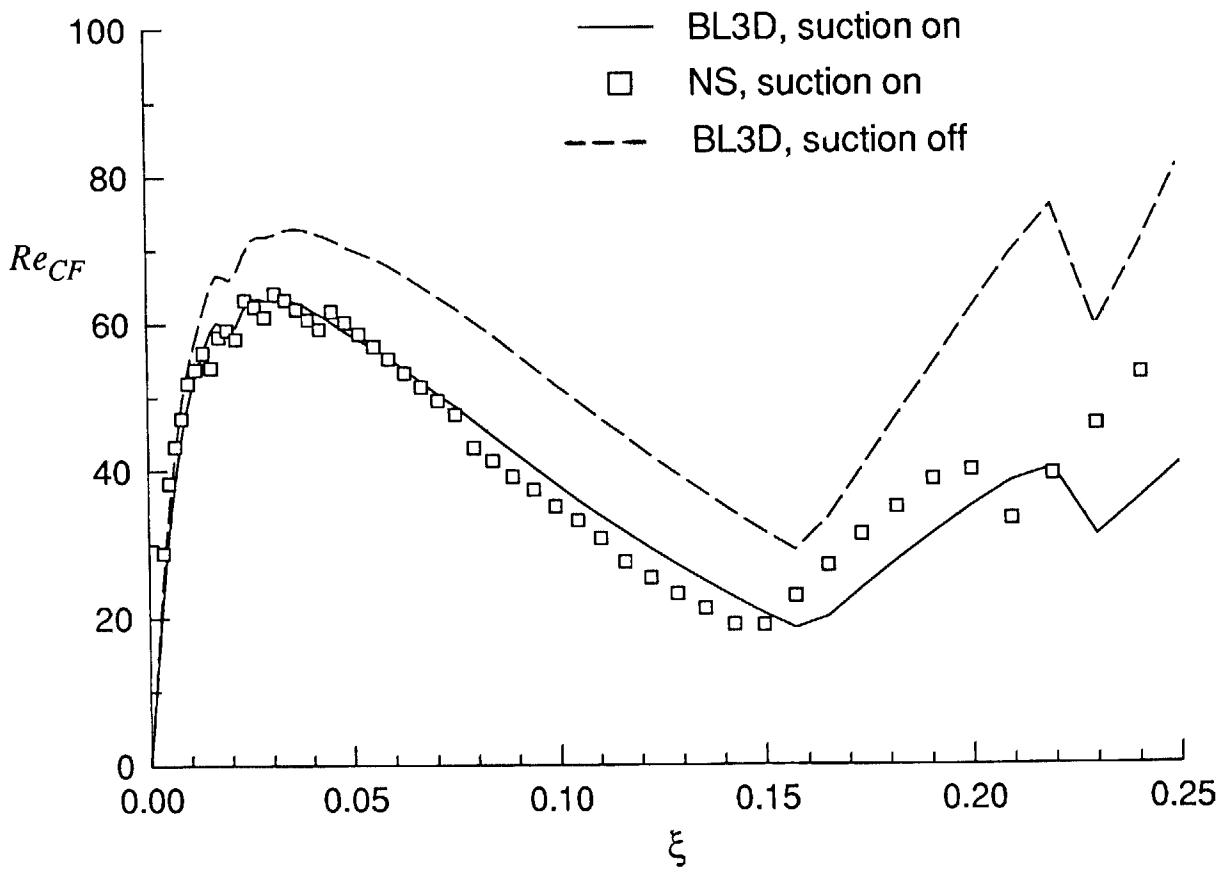

Figure 34. Comparison of crossflow Reynolds numbers from NS and BL3D at j(BL3D) = 15 with suction.

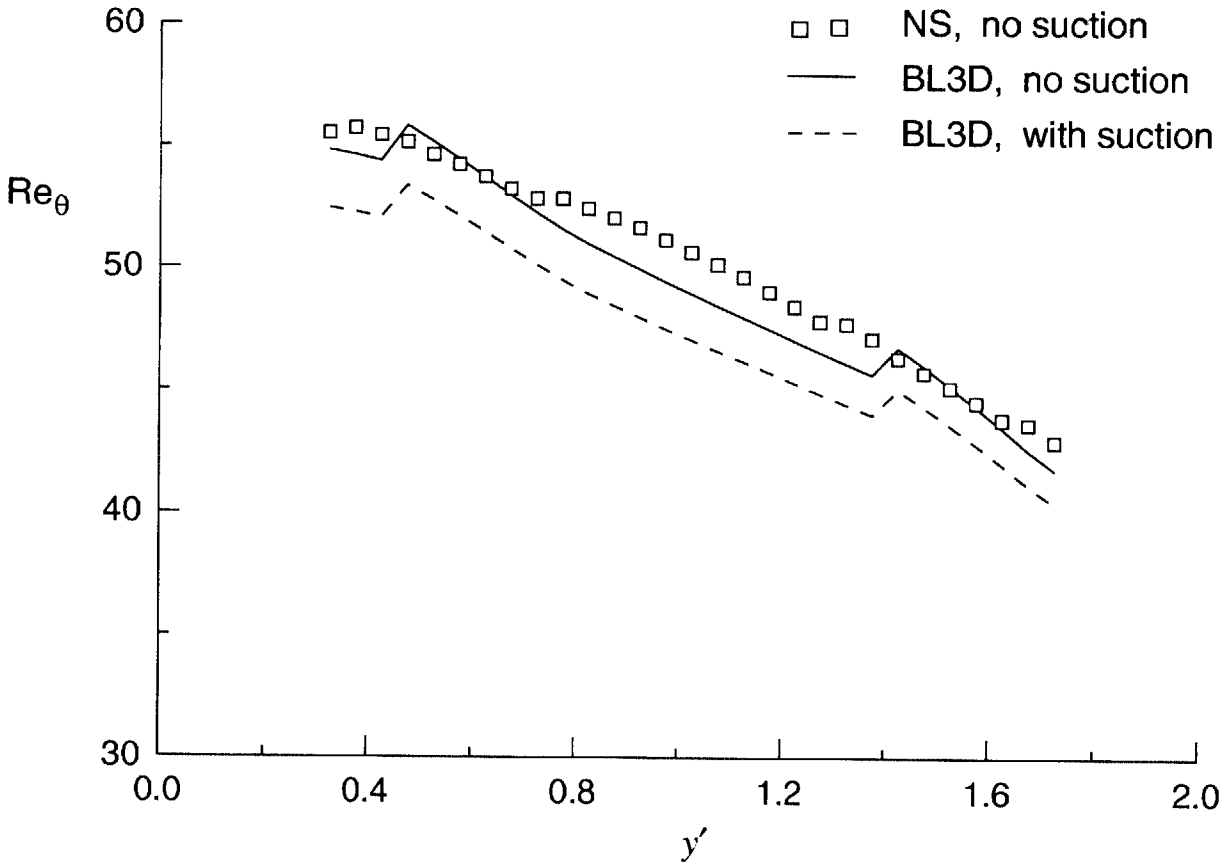

Figure 35. Variation of attachment-line Reynolds number for case 1 with or without suction.

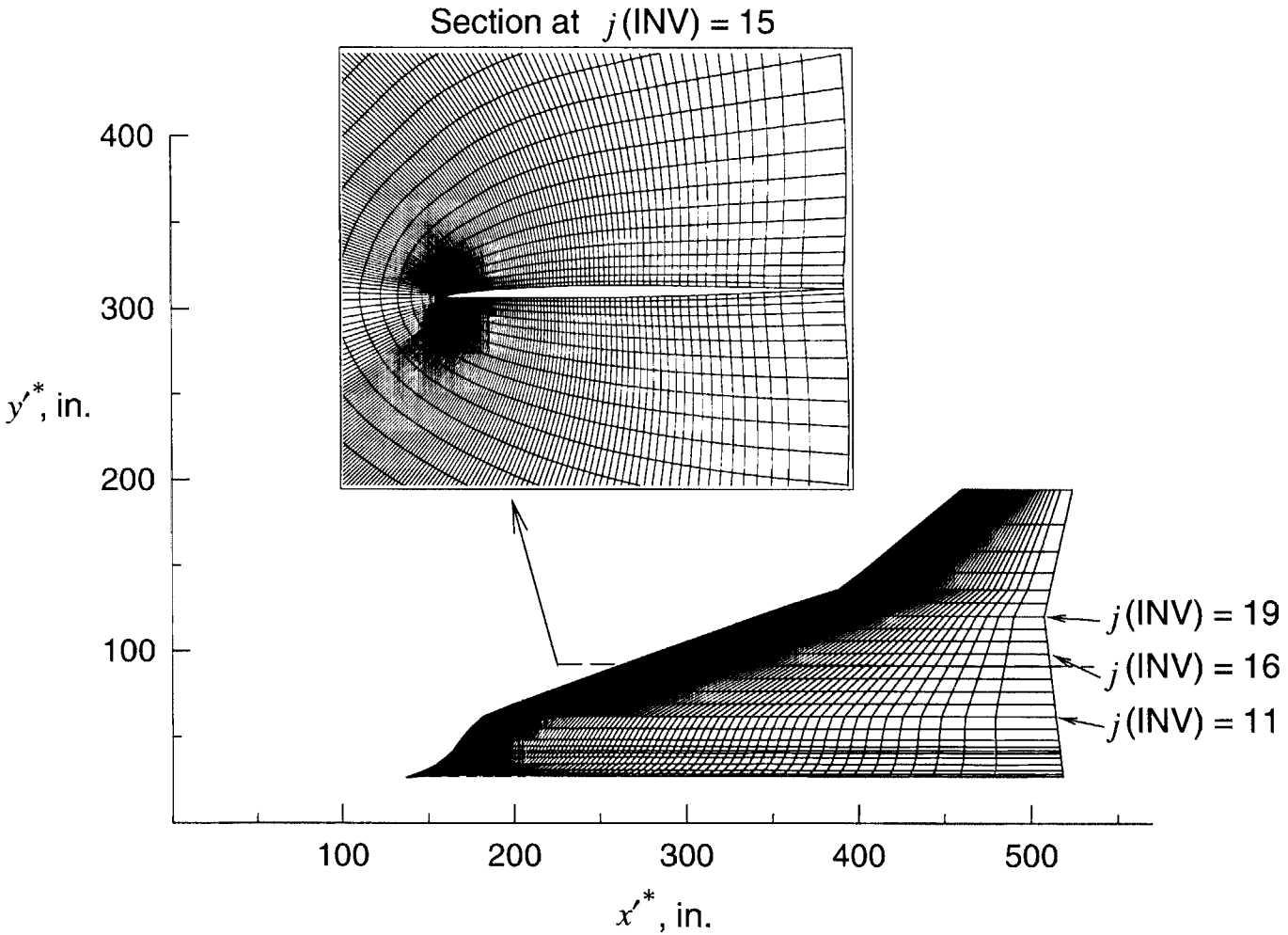

Figure 36. Euler grid for supersonic geometry, case 2.

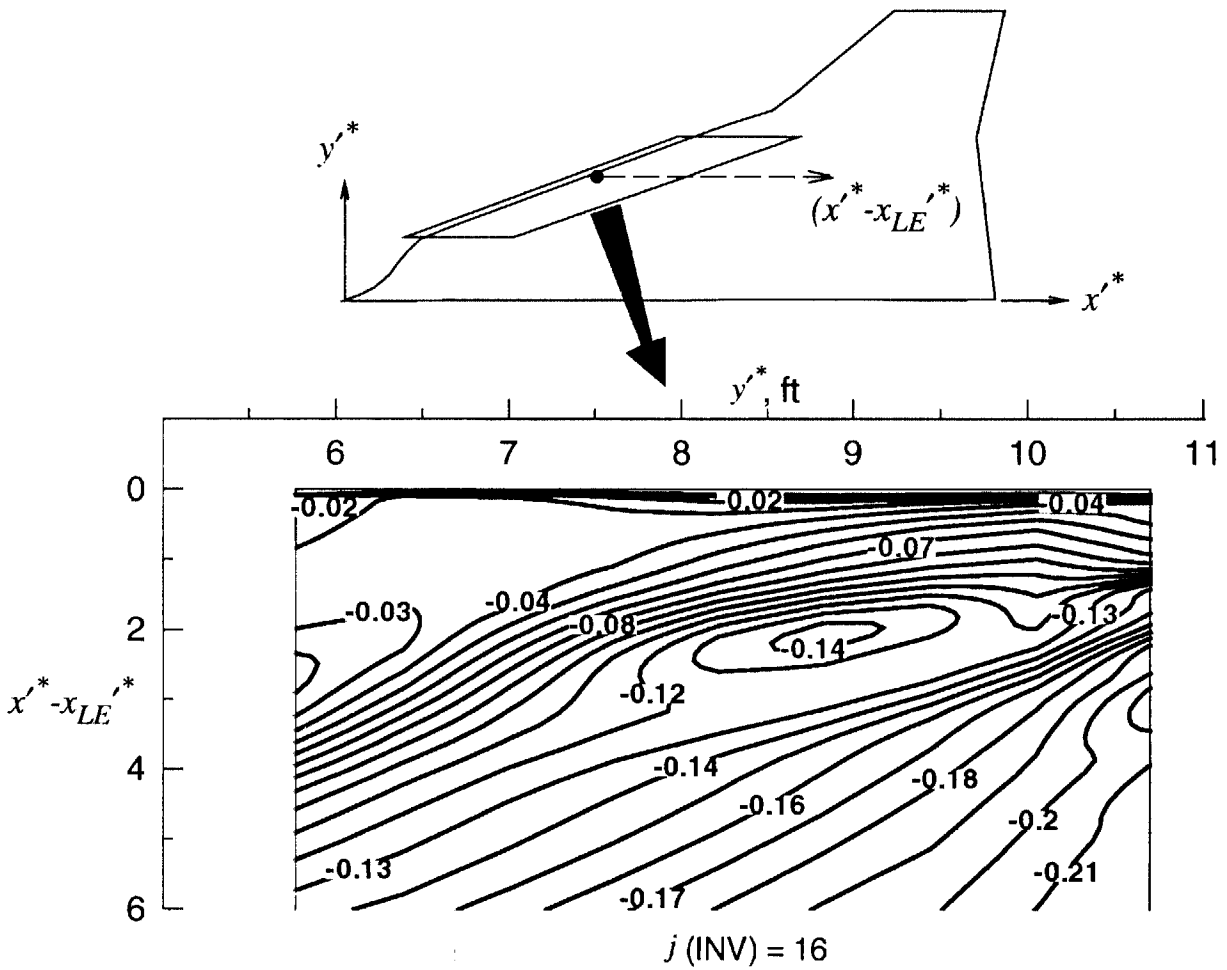

Figure 37. Contours of pressure coefficient for case 2, upper surface.

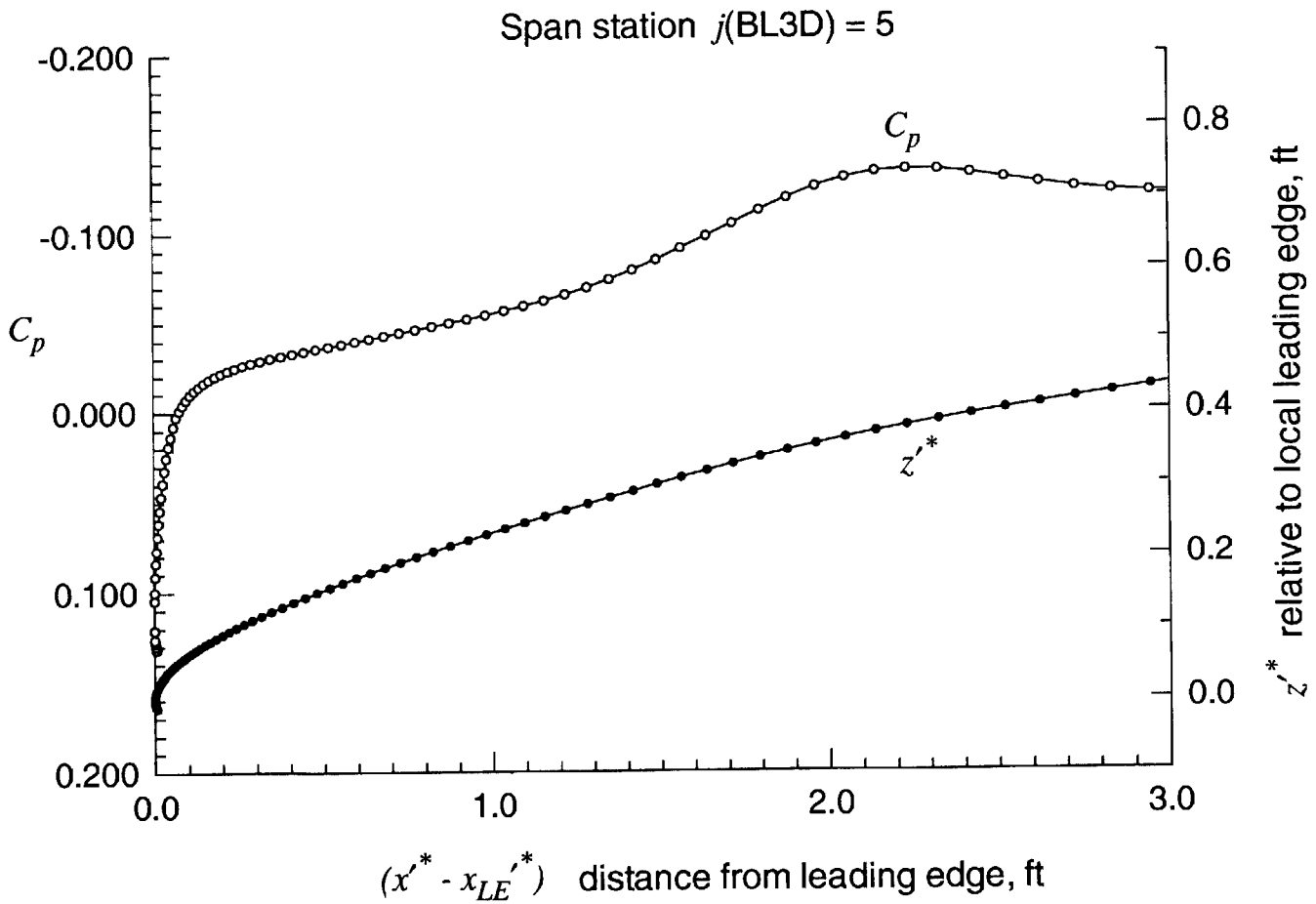

Figure 38. Pressure coefficient interpolated to BL3D grid, case 2.

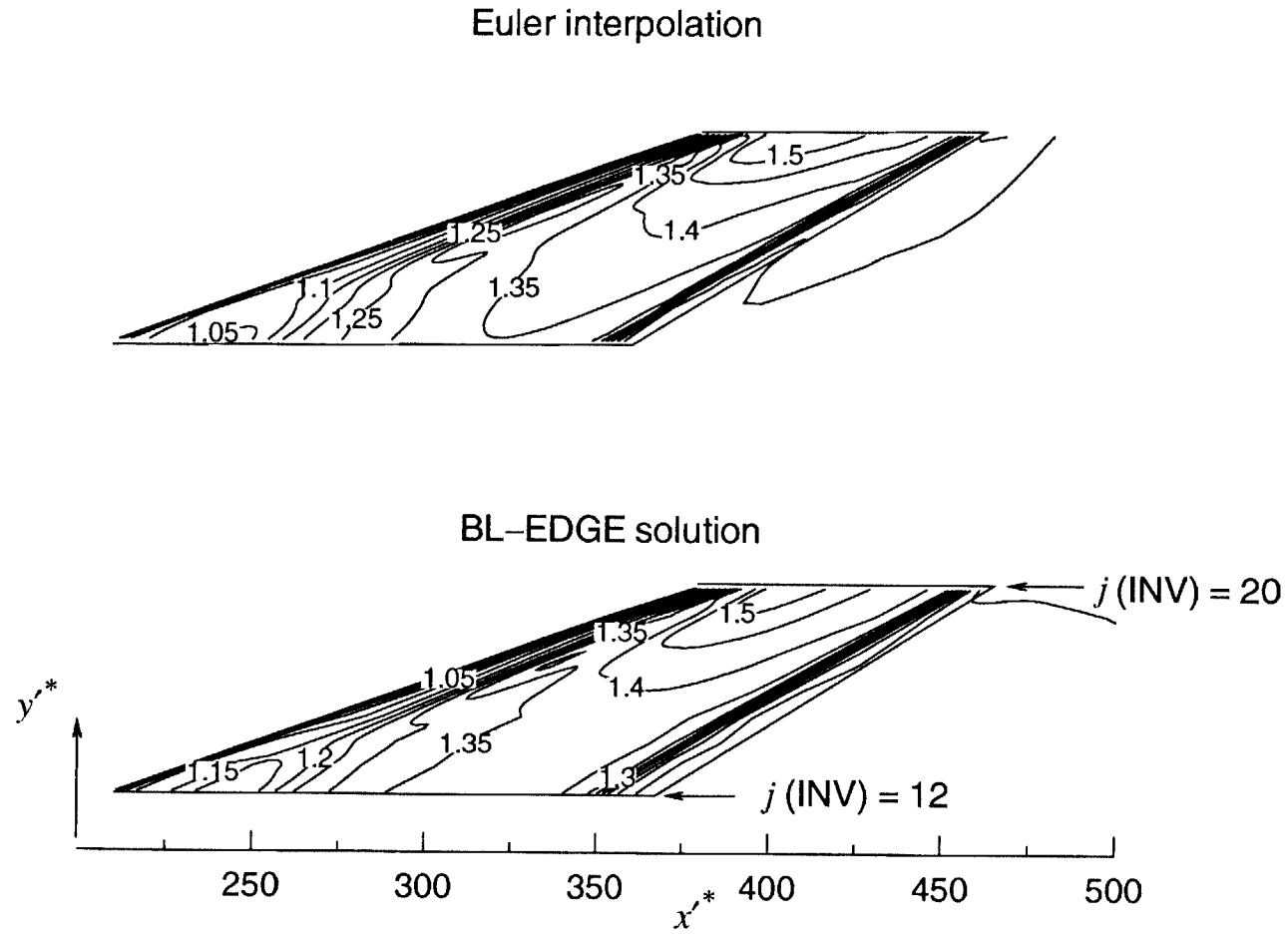

Figure 39. Comparison of contours of u_e from Euler and BL–EDGE solutions.

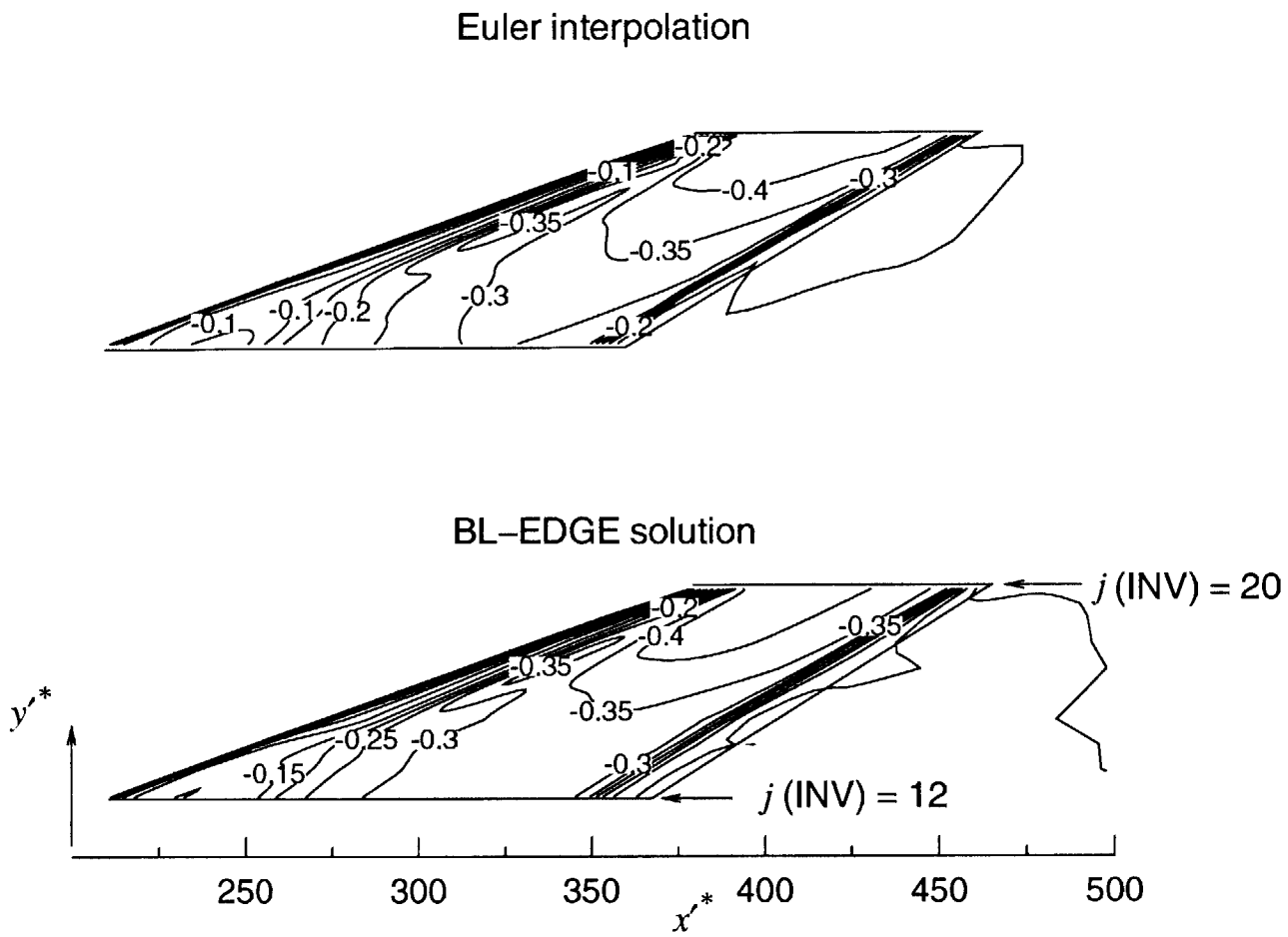

Figure 40. Comparison of contours of v_e from Euler and BL–EDGE solutions.

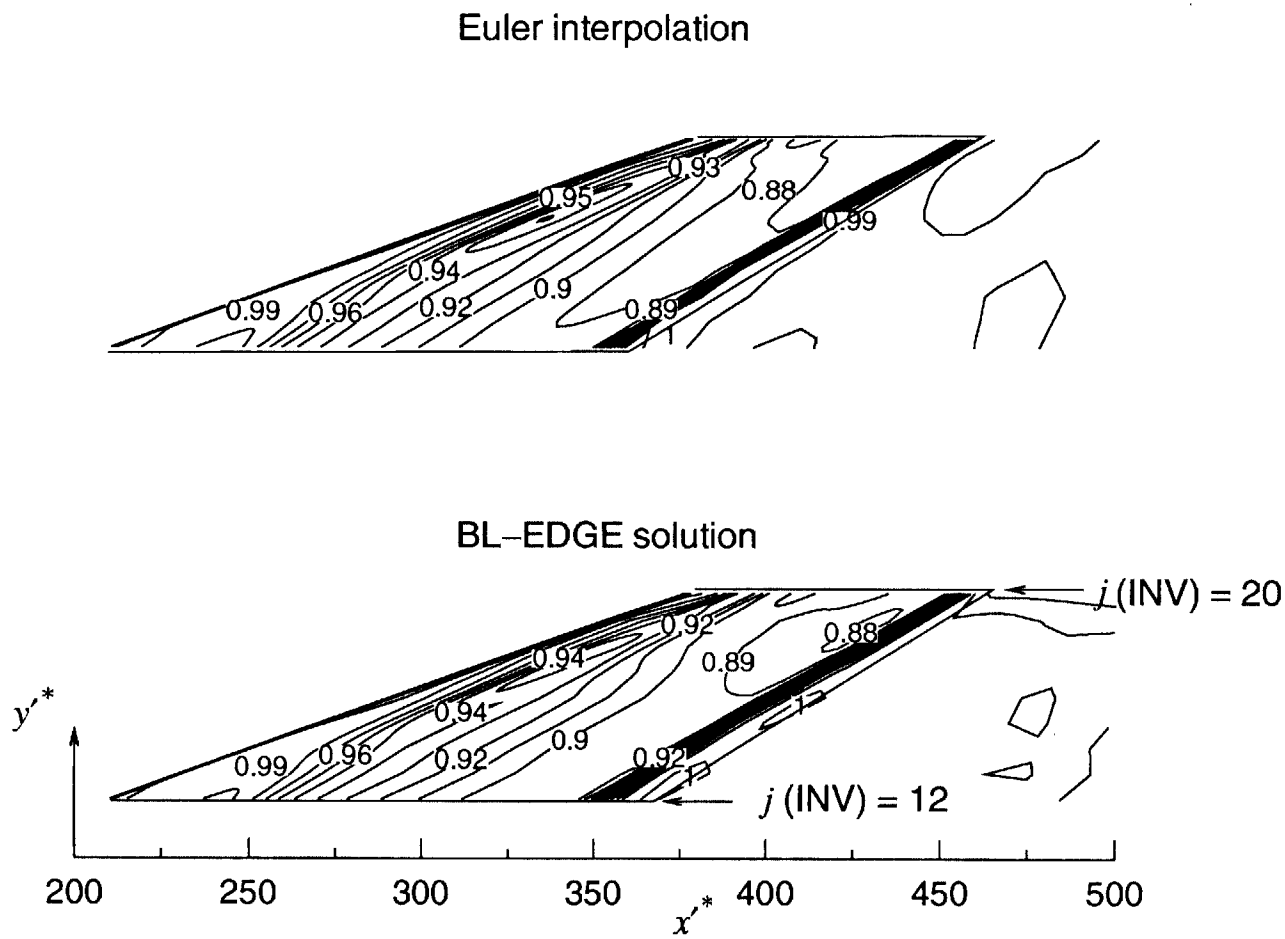

Figure 41. Comparison of contours of T_e from Euler and BL–EDGE solutions.

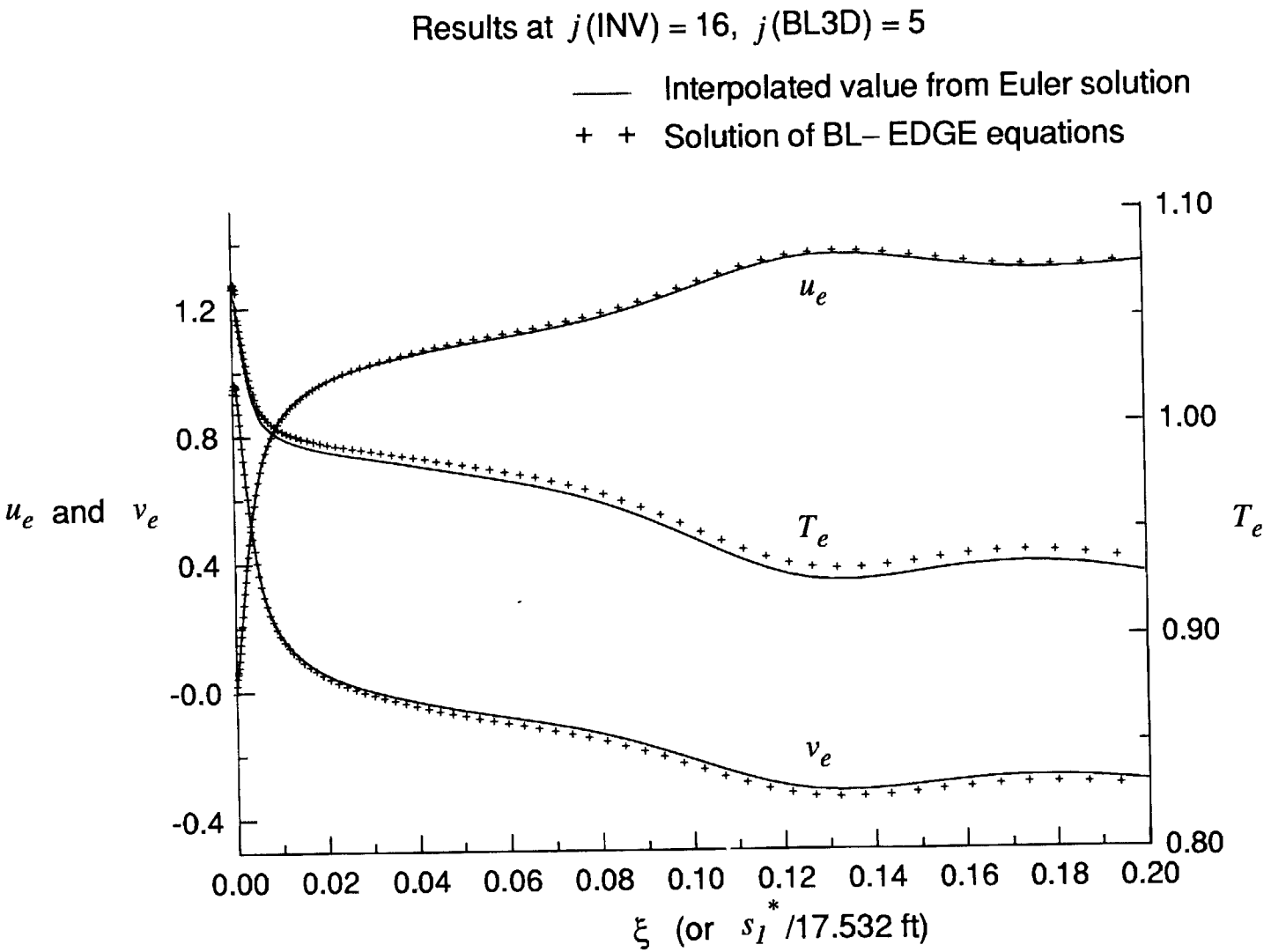

Figure 42. Comparison of BL– EDGE solution to Euler solution for case 2, upper surface.

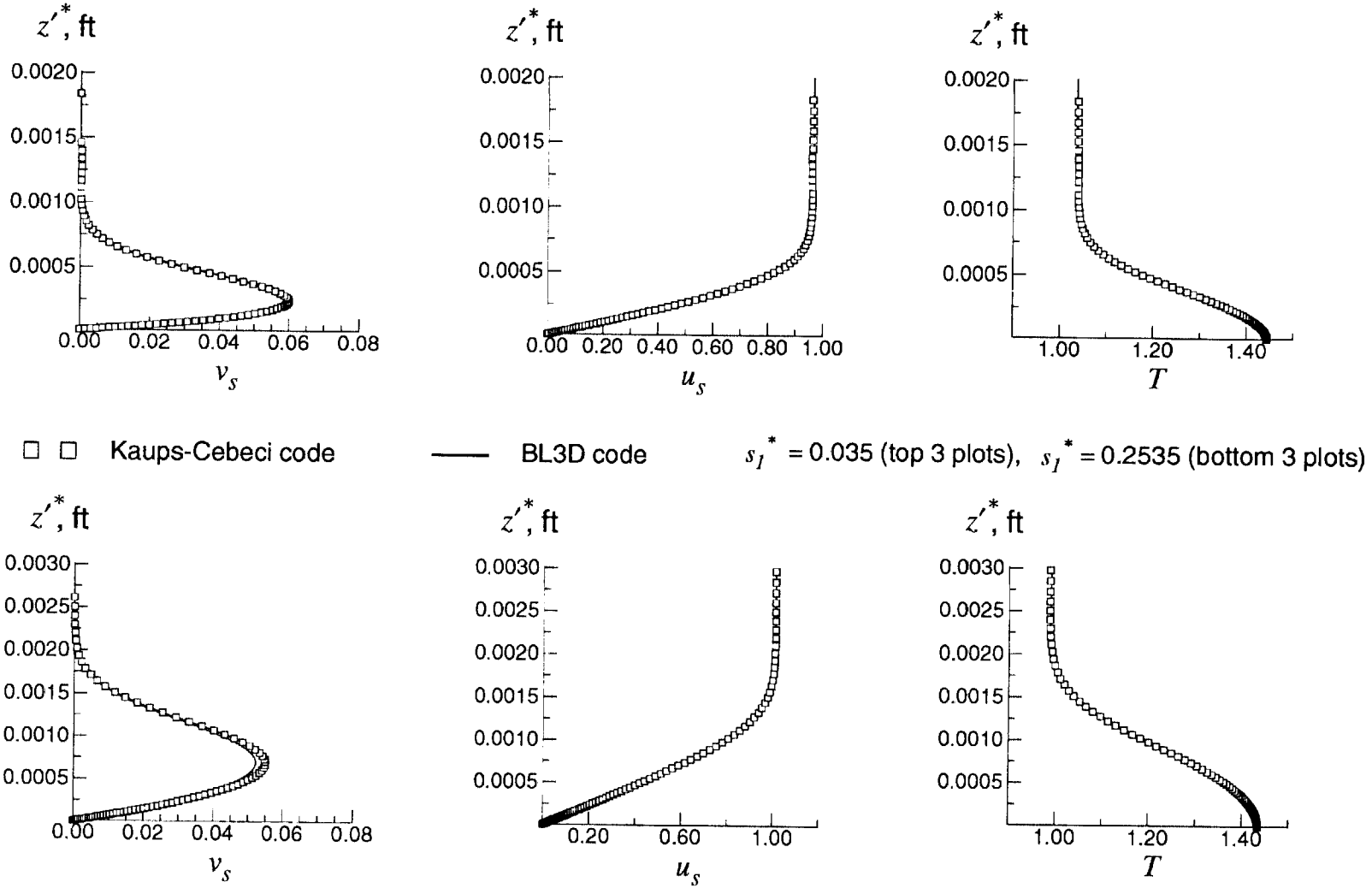

Figure 43. Comparison of solution profiles for case 2, s_1^* = 0.035 ft and s_1^* = 0.2535 ft.

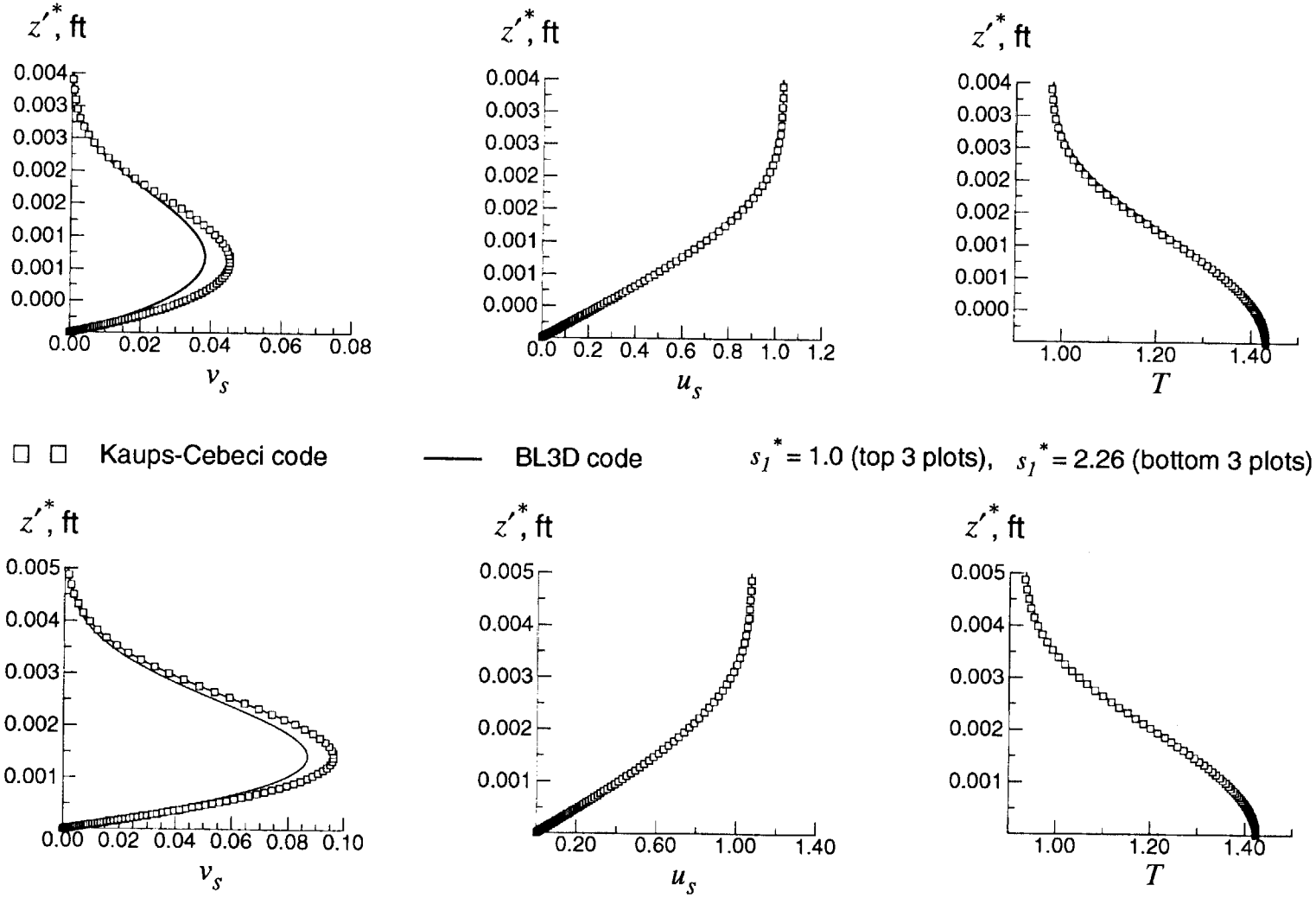

Figure 44. Comparison of solution profiles for case 2, s_1^* = 1.0 ft and s_1^* = 2.26 ft.

C-2

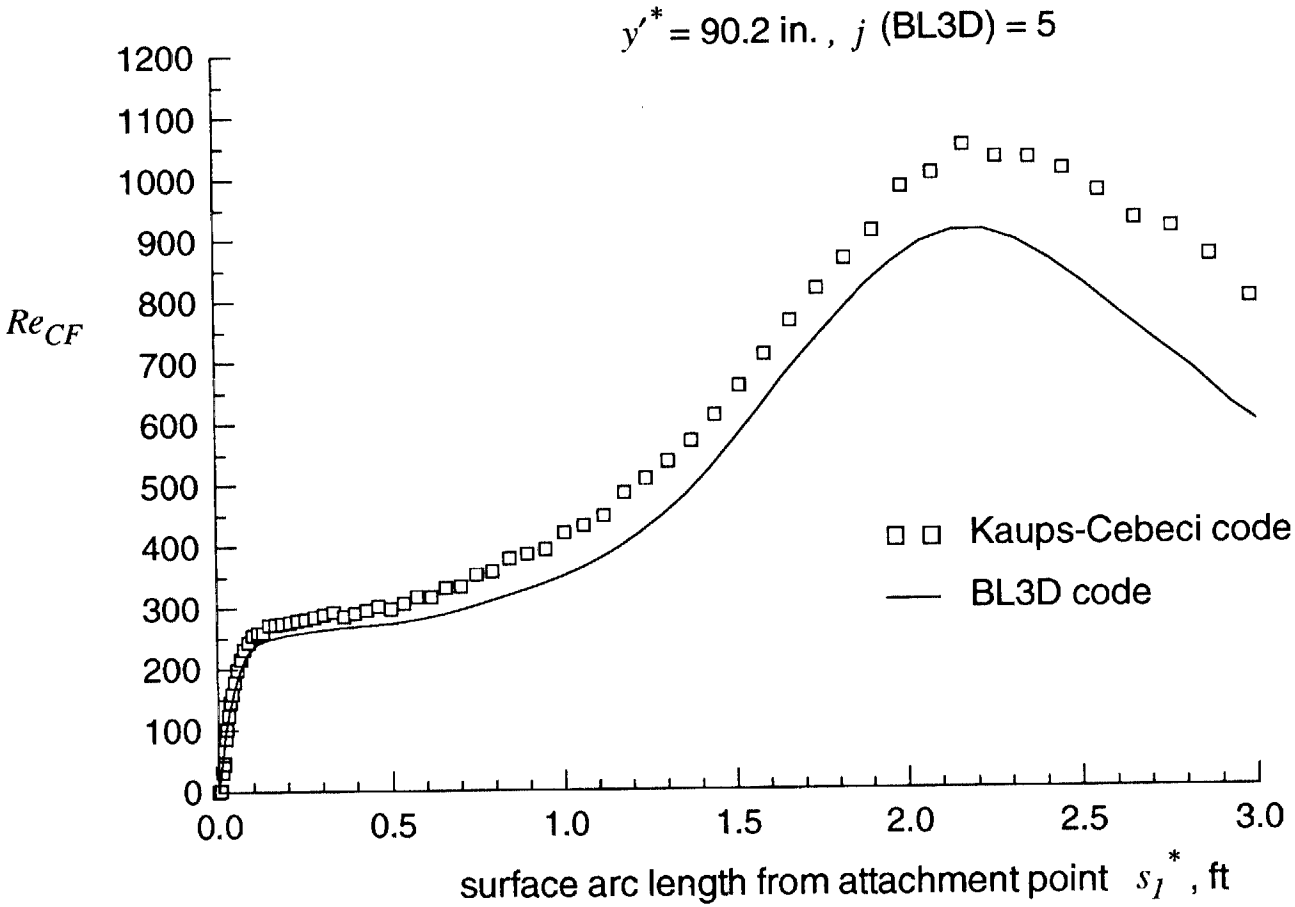

Figure 45. Comparison of crossflow Reynolds numbers at j(BL3D) = 5 for case 2.

Appendix A

Coefficients of the Linearized System of Compressible Three-Dimensional Boundary-Layer Equations Discretized With a Fourth-Order Pade Formula

(1) Coefficients of Continuity Equation:

$$a_{11}^k = -1$$
$$a_{12}^k = -c_{1k}(e_{11})_{k-1}$$
$$a_{13}^k = -c_{1k}(e_{12})_{k-1}$$
$$a_{14}^k = 0$$
$$a_{15}^k = -c_{2k}(e_{11})_{k-1}$$
$$a_{16}^k = -c_{2k}(e_{12})_{k-1}$$
$$a_{17}^k = 0$$

$$b_{11}^k = 1$$
$$b_{12}^k = -c_{1k}(e_{11})_k$$
$$b_{13}^k = -c_{1k}(e_{12})_k$$
$$b_{14}^k = 0$$
$$b_{15}^k = c_{2k}(e_{11})_k$$
$$b_{16}^k = c_{2k}(e_{12})_k$$
$$b_{17}^k = 0$$

$$r_1^k = -(q_{11})_k + (q_{11})_{k-1} + c_{1k}(q_{12})_k + c_{1k}(q_{12})_{k-1} - c_{2k}(q_{13})_k + c_{2k}(q_{13})_{k-1}$$

$$q_{11} = w$$
$$q_{12} = A_1 F_\xi + A_2 F + A_3 G_\eta + A_4 G$$
$$q_{13} = A_1 L_\xi + A_2 L + A_3 M_\eta + A_4 M$$
$$e_{11} = a_1 A_1 + A_2$$
$$e_{12} = b_1 A_3 + A_4$$

$$c_{1k} = \frac{1}{2}\Delta\zeta_k$$
$$c_{2k} = \frac{1}{12}\Delta\zeta_k^2$$
$$\Delta\zeta_k = \zeta_k - \zeta_{k-1}$$

(2) Coefficients of ξ Momentum Equation:

$$
\begin{aligned}
a_{21}^k &= F_{k-1} \\
a_{22}^k &= w_{k-1} - c_{1k}(e_{21})_{k-1} - c_{2k}(e_{22})_{k-1} \\
a_{23}^k &= -c_{1k}(e_{23})_{k-1} - c_{2k}(e_{24})_{k-1} \\
a_{24}^k &= -c_{1k}\tilde{B}_6 \\
a_{25}^k &= -l_{k-1} - c_{2k}(e_{21})_{k-1} \\
a_{26}^k &= -c_{2k}(e_{23})_{k-1} \\
a_{27}^k &= -c_{2k}\tilde{B}_6
\end{aligned}
$$

$$
\begin{aligned}
b_{21}^k &= -F_k \\
b_{22}^k &= -w_k - c_{1k}(e_{21})_k + c_{2k}(e_{22})_k \\
b_{23}^k &= -c_{1k}(e_{23})_k + c_{2k}(e_{24})_k \\
b_{24}^k &= -c_{1k}\tilde{B}_6 \\
b_{25}^k &= l_k + c_{2k}(e_{21})_k \\
b_{26}^k &= c_{2k}(e_{23})_k \\
b_{27}^k &= c_{2k}\tilde{B}_6
\end{aligned}
$$

$$
r_2^k = -(q_{21})_k + (q_{21})_{k-1} + c_{1k}(q_{22})_k + c_{1k}(q_{22})_{k-1} - c_{2k}(q_{23})_k + c_{2k}(q_{23})_{k-1}
$$

$$
\begin{aligned}
q_{21} &= (lL - wF) \\
q_{22} &= B_1\left(F^2\right)_\xi + B_2(FG)_\eta + \tilde{B}_3F^2 + \tilde{B}_4FG + \tilde{B}_5G^2 + \tilde{B}_6H \\
q_{23} &= 2B_1(FL)_\xi + B_2(FM + GL)_\eta + 2\tilde{B}_3FL + \tilde{B}_4(FM + GL) + 2\tilde{B}_5GM + \tilde{B}_6I \\
e_{21} &= \left(2a_1B_1 + 2\tilde{B}_3\right)F + \left(b_1B_2 + \tilde{B}_4\right)G \\
e_{22} &= \left(2a_1B_1 + 2\tilde{B}_3\right)L + \left(b_1B_2 + \tilde{B}_4\right)M \\
e_{23} &= \left(b_1B_2 + \tilde{B}_4\right)F + 2\tilde{B}_5G \\
e_{24} &= \left(b_1B_2 + \tilde{B}_4\right)L + 2\tilde{B}_5M
\end{aligned}
$$

(3) Coefficients of η Momentum Equation:

$$
\begin{aligned}
a_{31}^k &= G_{k-1} \\
a_{32}^k &= -c_{1k}(e_{31})_{k-1} - c_{2k}(e_{32})_{k-1} \\
a_{33}^k &= w_{k-1} - c_{1k}(e_{33})_{k-1} - c_{2k}(e_{34})_{k-1} \\
a_{34}^k &= -c_{1k}\tilde{C}_6 \\
a_{35}^k &= -c_{2k}(e_{31})_{k-1} \\
a_{36}^k &= -l_{k-1} - c_{2k}(e_{33})_{k-1} \\
a_{37}^k &= -c_{2k}\tilde{C}_6
\end{aligned}
$$

$$
\begin{aligned}
b_{31}^k &= -G_k \\
b_{32}^k &= -c_{1k}(e_{31})_k + c_{2k}(e_{32})_k \\
b_{33}^k &= -w_k - c_{1k}(e_{33})_k + c_{2k}(e_{34})_k \\
b_{34}^k &= -c_{1k}\tilde{C}_6 \\
b_{35}^k &= c_{2k}(e_{31})_k \\
b_{36}^k &= l_k + c_{2k}(e_{33})_k \\
b_{37}^k &= c_{2k}\tilde{C}_6
\end{aligned}
$$

$$
r_3^k = -(q_{31})_k + (q_{31})_{k-1} + c_{1k}(q_{32})_k + c_{1k}(q_{32})_{k-1} - c_{2k}(q_{33})_k + c_{2k}(q_{33})_{k-1}
$$

$$
\begin{aligned}
q_{31} &= (lM - wG) \\
q_{32} &= C_1(FG)_\xi + C_2\left(G^2\right)_\eta + \tilde{C}_3F^2 + \tilde{C}_4FG + \tilde{C}_5G^2 + \tilde{C}_6H \\
q_{33} &= C_1(FM + GL)_\xi + 2C_2(GM)_\eta + 2\tilde{C}_3FL + \tilde{C}_4(FM + GL) + 2\tilde{C}_5GM + \tilde{C}_6I \\
e_{31} &= 2\tilde{C}_3F + \left(a_1C_1 + \tilde{C}_4\right)G \\
e_{32} &= 2\tilde{C}_3L + \left(a_1C_1 + \tilde{C}_4\right)M \\
e_{33} &= \left(a_1C_1 + \tilde{C}_4\right)F + \left(2b_1C_2 + 2\tilde{C}_5\right)G \\
e_{34} &= \left(a_1C_1 + \tilde{C}_4\right)L + \left(2b_1C_2 + 2\tilde{C}_5\right)M
\end{aligned}
$$

(4) Coefficients of Energy Equation:

$$
\begin{aligned}
a_{41}^k &= H_{k-1} \\
a_{42}^k &= -c_{1k}(e_{41})_{k-1} - c_{2k}(e_{42})_{k-1} \\
a_{43}^k &= -c_{1k}(e_{43})_{k-1} - c_{2k}(e_{44})_{k-1} \\
a_{44}^k &= w_{k-1} - c_{1k}(e_{45})_{k-1} - c_{2k}(e_{46})_{k-1} \\
a_{45}^k &= -c_{2k}(e_{41})_{k-1} \\
a_{46}^k &= -c_{2k}(e_{43})_{k-1} \\
a_{47}^k &= -(l_p)_{k-1} - c_{2k}(e_{45})_{k-1}
\end{aligned}
$$

$$
\begin{aligned}
b_{41}^k &= -H_k \\
b_{42}^k &= -c_{1k}(e_{41})_k + c_{2k}(e_{42})_k \\
b_{43}^k &= -c_{1k}(e_{43})_k + c_{2k}(e_{44})_k \\
b_{44}^k &= -w_k - c_{1k}(e_{45})_k + c_{2k}(e_{46})_k \\
b_{45}^k &= c_{2k}(e_{41})_k \\
b_{46}^k &= c_{2k}(e_{43})_k \\
b_{47}^k &= (l_p)_k + c_{2k}(e_{45})_k
\end{aligned}
$$

$$
r_4^k = -(q_{41})_k + (q_{41})_{k-1} + c_{1k}(q_{42})_k + c_{1k}(q_{42})_{k-1} - c_{2k}(q_{43})_k + c_{2k}(q_{43})_{k-1}
$$

$$
\begin{aligned}
q_{41} &= (l_p I - wH) \\
q_{42} &= D_1(FH)_\xi + D_2(GH)_\eta + D_3 FH + D_4 GH + D_5 \\
q_{43} &= D_1(FI + HL)_\xi + D_2(GI + HM)_\eta + D_3(FI + HL) + D_4(GI + HM) + D_5' \\
e_{41} &= (a_1 D_1 + D_3)H \\
e_{42} &= (a_1 D_1 + D_3)I \\
e_{43} &= (b_1 D_2 + D_4)H \\
e_{44} &= (b_1 D_2 + D_4)I \\
e_{45} &= (a_1 D_1 + D_3)F + (b_1 D_2 + D_4)G \\
e_{46} &= (a_1 D_1 + D_3)L + (b_1 D_2 + D_4)M
\end{aligned}
$$

(5) Coefficients of F-L-L' Equation:

$$a_{51} = -c_{2k}\frac{1}{l_{k-1}}L_{k-1}$$
$$a_{52} = -1 - c_{2k}\frac{1}{l_{k-1}}(e_{51})_{k-1}$$
$$a_{53} = -c_{2k}\frac{1}{l_{k-1}}(e_{52})_{k-1}$$
$$a_{54} = -c_{2k}\frac{1}{l_{k-1}}\tilde{B}_6$$
$$a_{55} = -c_{1k} - c_{2k}\frac{1}{l_{k-1}}(-l' + w)_{k-1}$$
$$a_{56} = 0$$
$$a_{57} = 0$$

$$b_{51} = c_{2k}\frac{1}{l_k}L_k$$
$$b_{52} = 1 + c_{2k}\frac{1}{l_k}(e_{51})_k$$
$$b_{53} = c_{2k}\frac{1}{l_k}(e_{52})_k$$
$$b_{54} = c_{2k}\frac{1}{l_k}\tilde{B}_6$$
$$b_{55} = -c_{1k} + c_{2k}\frac{1}{l_k}(-l' + w)_k$$
$$b_{56} = 0$$
$$b_{57} = 0$$

$$r_5^k = -(q_{51})_k + (q_{51})_{k-1} + c_{1k}(q_{52})_k + c_{1k}(q_{52})_{k-1} - c_{2k}(q_{53})_k + c_{2k}(q_{53})_{k-1}$$

$$q_{51} = F$$
$$q_{52} = L$$
$$q_{53} = \frac{1}{l}\Big\{ B_1(F^2)_\xi + B_2(FG)_\eta + \hat{B}_3F^2 + \hat{B}_4FG + \tilde{B}_5G^2 + \tilde{B}_6H - Ll' + wL + A_1FF_\xi + A_3FG_\eta \Big\}$$
$$e_{51} = \Big(2a_1B_1 + 2\hat{B}_3 + a_1A_1\Big)F + \Big(b_1B_2 + \hat{B}_4\Big)G + A_1F_\xi + A_3G_\eta$$
$$e_{52} = \Big(b_1B_2 + \hat{B}_4 + b_1A_3\Big)F + 2\tilde{B}_5G$$

(6) Coefficients of G-M-M' Equation:

$$a_{61} = -c_{2k}\frac{1}{l_{k-1}}M_{k-1}$$
$$a_{62} = -c_{2k}\frac{1}{l_{k-1}}(e_{61})_{k-1}$$
$$a_{63} = -1 - c_{2k}\frac{1}{l_{k-1}}(e_{62})_{k-1}$$
$$a_{64} = -c_{2k}\frac{1}{l_{k-1}}\tilde{C}_6$$
$$a_{65} = 0$$
$$a_{66} = -c_{1k} - c_{2k}\frac{1}{l_{k-1}}(-l' + w)_{k-1}$$
$$a_{67} = 0$$

$$b_{61} = c_{2k}\frac{1}{l_k}M_k$$
$$b_{62} = c_{2k}\frac{1}{l_k}(e_{61})_k$$
$$b_{63} = 1 + c_{2k}\frac{1}{l_k}(e_{62})_k$$
$$b_{64} = c_{2k}\frac{1}{l_k}\tilde{C}_6$$
$$b_{65} = 0$$
$$b_{66} = -c_{1k} + c_{2k}\frac{1}{l_k}(-l' + w)_k$$
$$b_{67} = 0$$

$$r_6^k = -(q_{61})_k + (q_{61})_{k-1} + c_{1k}(q_{62})_k + c_{1k}(q_{62})_{k-1} - c_{2k}(q_{63})_k + c_{2k}(q_{63})_{k-1}$$

$$q_{61} = G$$
$$q_{62} = M$$
$$q_{63} = \frac{1}{l}\Big\{C_1(FG)_\xi + C_2(G^2)_\eta + \tilde{C}_3F^2 + \hat{C}_4FG + \hat{C}_5G^2 + \tilde{C}_6H$$
$$- Ml' + wM + A_1GF_\xi + A_3GG_\eta\Big\}$$

$$e_{61} = 2\tilde{C}_3F + \Big(a_1C_1 + \hat{C}_4 + a_1A_1\Big)G$$
$$e_{62} = \Big(a_1C_1 + \hat{C}_4\Big)F + \Big(2b_1C_2 + 2\hat{C}_5 + b_1A_3\Big)G + A_1F_\xi + A_3G_\eta$$

(7) Coefficients of H-I-I' Equation:

$$a_{71} = -c_{2k}\frac{1}{(l_p)_{k-1}}w_{k-1}$$
$$a_{72} = -c_{2k}\frac{1}{(l_p)_{k-1}}(e_{71})_{k-1}$$
$$a_{73} = -c_{2k}\frac{1}{(l_p)_{k-1}}(e_{72})_{k-1}$$
$$a_{74} = -1 - c_{2k}\frac{1}{(l_p)_{k-1}}(e_{73})_{k-1}$$
$$a_{75} = 0$$
$$a_{76} = 0$$
$$a_{77} = -c_{1k} - c_{2k}\frac{1}{(l_p)_{k-1}}(-l'_p + w)_{k-1}$$
$$b_{71} = c_{2k}\frac{1}{(l_p)_k}w_k$$
$$b_{72} = c_{2k}\frac{1}{(l_p)_k}(e_{71})_k$$
$$b_{73} = c_{2k}\frac{1}{(l_p)_k}(e_{72})_k$$
$$b_{74} = 1 + c_{2k}\frac{1}{(l_p)_k}(e_{73})_k$$
$$b_{75} = 0$$
$$b_{76} = 0$$
$$b_{77} = -c_{1k} + c_{2k}\frac{1}{(l_p)_k}(-l'_p + w)_k$$
$$r_7^k = -(q_{71})_k + (q_{71})_{k-1} + c_{1k}(q_{72})_k + c_{1k}(q_{72})_{k-1} - c_{2k}(q_{73})_k + c_{2k}(q_{73})_{k-1}$$
$$q_{71} = H$$
$$q_{72} = I$$
$$q_{73} = \frac{1}{l_p}\Big\{D_1(FH)_\xi + D_2(GH)_\eta + \tilde{D}_3FH + \tilde{D}_4GH + D_5 - Il'_p + wI + A_1HF_\xi + A_3HG_\eta\Big\}$$
$$e_{71} = \Big(a_1D_1 + \tilde{D}_3 + a_1A_1\Big)H$$
$$e_{72} = \Big(b_1D_2 + \tilde{D}_4 + b_1A_3\Big)H$$
$$e_{73} = \Big(a_1D_1 + \tilde{D}_3\Big)F + \Big(b_1D_2 + \tilde{D}_4\Big)G + A_1F_\xi + A_3G_\eta$$

Appendix B

User's Manual for the BL3D Program

The BL3D program package consists of a collection of program files, input files, and output files that relate to the solution of three-dimensional boundary-layer flow on a swept wing. In addition to the BL3D program files, the program package includes files related to the Euler and Navier-Stokes calculations for the two example cases and the interface programs. Some of these files are not directly related to the core program BL3D, but were developed for the validation of the code. These include Euler and Navier-Stokes grid and solution files as well as programs used in processing the Navier-Stokes results for comparison with the BL3D results. All the files have been archived on the NASA Langley Masstor system and can be made available per individual request.

Table 1 at the end of this section gives a list of important computer variable names used in the programs and the corresponding translation to the variables used in the formulation as listed in "Nomenclature". This list may be useful for customizing the program for a particular application.

Program Structure

The files are divided into subdirectories as follows. Each subdirectory contains a README file with a short description of the contents of the subdirectory and instructions for running the programs.

bl3d/euler/case1. Contains files that correspond to generation of the Euler solution for case 1 (subsonic swept wing) with the code CFL3D. The program CFL3D is not included.

bl3d/interface/case1. Contains interface programs and input files used in processing the Euler solution for case 1 and generation of the data file required in the BL3D run.

bl3d/bl/case1. Contains the BL3D program files used for case 1.

bl3d/ns/case1. Contains files that correspond to the Navier-Stokes solution with CFL3D for case 1.

Similarly, `bl3d/euler/case2`, `bl3d/interface/case2`, `bl3d/bl/case2`, `bl3d/ns/case2` are subdirectories that correspond to case 2 runs for a supersonic swept wing. The subdirectory `bl3d/ns/case2` contains files that relate to the application of the Kaups-Cebeci code for case 2.

The files in the subdirectories `bl3d/euler` and `bl3d/ns` are not of direct interest here. The `README` files in these subdirectories and comment statements in the program files may be consulted for more detailed information. Presented below are details on the interface and boundary-layer program files for the two test cases.

Interface Program Inputs

The inviscid results are assumed to be available on a grid that is generally (though not strictly) oriented along the constant span and constant chord directions. The boundary-layer grid stretching, the interpolation, and the BL–EDGE solution procedure are based on this assumption. The surface grid is also, in general, nonorthogonal. The inviscid Euler results are assumed to be available in either of the two following formats:

(a) Two separate files, one of which contains the grid points and the other, which contains the Euler solution at the cell center points. The actual read statement (e.g., from `bl3d/interface/case1/rinvis.f`) is as follows:

The grid file:

```
open(unit=1,file='grid',form='unformatted',status='old')
read(1) jdim,kdim,idim
read(1)(((xg(j,k,i),j=1,jdim),k=1,kdim),i=1,idim),
       (((yg(j,k,i),j=1,jdim),k=1,kdim),i=1,idim),
       (((zg(j,k,i),j=1,jdim),k=1,kdim),i=1,idim)
```

The solution file:

```
dimension titlw(20)
open(unit=1,file='rest.bin',form='unformatted',status='old')
read(2) titlw,xmachw,jt,kt,it,alphw,ntr,ntime
read(2)((((q(j,k,i,l),j=1,jdim-1),k=1,kdim-1),i=1,idim-1),l=1,5)
```

The above file format corresponds to output from the program CFL3D. The `i,j,k` indices in the read statement are defined differently compared to the BL3D terminology. Here, `i` refers to the span direction, and `j` refers to the chord wraparound direction that starts from the wing lower surface trailing edge or the downstream plane of the lower surface wake. Note that in this case the solution points are one less than the grid points because they are obtained at the cell centers. Following these read statements, the `i,j` indices are switched to correspond to BL3D notation and are normalized with the reference length `reflen`. The coordinates and solution on the wing surface alone are then extracted. In some cases, the sign of the coordinate `y` and velocity component `vc` may have to be switched because in BL3D the coordinate system assumes a right wing. The variable `q` contains the solution vector in standard CFL3D notation (see the `README` file for more detailed information).

(b) A provision is included in the interface program to input the inviscid data on the surface only from a single ASCII file in the following format:

```
open(unit=21,file='edge.dat',status='unknown')
read(21,*)iv,jv
read(21,*)((xc(i,j),i=1,iv),j=1,jv)
read(21,*)((yc(i,j),i=1,iv),j=1,jv)
read(21,*)((zc(i,j),i=1,iv),j=1,jv)
read(21,*)((uc(i,j),i=1,iv),j=1,jv)
read(21,*)((vc(i,j),i=1,iv),j=1,jv)
read(21,*)((wc(i,j),i=1,iv),j=1,jv)
read(21,*)((tc(i,j),i=1,iv),j=1,jv)
read(21,*)((pc(i,j),i=1,iv),j=1,jv)
read(21,*)((xs(i,j),i=1,iv+1),j=1,jv+1)
read(21,*)((ys(i,j),i=1,iv+1),j=1,jv+1)
read(21,*)((zs(i,j),i=1,iv+1),j=1,jv+1)
```

The variables `iv,jv` refer to the surface grid cell center dimensions in the chord wraparound direction and the span direction. The variables `xc,yc,zc` are coordinates of the cell centers (assumed to be nondimensionalized with `reflen`) and `uc,vc,wc` are

the Cartesian velocity components (normalized by free-stream velocity) from the inviscid solution at the cell centers. The variables `tc,pc` are nondimensional temperature and pressure coefficient values at the cell centers. The variables `xs,ys,zs` are the actual normalized grid locations (not used in the program except for plot output).

The input file for the interface run is in the following format:

bl3d/interface/case1/inp.dat

```
CASE 1, INTERFACE RUN
amach      gam        isurf      istart
0.5        1.40       1          0
ite1       ite2       jte1       jte2
33         289        1          43
j1         j2         reflen
7          35         1.0
ncp        xcp
40         0.05
itat       uerlim     omatt
50         0.0002     0.8
nxw        j1w        j2w        iout
100        7          35         1
```

Note that each input line is preceded by a line that contains a description of the input variables (read as a character variable and ignored). The description of the input variables is as follows:

amach	Mach number
gam	ratio of specific heats
isurf	upper or lower surface (1 or 0)
istart	restart option =0 full run, input from inviscid files 'grid', 'rest.bin' =1 run with data read from 'edge.dat' =2 read inviscid files, write 'edge.dat' and stop
ite1,ite2,jte1,jte2	indices corresponding to wing edges ite1,ite2: lower and upper surface TE indices (inviscid data assumed to be indexed in the chord-wrap-around direction from lower TE to LE to upper TE) jte1,jte2; span direction wing boundaries
j1,j2	limit inviscid data processing to (j1->j2)
reflen	normalizing length, usually root chord; if grid units are in inches for example,

	reflen can be used to be consistent with units
ncp,xcp	number of points in the BL grid between attachment point and local chord fraction =xcp (30,0.05 for example for 30 points from attach. point to 5% chord location)
itat,uerlim,omatt	max number or attachment point relocation iterations and error tolerance on ue (20,0.001 recommended) omatt is a relaxation factor for attachment point relocation iteration,<1; smaller values give slower convergence, but less oscillation
nxw,j1w,j2w	BL3D output option output file write will be from i=1 to i=nxw, j=j1w to j=j2w nxw.LE.nx; j1w.GE.j1 ; j2w.LE.j2 if nxw is set to 0, nxw taken to be=nx
iout	=1, output interpolated ue,ve,te values =2, output ue,ve,te from solution of BL-EDGE equations

Note that the `istart=1` option corresponds to the input of inviscid data from a single ASCII file as described previously. If the calculation is for the lower surface (`isurf=0`) and if `istart=0`, then the program reverses the `i` indexing direction (in effect, the lower surface becomes the upper surface of an inverted wing).

Interface Program Output

The output for the BL3D code is written to a binary file called `bl.bin`. The format for this write is as follows (see also the file `blout.f`):

```
nyw=j2w-j1w+1
write(10)nxw,nyw
write(10)((x(i,j),i=1,nxw),j=j1w,j2w)
write(10)((y(i,j),i=1,nxw),j=j1w,j2w)
write(10)((h1(i,j),i=1,nxw),j=j1w,j2w)
write(10)((h2(i,j),i=1,nxw),j=j1w,j2w)
write(10)((g12(i,j),i=1,nxw),j=j1w,j2w)
if(iout.eq.1)then
write(10)((ue(i,j),i=1,nxw),j=j1w,j2w)
write(10)((ve(i,j),i=1,nxw),j=j1w,j2w)
else
write(10)((use(i,j),i=1,nxw),j=j1w,j2w)
write(10)((vse(i,j),i=1,nxw),j=j1w,j2w)
```

```
endif
write(10)((pb(i,j),i=1,nxw),j=j1w,j2w)
if(iout.eq.1)then
write(10)((tb(i,j),i=1,nxw),j=j1w,j2w)
else
write(10)((tse(i,j),i=1,nxw),j=j1w,j2w)
endif
write(10)((xb(i,j),i=1,nxw),j=j1w,j2w)
write(10)((yb(i,j),i=1,nxw),j=j1w,j2w)
write(10)((zb(i,j),i=1,nxw),j=j1w,j2w)
write(10)((ub(i,j),i=1,nxw),j=j1w,j2w)
write(10)((vb(i,j),i=1,nxw),j=j1w,j2w)
write(10)((wb(i,j),i=1,nxw),j=j1w,j2w)
write(10)(xsave(nx,j),j=j1w,j2w)
```

The output of `xsave` corresponds to the normalizing arc length values used in each span station `j=j1w,j2w`. Note that the dimensional distance from the attachment line in the x direction (i.e., surface arc length) is given by `x(i,j)*xsave(j)*reflen`. Other output files contain information about attachment-line iteration convergence, the accuracy of the interpolation, and the BL–EDGE solution. The files `README`, `main.f`, as well as comment statements throughout the various subroutines, may be consulted for more information on these outputs.

Running the Interface Program

The program routines are contained in the following files:

```
main.f
attach.f
blout.f
inputs.f
metrix.f
pack.f
ploti.f
rinvis.f
sdist.f
solv3.f

surf.f
```

In addition, the `include` files `com`, `compack`, the makefile `makefile`, and the input file `inp.dat` are also provided. A brief description of some of these files follows:

`inputs.f`. Reads the input file `inp.dat`.

`rinvis.f`. Reads the inviscid data; extracts required data needed for the upper or lower surface; normalization of coordinates and flow quantities.

`attach.f`. Locates the initial attachment line (for first pass only); generates a boundary-layer surface grid that originates from the currently defined attachment line; calls `sdist.f` for a suitable grid stretching.

`metrix.f`. Calculates metric quantities `h1,h2,g12` based on currently defined boundary-layer grid.

`surf.f`. Solves the BL–EDGE equations if this input option is selected.

`blout.f`. Outputs the file `bl.bin` required for BL3D run.

`pack.f`. Library of cubic tension spline interpolation routines.

The `include` file `com` has the following parameter statements (which correspond to case 1 in this example):

```
parameter(jdim=321,kdim=49,idim=53)
parameter(ivm=257,jvm=43)
parameter(nxm=300,nym=jvm)
```

The dimensions depend on the inviscid grid size and the boundary-layer grid size; see comment statements in the file `com` for selection of these values.

The `include` file `compack` is used in conjunction with the spline routines in `pack.f`.

The program is run as follows: choose appropriate dimensions in the `parameter` statements in the file `com`; remove all `.o` files if `com` is modified; then type `make` followed by `a.out` to run the program. The output files `fort.3, fort.20, fort.30, fort.31, fort.32, fort.50, fort.51, fort.99` are useful for plotting or checking the results. Please refer to the various subroutines for a description of these outputs.

An appropriate selection of input quantities and inviscid data of good resolution are required for successful completion of the interface run. Run times on the Cray are only a

few CPU seconds so that runs can usually be made interactively. Some error messages and suggested fixes are given below.

```
error from s/r SDIST; ipass=...
no solution for ak found in the range ... to ...',
change ak or dak values in s/r ATTACH or

change input values of ncp,xcp ...'
```

The possible problem here is the use of inappropriate boundary-layer grid stretching; try a different combination of `ncp,xcp`. The inviscid grid may also be too coarse near the leading edge.

```
Convergence to uerlim not achieved
```

This problem is due to the lack of convergence in the attachment-line relocation loop; choose a lower value of `omatt` or increase `itat,uerlim` values. If various combinations do not work, inviscid data is too coarse or the solution near the attachment line is not smooth enough or the inviscid attachment line is too curved.

```
no convergence; s/r surf
i,j =...
ii,use(ii,j),vse(ii,j),hse(ii,j),pb(ii,j)

..      ..          ..          ..          ..
```

This problem is due to lack of convergence in the BL–EDGE equations, which is invariably caused by a small nonnegative $\partial P/\partial x$ at the attachment line. The nonnegative $\partial P/\partial x$ is caused by an amplification in the oscillations in pressure near the attachment line from the spline interpolation caused by a coarse inviscid grid. One possible fix is to drop back to linear interpolation for P for a few points near the attachment line. Some comment statements can be found in `attach.f`, which can be "uncommented" to drop back to linear interpolation.

Boundary-Layer Program Inputs

The inputs to the boundary-layer program are composed of two files:

(a) The boundary-layer edge data file `bl.bin`. This binary file is created by running the interface program and is assumed to be available in the current directory (`bl/case1`, for example). The format for this file has been described previously. This file is read in the subroutine `rinvis`.

(b) The boundary-layer input options file `inp.dat`. This file is read in the subroutine `inputs` and is assumed to be in the following format (note that each input line is preceded by a line that contains a description of the input variables, which is read as a character variable and ignored):

bl3d/bl/case1/inp.dat

```
CASE 1 : BL INPUTS
AMACH      PFS        TFS        PRL        IWALL      REFLEN     IUNIT
0.5        2000       520        0.72         0        1.0        0
ZMAX       AK         NXLIM      NYLIM
8.0        1.05       68         29
ITMAX      EPSF       EPSG       EPSH       IORD

20        1.e-6     1.e-6      1.e-06       5
```

The description of the input variables is given below:

```
amach           free-stream Mach number

pfs             free-stream static pressure (lb/ft2)

tfs             free-stream static temperature (deg R)

prl             laminar Prandtl number

iwall           wall boundary condition
                =0  adiabatic wall
                =1  wall temperature, deg R specified
                    (read in 'main.f')
                =2  wall heat flux specified ,lb/(ft.sec)
                    (read in main.f)
                 note: suction rates are also specified in 'main.f'

reflen          reference length in ft.
                (similar to input in interface program, but in ft.)
```

iunit	US or SI units, =0 for US units SI units not currently implemented
zmax	maximum value of transformed variable 'zeta' corresponding to boundary-layer edge
ak	stretching coefficient by which points are distributed away from the wall
nxlim	number of stations to march in x direction
nylim	number of span-wise stations in y direction
itmax	maximum number of iterations at each (i,j) point
epsf	convergence criterion for f-prime at wall
epsh	convergence criterion for h-prime at wall
iord	value of i for which scheme becomes fully second- order in the stream-wise direction

Boundary-Layer Program Outputs

The output from the boundary-layer program is output to several `fort.` files. The convergence information can be found in `fort.2`. Most of the results are output from `subroutine phys` and can be modified as required. The output quantities include z^*, u, v, T profiles; boundary-layer thickness, displacement thickness, and skin-friction coefficient; streamwise and crossflow profiles; and crossflow Reynolds number. Please refer to `subroutine phys` for more details. Note that these "writes" are for each (i, j) location (with j as the inner loop).

Output Format for Stability Analysis

The output of profiles and their derivatives to first and second order, as well as edge-normalizing quantities, are made in the format described below.

```
open(unit=7,file='fort.7',form='unformatted',status='unknown')
write(7)title
```

Title in `character*80`.

```
write(7)nxlim,nylim,reflen
```

nxlim is number of chordwise stations.

nylim is number of spanwise stations.

reflen is reference length, dimensional.

```
write(7)pfs,tfs,ufs,amach,rofs
```

Quantities $P_\infty^*, T_\infty^*, U_\infty^*, M_\infty, \rho_\infty^*$.

For each profile i=1,nxlim; j=1,nylim:

```
write(7)i,j,nz,x(i,j),y(i,j),xbs,ybs,zbs
write(7)h1(i,j),h2(i,j),g12(i,j),s1s
write(7)ues,ves,tes,roes,pes,res,ales,prl,deltax,thetax,rcr
```

i is streamwise index.

j is spanwise index.

nz is no. of points in profile (constant).

x(i,j) is boundary-layer coordinate x.

y(i,j) is boundary-layer coordinate y.

xbs,ybs,zbs are Cartesian coordinates x'^*, y'^*, z'^*.

h1(i,j),h2(i,j),g12(i,j) are metrics h_1, h_2, g_{12}.

s1s is $s_1{}^*$, dimensional arc-length in the x direction.

ues,ves,tes,roes,pes are edge quantities $u_e{}^*$, $v_e{}^*$, $T_e{}^*$, $\rho_e{}^*$, $P_e{}^*$.

For i=1, $\partial u_e^*/\partial s_1^*$ is output instead of $u_e{}^*$.

res is local Reynolds number based on $s_1{}^*$, $u_e{}^*$, $\nu_e{}^*$.

ales is reference length by which normal distance is scaled.

ales $= l^* = \sqrt{\nu_e^*/\frac{\partial u_e^*}{\partial s_1^*}}$ for i=1.

ales = $l^* = \sqrt{\nu_e^* s_1^* / u_e^*}$ for i>1.

prl is laminar Prandtl number.

deltax is boundary-layer thickness (99 percent) based on u, dimensional.

thetax is momentum thickness based on u, dimensional.

rcr is radius of curvature, dimensional.

Profile outputs:

```
write(7)(zp(k),k=1,nz)
```

zp is $z_p = (z^*/l^*)$; note l^* definition for i=1 and i>1.

This box only for i>1:

```
write(7)(up(k),k=1,nz)
write(7)(upz(k),k=1,nz)

write(7)(upzz(k),k=1,nz)
```

up is u^*/u_e^*; upz is $\partial u_p/\partial z_p$; upzz is $\partial^2 u_p/\partial z_p^2$

```
write(7)(vp(k),k=1,nz)
write(7)(vpz(k),k=1,nz)

write(7)(vpzz(k),k=1,nz)
```

vp is v^*/v_e^* if i=1, v^*/u_e^* if i>1;

vpz, vpzz are derivatives defined similar to upz, upzz.

```
write(7)(tp(k),k=1,nz)
write(7)(tpz(k),k=1,nz)

write(7)(tpzz(k),k=1,nz)
```

tp is T^*/T_e^*; tpz, tpzz are defined similar to upz, upzz.

```
write(7)(wp(k),k=1,nz)
write(7)(wpz(k),k=1,nz)

write(7)(wpzz(k),k=1,nz)
```

wp is $\hat{w}^*/v_e^*$ if i=1, $\hat{w}^*/u_e^*$ for i>1; wpz,wpzz are defined similar to upz,upzz.

This box only for i>2; output of streamwise derivatives:

```
write(7)(duds(k),k=1,nz)
write(7)(dvds(k),k=1,nz)
write(7)(dtds(k),k=1,nz)
write(7)(dwds(k),k=1,nz)
```

duds=$(\partial u^*/\partial s_1^*)/(U_\infty^*/l^*)$

dvds=$(\partial v^*/\partial s_1^*)/(U_\infty^*/l^*)$

dtds=$(\partial T^*/\partial s_1^*)/(U_\infty^*/l^*)$

dwds=$(\partial \hat{w}^*/\partial s_1^*)/(U_\infty^*/l^*)$

These output writes are implemented in subroutine out in the subdirectory, bl3d/bl/case1 (and also bl3d/bl/case2).

Running the Boundary-Layer Program

The program routines are contained in the following files:

```
blk.f
der.f
etac.f
main.f
phys.f
rinvis.f
sumk.f
c13phi.f
derk.f
initial.f
nextep.f
read7.f
solve.f
updte.f
```

```
conv.f
edge.f
inputs.f
out.f
ref.f
sum.f
```

In addition, the `include` files `com` and `compack`, the makefile `makefile`, and the input file `inp.dat` are also provided. A brief description of important subroutines follows:

`inputs.f`. Reads input file `inp.dat`.

`ref.f`. Calculates reference quantities.

`rinvis.f`. Reads boundary-layer edge data `bl.bin`.

`initial.f`. Sets up initial profile at the attachment point $i = 1, j = 1$.

`main.f`. Calls various routines; specification of wall temperature or wall heat flux; specifies wall suction rate.

`edge.f`. Specifies edge coefficients depending on boundary point or interior point; calls `c13phi.f`, `etac.f` to calculate some additional edge parameters.

`etac.f`. Sets up the y differencing coefficients based on the local crossflow direction (L scheme or Z scheme).

`blk.f`. Sets up and solves the `(7x7xnz)` block tridiagonal system.

`updte.f`. Updates nonlinear quantities θ, θ', l, l', D_5, and l at $k = 1$ for the current iteration.

`updte.f`. Checks convergence.

`phys.f`. Outputs dimensional quantities, boundary-layer properties; calculates crossflow.

`nexstep.f`: storing of variables prior to stepping in i.

`out.f`: output of quantities and profiles for boundary-layer stability analysis.

The `include` file `com` has the following `parameter` statement (for `case1` in this example):

```
parameter(nx=100,ny=29,nz=61)
```

The nx and ny values are as written out from the interface program. The value of nz corresponds to the number of points in the boundary-layer normal direction.

The program is run with input files inp.dat and bl.bin. Appropriate dimensions in parameter statement in the file com are selected; then remove all .o files if com was modified. Type make, followed by a.out to run the program. Runs can be made interactively for moderate grids. The program execution stops at the *(i, j)* location where the boundary layer separates; this results from the calculation of negative temperature in subroutine update. An error message is printed out, and the incipient separation condition can be checked by the local skin-friction coefficient.

Table 1

List of Important Program Variables

Computer variable	Symbol	Description
a,b,c	$\alpha^k_{l,m}, \beta^k_{l,m}, \gamma^k_{l,m}$	elements of linearized system (eq. (120))
a1,a2,a3,a4	A_1, A_2, A_3, A_4	coefficients of transformed continuity equations (eqs. (47)–(50))
ad1,ad2,ad3	a_1, a_2, a_3	ξ direction coefficients (eq. (129))
ak	k_s	stretching constant for ζ distribution (eq. (128))
al	l	ratio $(\rho\mu)/(\rho_e\mu_e)$
alp	l'	$\partial l/\partial\zeta$
alpr	l/Pr	
alprp	l'/Pr	
amach	M_∞	Mach number
amue	μ_e	edge viscosity, nondimensional, (eq. (33))
amuel	μ_e at *(i,j)*	local value of μ_e
amufs	μ^*_∞	free-stream viscosity, dimensional
amur	μ_r	reference viscosity function, nondimensional (eq. (33))
b1,b2,b3,b4,b5,b6	$B_1, B_2, B_3, B_4, B_5, B_6$	coefficients (eqs. (55)–(60))
b3h,b4h	$\hat{B}_3, \hat{B}_4$	coefficients (eq. (94))

Computer variable	Symbol	Description
b3t,b4t,b5t,b6t	$\tilde{B}_3, \tilde{B}_4, \tilde{B}_5, \tilde{B}_6$	coefficients (eq. (91))
bd1,bd2,bd3,bd4, bd5	b_1, b_2, b_3, b_4, b_5	η direction differencing coefficients (eq. (132))
bet	$\gamma/(\gamma-1)$	
bet2	$(\gamma-1)/2$	
c1,c2,c3,c4,c5,c6	$C_1, C_2, C_3, C_4, C_5, C_6$	coefficients (eqs. (62)–(67))
c4h,c5h	$\hat{C}_4, \hat{C}_5$	coefficients (eq. (95))
c3t,c4t,c5t,c6t	$\tilde{C}_3, \tilde{C}_4, \tilde{C}_5, \tilde{C}_6$	coefficients (eq. (92))
c13	C_{13}	metric coefficient (eq. (6))
c132	${C_{13}}^2$	
c13phix	$(C_{13}\phi/h_1)_{,x}$	metric coefficient (eq. (48))
c13phiy	$\{C_{13}\phi v_r/(h_2 u_e)\}_{,y}$	metric coefficient (eq. (50))
c24,c25,c26	C_{24}, C_{25}, C_{26}	coefficients (eq. (19))
c26x	$\partial C_{26}/\partial x$	coefficient (eq. (80))
c34,c35,c36	C_{34}, C_{35}, C_{36}	coefficients (eq. (20))
cbeta1	$\cos(\beta)_{i,j}$	angle between grid lines (eq. (3))
cd1,cd2	$\frac{1}{2}, \frac{1}{12}$	constants (eq. (101))
chi1,chi2,chi3	χ_1, χ_2, χ_3	coefficients (eq. (87))

Computer variable	Symbol	Description
d1,d2,d3,d4,d5	D_1, D_2, D_3, D_4, D_5	coefficients (eqs. (68)–(69))
d5p	$\partial D_5/\partial\zeta$	
d3t,d4t	$\tilde{D_3}$,$\tilde{D_4}$	coefficients (eq. (96))
delfp,delgp, delhp	$\partial S_5, \partial S_6, \partial S_7$	solution vector elements (eq. (108))
delfpmax, delgpmax, delhpmax,	max. of $\partial S_5, \partial S_6, \partial S_7$	convergence indicators
deltax		boundary-layer thickness based on F reaching 99 percent value, dimensional
duds	$(\partial u_e/\partial x)_{i=1}$	attachment-line velocity gradient
e1,e2,e3,e4	E_1, E_2, E_3, E_4	coefficients (eq. (87))
epsf,epsg,epsh		convergence criterion for change in f', g', h' at wall (k = 1)
f	F	u/u_e
f1,f2		F at $i-1$ and $i-2$
fe	$(\partial u_e/\partial x)_{i=1}$	attachment-line velocity gradient
fel		local value of fe
fey	$(\partial^2 u_e/\partial x\,\partial y)_{i=1}$	used in eq. (76)
fp	F'	$\partial(u/u_e)/\partial\zeta$
fp1,fp2		F' at $i-1$ and $i-2$

Computer variable	Symbol	Description
g	G	v/v_r
f1, f2		F at $i-1$ and $i-2$
g1, g2		G at $i-1$ and $i-2$
g12, g121	g_{12}	metric coefficient
g12x	$\partial g_{12}/\partial x$	
g12y	$\partial g_{12}/\partial y$	
gam	γ	
gel		local value of $G_{k=ke}$
gex, gey		x,y gradients of $G_{k=ke}$
gp	G'	$\partial(v/v_r)/\partial\zeta$
gp1, gp2		G' at $i-1$ and $i-2$
h	H	nondimensional total enthalpy (eq. (24))
h1	h_1	metric coefficient
h11	h_1	local value of metric coefficient
h1x, h1y	$h_{1,x}, h_{1,y}$	x,y gradients of h_1
h2	h_2	metric coefficient
h21	h_2	local value of metric coefficient
h2x, h2y	$h_{2,x}, h_{2,y}$	x,y gradients of h_2
he	$H_{k=ke}$	boundary-layer edge value of H

Computer variable	Symbol	Description
hel		local value of H
hfs	H^*_∞	free-stream value of total enthalpy (eq. (23))
hh1,hh2		H at $i-1$ and $i-2$
hp	H'	$\partial H/\partial\zeta$
hp1,hp2		H' at $i-1$ and $i-2$
hse		H_e from BL-EDGE equations
i	i	streamwise index
iat		attachment-line iteration count
idim		Euler grid maximum dimension
ile		i index of leading edge
iord		value of i at which scheme is fully second order in x
iout		flag to output edge values by interpolation or from BL–EDGE solution
istart		flag for interface run mode
isurf		flag for upper or lower surface
it	superscript n	boundary-layer iteration count
itat		maximum number of attachment-line iterations
ite1,ite2		wing trailing edge indices

Computer variable	Symbol	Description
itmax		maximum number of boundary-layer iterations
iunit		flag for U.S. units or S.I. units
iv		number of points in streamwise direction, from interface run
ivm		maximum dimension for iv
iwall		flag for wall boundary condition
j		spanwise index
j1,j2,j3,j4,j5		neighboring points of (i,j) used in y differencing
j1w,j2w		spanwise indices that correspond to interface output
jdim		Euler grid maximum dimension
jte1,jte2		wing symmetry plane and tip indices
jv		number of points in spanwise direction from interface run
jvm		maximum dimension for jv
kdim		Euler grid maximum dimension
lflagx		flag to signify attachment-point solution or three-dimensional solution
lflagy		flag to signify LISW or general three-dimensional case

Computer variable	Symbol	Description
ncp		number of points in boundary-layer grid between attachment point and point at which local chord fraction = xcp
nx		streamwise dimension of boundary-layer grid
nxlim		value of i<nx limiting march in x
nxm		maximum dimension for nx
nxw		number of streamwise stations written out from interface code
ny		spanwise dimension of boundary-layer grid
nylim		value of j (<ny) limiting sweep in y
nym		maximum dimension for ny
nz		number of points in normal direction
nz1		nz-1
omatt		relaxation factor ω_a for attachment-line iteration
omega		blending factor between LISW and three-dimensional solutions
pb	C_p	pressure coefficient on boundary-layer grid
pc	C_p	pressure coefficient on Euler grid
pfs	P^*_∞	free-stream static pressure, dimensional
phil	ϕ	local value of ϕ

Computer variable	Symbol	Description
pi	π	
prl	Pr	laminar Prandtl number
q	q	absolute velocity, nondimensional
qel		local value of absolute edge velocity
reflen	L^*_∞	reference length
refls	Re_∞	free-stream Reynolds number based on L^*_∞ (eq. (29))
refs	Re_∞ / L^*_∞	free-stream Reynolds number per unit length
roe	ρ_e	boundary-layer edge density, nondimensional
roel	ρ_e	local value of boundary-layer edge density
rofs	ρ^*_∞	free-stream density, dimensional
rstar	R^*	gas constant
s1l	s_1	nondimensional arc length
tb	T_e	nondimensional boundary-layer edge temperature
tc		nondimensional temperature from Euler solution
te,tel	T_e	nondimensional boundary-layer edge temperature
tfs	T^*_∞	free-stream dimensional temperature

Computer variable	Symbol	Description
the1, the2	θ, θ'	temperature ratio and gradient (eqs. (54) and (89))
thetax		momentum thickness based on F, dimensional
ti1, ti2		temperature profiles at $i-1$ and $i-2$
tr	T_r	reference temperature (eq. (33))
trs	T_r^*	reference temperature, dimensional (eq. (32))
tse		edge temperature from the solution of the BL–EDGE equations
tst		streamwise derivative of T
tw	T_W	wall temperature, nondimensional (eq. (119))
ub		Cartesian velocity component, nondimensional
uc		Cartesian velocity component from Euler solution, nondimensional
ue	u_e	streamwise edge velocity
uel	u_e	local value of streamwise edge velocity
uerlim		error tolerance on streamwise velocity u_e at attachment line
uex	$\partial u_e/\partial x$	streamwise velocity gradient
uey	$\partial u_e/\partial y$	spanwise velocity gradient

Computer variable	Symbol	Description
ufs	U_∞^*	freestream velocity, dimensional
ui1,ui2		velocity profiles at $i-1$ and $i-2$
url		= 0 on attachment line, = 1, away from attachment line; used to compute q
use		edge velocity from the solution of the BL–EDGE equations
ustr		velocity profile in the edge streamline direction
vb		Cartesian velocity component, nondimensional
vc		Cartesian velocity component from Euler solution, nondimensional
vcross		crossflow velocity (orthogonal to edge streamline)
ve	v_e	edge velocity in span direction, nondimensional
vel	v_e	local value of v_e
vi1,vi2		velocity profiles at $i-1$ and $i-2$
vrl	v_r	reference velocity used in the definition of G (eq. (43))
vrx,vry		derivatives in x,y of v_r
vse		edge velocity from the solution of the BL–EDGE equations
w	w	transformed normal velocity (eq. (44))

Computer variable	Symbol	Description
wb		Cartesian velocity component, nondimensional
wc		Cartesian velocity component from Euler solution, nondimensional
wi1,wi2		velocity profiles at $i-1$ and $i-2$
x,y	x,y	streamwise boundary-layer coordinates
xb,yb,zb	x'	Cartesian coordinate of boundary-layer grid
xc,yc,zc		Cartesian coordinate of Euler grid
xcp		percent chord value at which i=ncp
xnorm		normalizing arc length, nondimensional
z		transformed boundary-layer normal coordinate
zcon		coefficient to calculate zphys from z
zi1,zi2		zphys at $i-1$ and $i-2$
zphys	z^*	boundary-layer grid normal coordinate, dimensional
zphysx		streamwise gradient of z^*
zphysy		spanwise gradient of z^*

REPORT DOCUMENTATION PAGE

Form Approved
OMB No. 0704-0188

1. AGENCY USE ONLY *(Leave blank)*	2. REPORT DATE	3. REPORT TYPE AND DATES COVERED
	August 1993	Contractor Report

4. TITLE AND SUBTITLE

Three-Dimensional Boundary-Layer Program (BL3D) for Swept Subsonic or Supersonic Wings With Application to Laminar Flow Control

5. FUNDING NUMBERS

C NAS1-19672

WU 537-03-23-03

6. AUTHOR(S)

Venkit Iyer

7. PERFORMING ORGANIZATION NAME(S) AND ADDRESS(ES)

ViGYAN, Inc.
30 Research Drive
Hampton, VA 23666-1325

8. PERFORMING ORGANIZATION REPORT NUMBER

9. SPONSORING / MONITORING AGENCY NAME(S) AND ADDRESS(ES)

National Aeronautics and Space Administration
Langley Research Center
Hampton, VA 23681-0001

10. SPONSORING / MONITORING AGENCY REPORT NUMBER

NASA CR-4531

11. SUPPLEMENTARY NOTES

Langley Technical Monitor: Julius E. Harris

12a. DISTRIBUTION / AVAILABILITY STATEMENT

Unclassified/Unlimited

Subject Category 34

12b. DISTRIBUTION CODE

13. ABSTRACT ***(Maximum 200 words)***

The theory, formulation, and solution of three-dimensional, compressible attached laminar flows, applied to swept wings in subsonic or supersonic flow are discussed. This report incorporates several new features and modifications to an earlier general procedure described in NASA CR 4269, January 1990. Details of interfacing the boundary-layer computation with solution of the inviscid Euler equations are discussed. The report also includes a description of the computer program, complete with user's manual and example cases. Comparison of solutions with Navier-Stokes computations with or without boundary-layer suction is given. Output of solution profiles and derivatives required in boundary-layer stability analysis is provided.

14. SUBJECT TERMS	15. NUMBER OF PAGES
boundary layer; compressible flow; laminar flow control; transition prediction; swept-wing flow	136
	16. PRICE CODE A07

17. SECURITY CLASSIFICATION OF REPORT	18. SECURITY CLASSIFICATION OF THIS PAGE	19. SECURITY CLASSIFICATION OF ABSTRACT	20. LIMITATION OF ABSTRACT
Unclassified	Unclassified	Unclassified	